Title
Role of PAK4 in immune cell exclusion and resistance to PD-1 blockade immunotherapy

Author
Abril Rodriguez, Gabriel

Publication Date
2021

Peer reviewed|Thesis/dissertation

UNIVERSITY OF CALIFORNIA

Los Angeles

Role of PAK4 in immune cell exclusion and resistance to PD-1 blockade immunotherapy

A dissertation submitted in partial satisfaction of the requirements for the degree Doctor of Philosophy in Molecular and Medical Pharmacology

by

Gabriel Abril Rodriguez

2021

ABSTRACT OF THE DISSERATION

Role of PAK4 in immune cell exclusion and
resistance to PD-1 blockade immunotherapy

By

Gabriel Abril Rodriguez
Doctor of Philosophy in Molecular and Medical Pharmacology
University of California, Los Angeles, 2021
Professor Antoni Ribas, Chair

Immune checkpoint blockade therapies constitute one of the major advances in cancer treatment. Despite the long-lasting responses observed in a wide range of tumor types, the majority of patients do not respond or relapse shortly after. In order to increase response rates, we need to better predict patients that would benefit from the treatment as well as identify resistance mechanisms to find novel treatment strategies. However, the interplay between the immune system, the cancer cells and the tumor microenvironment is complex and dynamic, rendering the understanding of resistant mechanisms particularly challenging.

Lack of immune cell infiltration constitutes one of the main mechanisms of primary resistance to checkpoint blockade. The absence of T cells on the tumor margin leaves the therapeutic targeting of immune checkpoints ineffective. Interestingly, cancer cell-intrinsic mechanisms could actively participate in the process of immune evasion and importantly, could be pharmacologically targeted to reverse immune exclusion. The finding of actionable molecules that increases T cell infiltration in the tumor could be used in combination with PD-1 blockade, in order to reverse adaptive immune resistance.

Here, we characterized the tumors of melanoma patients treated with PD-1 blockade. Our analyses further validated lack of immune cell infiltration as one mechanism of resistance. Importantly, we identified PAK4 as a novel and actionable target that is enriched in biopsies with poor immune infiltration and lack of response to PD-1 blockade. We show how genetically and pharmacologically that inhibition of PAK4 increases immune cell infiltration and improves checkpoint blockade therapy in several *in vivo* mouse models. We further characterized the impact of inhibiting PAK4 expression. The transcriptomic profiles of PAK4 KO tumors revealed the profound effect that has on the tumor microenvironment, particularly in the genes related to the extracellular matrix and blood vessel formation. This work serves as an example of how direct changes in cancer cells impact the tumor microenvironment and influence the anti-tumor immune response. Importantly, this work also provides the scientific rationale for a novel treatment strategy to combine PAK4 inhibitor with checkpoint blockade.

The dissertation of Gabriel Abril Rodriguez is approved.

David Baltimore

Thomas G. Graeber

Anna Wu

Antoni Ribas, Committee Chair

University of California, Los Angeles

2021

This work is dedicated to my family

TABLE OF CONTENTS

List of Figures

Chapter 1: Immune checkpoint blockade

Chapter 2: PAK4 inhibition improves PD-1 blockade immunotherapy

Chapter 3: PAK4 inhibition remodels the tumor microenvironment to increase PD-1 blockade efficacy

List of Tables

Chapter 2: PAK4 inhibition improves PD-1 blockade immunotherapy

Acknowledgements

This has been an exciting, challenging and highly rewarding journey, and it would not be fair to start this section in any other way but to showing my gratitude to the person who made it all possible, my outstanding mentor, Toni Ribas. Toni, I do not have any other alternative but to take advantage of this section to say how mindful and supportive you have been all along the way. And you know I have to write this down, in these sentences, because if I'll try to say it out loud, as I will do after my oral defense, you would stop my right away and say: "this is not about me, this is about you". You are a leader in several ways, not only in your professional career, but also in the way you treat others. You have taught me more than I could ever give you back. Thank you.

Also, I want to take this opportunity to say sorry to the whole Ribas lab family for having to deal with me during these 5 years (you didn't have a choice), as well as all the rest of collaborators and friends that made this work possible. I would be always grateful that our paths crossed along this journey.

Thanks to my colleague, that I'm lucky to also call him friend, Davis, who perhaps owns as much as I do, the success of this project. Thanks for your time, help and your relentless commitment to advance cancer research.

To the UCLA lunch family, specially to Ignacio and Cristina, to make me feel like at home even 10.000km away. Looking back, it would be impossible to find any single day you didn't make me laugh and smile. Without any doubt, you were one of the most valuable findings in my life.

Last but not least, this work is dedicated to my family. You mean the world to me. It has been tough to get used to receive "good night" messages in the middle of the afternoon

(consequences of being 9 hours behind you), but it did help to express more easily how much

I miss you and love you. Thanks for always being there for me. Os quiero.

Chapter 1 was adapted and extended from an original publication by Gabriel Abril-Rodriguez and Antoni Ribas.
Abril-Rodriguez G, Ribas A. SnapShot: Immune Checkpoint Inhibitors. Cancer Cell. 2017;31(6):848-848.e1. doi:10.1016/j.ccell.2017.05.010

Chapter 2 is a reproduction of the publication led by Gabriel Abril-Rodriguez and supervised by Antoni Ribas.
Abril-Rodriguez G, Torrejon DY, Liu W, et al. PAK4 inhibition improves PD-1 blockade immunotherapy. Nat Cancer. 2020;1(1):46-58. doi:10.1038/s43018-019-0003-0

Chapter 3 was adapted from an article in submission from work that was led by Gabriel Abril-Rodriguez and supervised by Antoni Ribas.
“PAK4 inhibition remodels the tumor microenvironment to increase PD-1 blockade efficacy” by Gabriel Abril-Rodríguez, Davis Y. Torrejon, Katie M. Campbell, Egmidio Medina, Justin D. Saco, Ameya S. Champhekar, Ivan Perez Garcilazo, Ignacio Baselga Carretero, Jas Singh, Jenna Jeffrey, Daniel DiRenzo, Juan Jaen, Begoña Comin-Anduix, Cristina Puig-Saus, Antoni Ribas.
In submission to Cancer Immunology Research, September 2021

Gabriel Abril Rodriguez was funded by the Isabel & Harvey Kibel Fellowship Award and the Alan Ghitis Fellowship Award for Melanoma Research

VITA

Education

Vrije University, Amsterdam, The Netherlands
M.S: Oncology 2014-2016

University of Barcelona, Barcelona, Spain
M.S: Biomedicine 2013-2014

University of Barcelona, Barcelona, Spain
B.S: Biochemistry 2009-2013

Honors and Awards

Alan Ghitis Fellowship Award for Melanoma Research 2020-2021
Alan Ghitis Fellowship Award for Melanoma Research 2019-2020
Isabel & Harvey Kibel Fellowship Award 2018-2019
UCLA Bioscience Innovation Day Pearl Cohen Poster Award 2019
Selected SITC Presidential Travel Award 2018
Isabel & Harvey Kibel Fellowship Award 2017-2018
Selected for the Oncology Topmaster program by the Vrije University 2016

Publications

Research articles

1. **Abril-Rodriguez, G**., Torrejon, D.Y., Liu, W. *et al.* PAK4 inhibition improves PD-1 blockade immunotherapy. *Nat Cancer* **1,** 46–58 (2020). doi.org/10.1038/s43018-019-0003-0

2. Kim YJ, Sheu KM, Tsoi J, **Abril-Rodriguez G,** et al. Melanoma dedifferentiation induced by IFN-γ epigenetic remodeling in response to anti-PD-1 therapy. J Clin Invest. 2021;131(12):e145859. doi:10.1172/JCI145859

3. Torrejon DY, **Abril-Rodriguez G**, Champhekar AS, et al. Overcoming Genetically Based Resistance Mechanisms to PD-1 Blockade. *Cancer Discov*. 2020;10(8):1140-1157. doi:10.1158/2159-8290.CD-19-1409

4. Grasso CS, Tsoi J, Onyshchenko M, **Abril-Rodriguez G**, et al. Conserved Interferon-γ Signaling Drives Clinical Response to Immune Checkpoint Blockade Therapy in Melanoma. *Cancer Cell*. 2020;38(4):500-515.e3. doi:10.1016/j.ccell.2020.08.005

5. Gruber, T., Kremenovic, M., Sadozai, H., Rombini, N., Baeriswyl, L., Maibach, F., Modlin, R. L., Gilliet, M., von Werdt, D., Hunger, R. E., Seyed Jafari, S. M., Parisi, G., **Abril-Rodriguez, G.,** Ribas, A., & Schenk, M. (2020). IL-32γ potentiates tumor immunity in melanoma. *JCI insight*, *5*(18), e138772. doi.org/10.1172/jci.insight.138772

6. Grasso, C. S., Giannakis, M., Wells, D. K., Hamada, T., Mu, X. J., Quist, M., Nowak, J. A., Nishihara, R., Qian, Z. R., Inamura, K., Morikawa, T., Nosho, K., **Abril-Rodriguez, G**., Connolly, C., Escuin-Ordinas, H., Geybels, M. S., Grady, W. M., Hsu, L., Hu-Lieskovan, S., Huyghe, J. R., … Peters, U. (2018). Genetic Mechanisms of Immune Evasion in Colorectal Cancer. *Cancer discovery*, *8*(6), 730–749.

doi.org/10.1158/2159-8290.CD-17-1327

7. **Abril-Rodriguez, G**., & Ribas, A. (2017). SnapShot: Immune Checkpoint Inhibitors. *Cancer cell*, *31*(6), 848–848.e1. doi.org/10.1016/j.ccell.2017.05.010

8. Garcia-Diaz, A., Shin, D. S., Moreno, B. H., Saco, J., Escuin-Ordinas, H., **Rodriguez, G. A**., Zaretsky, J. M., Sun, L., Hugo, W., Wang, X., Parisi, G., Saus, C. P., Torrejon, D. Y., Graeber, T. G., Comin-Anduix, B., Hu-Lieskovan, S., Damoiseaux, R., Lo, R. S., & Ribas, A. (2017). Interferon Receptor Signaling Pathways Regulating PD-L1 and PD-L2 Expression. *Cell reports*, *19*(6), 1189–1201. doi.org/10.1016/j.celrep.2017.04.031

9. Shin, D. S., Zaretsky, J. M., Escuin-Ordinas, H., Garcia-Diaz, A., Hu-Lieskovan, S., Kalbasi, A., Grasso, C. S., Hugo, W., Sandoval, S., Torrejon, D. Y., Palaskas, N., **Rodriguez, G. A.,** Parisi, G., Azhdam, A., Chmielowski, B., Cherry, G., Seja, E., Berent-Maoz, B., Shintaku, I. P., Le, D. T., … Ribas, A. (2017). Primary Resistance to PD-1 Blockade Mediated by JAK1/2 Mutations. *Cancer discovery*, *7*(2), 188–201. doi.org/10.1158/2159-8290.CD-16-1223

10. Zaretsky, J. M., Garcia-Diaz, A., Shin, D. S., Escuin-Ordinas, H., Hugo, W., Hu-Lieskovan, S., Torrejon, D. Y., **Abril-Rodriguez, G.,** Sandoval, S., Barthly, L., Saco, J., Homet Moreno, B., Mezzadra, R., Chmielowski, B., Ruchalski, K., Shintaku, I. P., Sanchez, P. J., Puig-Saus, C., Cherry, G., Seja, E., … Ribas, A. (2016). Mutations Associated with Acquired Resistance to PD-1 Blockade in Melanoma. *The New England journal of medicine*, *375*(9), 819–829. doi.org/10.1056/NEJMoa1604958

11. Orlando, S., Gallastegui, E., Besson, A., **Abril, G**., Aligué, R., Pujol, M. J., & Bachs, O. (2015). p27Kip1 and p21Cip1 collaborate in the regulation of transcription by recruiting cyclin-Cdk complexes on the promoters of target genes. *Nucleic acids research*, *43*(14), 6860–6873. doi.org/10.1093/nar/gkv593

Abstracts

Oral Presentations

Gabriel Abril-Rodriguez, Davis Y. Torrejon, Jesse M. Zaretsky, Theodore S. Nowicki, Siwen Hu-Lieskovan, Beata Berent-Maoz, Begoña Comin-Anduix, Catherine S. Grasso and Antoni Ribas. PAK4 inhibition reverses immune cell exclusion and overcomes resistance to checkpoint blockade therapy. Society for Immunotherapy for Cancer (SITC). Presidential Session, 2018.

Gabriel Abril-Rodriguez, Davis Y. Torrejon, Wei Liu, Jesse M. Zaretsky, Theodore S. Nowicki, Siwen Hu-Lieskovan, Beata Berent-Maoz, Begoña Comin-Anduix, Cun-Yu Wang, Catherine S. Grasso and Antoni Ribas. PAK4 inhibition improves PD-1 blockade therapy. Molecular and Medical Pharmacology Annual Retreat, 2019.

Gabriel Abril-Rodriguez. Role of PAK4 in immune cell exclusion and resistance to PD-1 blockade immunotherapies. University of California, Los Angeles. Research in Progress Seminars, 2019.

Gabriel Abril-Rodriguez. PAK4 inhibition reverses immune cell exclusion and overcomes resistance to checkpoint blockade therapy. Parker Institute for Cancer Immunotherapy, annual research meeting at UCLA, 2018.

Gabriel Abril-Rodriguez. PAK4 inhibition reverses immune cell exclusion and overcomes resistance to checkpoint blockade therapy. Parker Institute for Cancer Immunotherapy, UCLA retreat, 2017.

Poster Presentations

Gabriel Abril-Rodriguez, Davis Y. Torrejon, Wei Liu, Jesse M. Zaretsky, Theodore S. Nowicki, Jennifer Tsoi, Cristina Puig-Saus, Ignacio Baselga Carretero, Egmidio Medina, Michael J. Quist, Alejandro J. Garcia, William Senapedis, Erkan Baloglu, Anusha Kalbasi, Gardenia Cheung-Lau, Beata Berent-Maoz, Begoña Comin-Anduix, Siwen Hu-Lieskovan, Cun-Yu Wang, Catherine S. Grasso and Antoni Ribas. PAK4 inhibition improves PD-1 blockade immunotherapy. UCLA Biosciences Innovation Day, 2019.

Gabriel Abril-Rodriguez, Davis Y. Torrejon, Wei Liu, Jesse M. Zaretsky, Theodore S. Nowicki, Siwen Hu-Lieskovan, Beata Berent-Maoz, Begoña Comin-Anduix, Cun-Yu Wang, Catherine S. Grasso and Antoni Ribas. PAK4 inhibition improves PD-1 blockade immunotherapy. Biotechnology 2.0: Next Generation Biologic Therapeutics at Amgen, 2019.

Gabriel Abril-Rodriguez, Davis Y. Torrejon, Jesse M. Zaretsky, Theodore S. Nowicki, Siwen Hu-Lieskovan, Beata Berent-Maoz, Begoña Comin-Anduix, Catherine S. Grasso and Antoni Ribas. PAK4 inhibition reverses immune cell exclusion and overcomes resistance to checkpoint blockade therapy. Parker Institute for Cancer Immunotherapy, UCLA retreat, 2018.

Gabriel Abril-Rodriguez, Davis Y. Torrejon, Jesse M. Zaretsky, Theodore S. Nowicki, Siwen Hu-Lieskovan, Beata Berent-Maoz, Begoña Comin-Anduix, Catherine S. Grasso and Antoni Ribas. PAK4 inhibition reverses immune cell exclusion and overcomes resistance to checkpoint blockade therapy. Society for Immunotherapy for Cancer (SITC), 2018.

Gabriel Abril-Rodriguez, Catherine S. Grasso, Jesse M. Zaretsky, Beata Berent-Maoz, Siwen Hu-Lieskovan and Antoni Ribas. Role of PAK4 in cancer immune cell exclusion. Parker Institute for Cancer Immunotherapy, UCLA retreat, 2017.

Gabriel Abril-Rodriguez, Catherine S. Grasso, Jesse M. Zaretsky, Beata Berent-Maoz, Siwen Hu-Lieskovan and Antoni Ribas. Role of PAK4 in cancer immune cell exclusion. American Association for Cancer Research (AACR) meeting, 2017.

Teaching Experience

University of California, Los Angeles (UCLA)
Teaching Assistant: Immunology (185A)
Assisted with instruction by leading review sections, individual tutoring, and writing and grading exams.

Academic Peer Reviewer

Reviewer for Nature Reviews Drug Discovery, 1 manuscript	2021
Reviewer for Cancer Discovery, *3 manuscripts*	2020-2021
Reviewer for Communications Biology, *1 manuscript*	2020
Reviewer for JNCI, Journal of the National Cancer Institute, *1 manuscript*	2017

Patents and inventions

Pak4 Inhibitors And Methods Of Use: 17/048473 Application number: 20210161943

Chapter 1:

Immune checkpoint blockade

1.- Immune checkpoint blockade: main concepts

Checkpoint blockade therapies induce major responses by releasing the inhibitory mechanisms that control T cell mediated immunity[1]. Immune checkpoints refer to the set of inhibitory pathways that immune cells possess in order to regulate and control the durability of the immune response while maintaining self-tolerance. Among the different immune-checkpoint receptors, antibodies blocking two of them have been approved by the FDA for clinical use: cytotoxic T lymphocyte-associated antigen 4 (CTLA-4) and programmed cell death 1 (PD-1) or its ligand PD-L1.

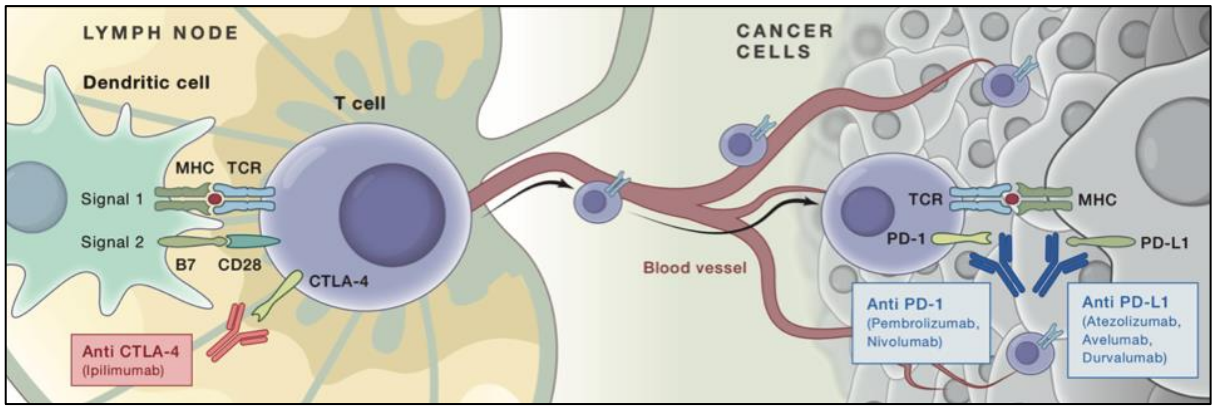

Figure 1. Checkpoint blockade: mechanism of action. Reprinted from Abril-Rodriguez and Ribas 2017.

CTLA-4 is expressed by T cells and controls T cell activation during early stages at the lymph nodes. CTLA-4 competes with the co-stimulatory receptor CD28 for the binding to ligands CD80 (B7.1) and CD86 (B7.2). Upon MHC-TCR engagement (signal 1), CD28 binds to CD80/86 (signal 2) to expand TCR signaling and T cell activation. This process also triggers the surface expression of CTLA-4 which was previously located in intracellular vesicles in the naive T cell. CTLA-4 presents higher affinity for the CD80/86 ligands than CD28. Therefore, CTLA-4 out competes CD28 in the binding of these ligands and by doing so prevents and controls further proliferation of the initial T-cell response[2]. On the other hand, PD-1 is expressed on activated T cells, B lymphocytes and natural killer cells and constitutes a main

mechanism of tumor immune resistance in peripheral tissues. PD-1 contains a tyrosine-based inhibitory motif (ITIM) together with an immune-receptor tyrosine-based switch motif (ITSM), which is phosphorylated upon binding with the B7-family of ligands PD-L1 (B7-H1 or CD274) or PD-L2 (B7-DC or CD273). Ligand engagement leads to the recruitment of SH2-domains containing tyrosine phosphatase 2 (SHP-2) resulting in the suppression of T cell proliferation and response[3]. The blockade of PD-1 receptor or its ligand PD-L1 with antibodies enhances pre-existent antitumor immune activity providing patients with major and durable immune responses against the tumor.

2.- PD-1 blockade mechanism of action: Interferon induced adaptive immune resistance

Interferons play a major role in mediating antitumor responses and they constitute the basis of adaptive immune resistance through the PD-1/PD-L1 interaction. There are three main types of IFNs: (1) type I which includes IFN-α and IFN-β, (2) type II IFN-γ and (3) type III IFN-λ. All three types of IFNs involve similar mechanisms of action. Binding to its specific receptor activates the associated Janus kinases (JAKs) and results in the recruitment of signal transducers and activators of transcription (STATs). Signal transduction is then completed by translocation of the activated STATs to the nucleus where they bind to specific elements of target promoters to amplify and regulate the expression of critical mediators of the immune response involved in cell proliferation, apoptosis, antigen processing machinery or migration[4]. However, interferons might also lead to the expression of genes that are involved in immunosuppression such as PD-L1 or indoleamine-2,3-dioxygenase (IDO), which can be induced in response to both type I and II IFNs. Although PD-L1 could also be constitutively expressed by activation of different oncogenic pathways[5–7], interferon induced PD-L1 expression seems to be a major mechanism whereby cancer cells evade T cell attack[8] . In short, antigen specific T cells release IFN-γ upon activation of their T cell receptor (TCR) after recognition of cognate antigen presented by major histocompatibility complexes (MHC). Consequent IFN-γ engagement to IFNGR1 and IFNGR2 on tumor cells leads to JAK1 and JAK2 activation resulting in STAT1 and STAT3 recruitment and phosphorylation. The complex

is then translocated to the nucleus where it binds to the gamma activated sequence (GAS) leading to interferon regulatory factor 1 (IRF1) activation. IRF1 induces PD-L1 expression[9] which is predominant at the invasive tumor margins where initial T cell/cancer cell interaction occurs and blocks the antitumor response of the pre-existing T cells (Tumeh et al., 2014). This process, termed adaptive immune resistance, allows cancer cells to evade the immune response by expressing PD-L1 which inhibits the initial T cell attack. PD-1 blockade therapies induce responses by inhibiting the adaptive immune resistance.

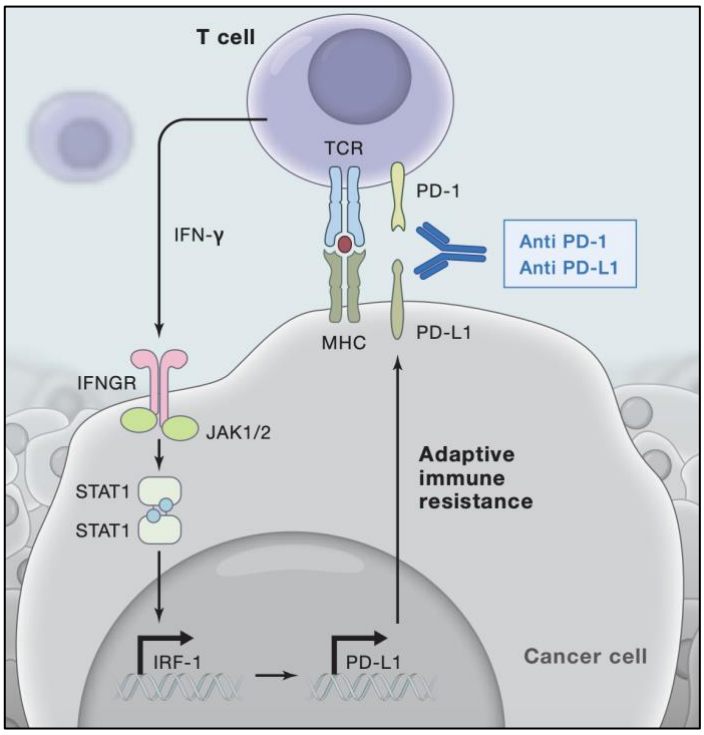

Figure 2. Interferon-induced adaptive immune resistance. Reprinted from Abril-Rodriguez and Ribas 2017.

3.- Tumor cell intrinsic mechanisms of resistance to checkpoint blockade

PD-1 blockade works by reinvigorating the pre-existing T cell anti-tumor response. However, in order to fully understand why tumors are or become resistant to checkpoint blockade, we need to first recapitulate what are the key steps involved in the generation of this pre-existing T cell anti-tumor immune response. In short, as described in the review Oncology Meets

Immunology: The Cancer-Immunity Cycle by Chen and Mellman[10], there are seven required steps: 1) Release of cancer cell antigens. 2) Uptake of this specific tumor antigens by antigen presentation cells (APCs). 3) Priming and activation of T cells in the lymph node. 4) Trafficking of tumor-specific T cells to the tumor. 5) Infiltration of T cells into the tumors. 6) Recognition of cancer by T cells and 7) killing of cancer cells. Now, one could imagine that defects in any of these critical steps could have an impact on the outcome of checkpoint blockade immunotherapy[11]. Here, we will describe some of the primary or acquired resistance mechanisms that are relevant for this thesis.

3.1.- Absence of tumor antigens

Since immune checkpoint blockade therapies reactive T cells that recognize tumor specific antigens, alterations that disrupt the TCR-peptide-HLA axis could despair treatment efficacy. For instance, this could be accomplished through mutations in genes that play a key role in the antigen presentation machinery, such as deletions in TAP or B2M[12,13]. In addition, tumors could have antigens that could be potentially recognized by T cells but develop mechanisms to block HLA expression, and hence, preventing the presentation and recognition of such tumor antigens by T cells[14–16]. Similarly, tumors with low mutational burden might not present tumor antigens that could be recognized by T cells[17]. In this scenario, blocking the PD-1/PD-L1 axis would not result in any clinical benefit as there is no pre-existing T cell army to re-activate. Interestingly, it has also been observed that dedifferentiation could also lead to the loss of tumor antigens, such as MART-1 in melanoma[18]. Although this resistance mechanism could be more relevant in adoptive T cell transfer therapies[19], it highlights the possibility that tumor antigens could be loss in response to inflammatory stimuli which could also impact checkpoint blockade outcome[20].

3.2.- Disruption of the IFN-γ axis

The understanding of how PD-L1 expression is regulated highlights the critical role of the IFN-γ pathway in PD-1 blockade. Hence, mutations or epigenetic silencing in mediators of the IFN-

γ/IFNGR1-IFNGR2/JAK1-JAK2/STAT1-STAT3/IRF1 axis, which results in the loss of sensitivity to IFN-γ pathway[9,21], could lead to the loss of PD-L1 expression, rendering checkpoint blockade ineffective. In addition to PD-L1 up-regulation, IFN-γ exhibits a potent anti-proliferative effect on cancer cells together with an increase in the expression of T cell attracting chemokines and antigen-presenting machinery components[22]. Given the scenario where PD-1/PD-L1 engagement is already being blocked, continued exposure of cancer cells to T cell released IFN-γ induces a selective pressure that promotes the selection of cancer cells that have acquired defects in the IFN-γ pathway. Here, insensitivity to IFN-γ functions as an acquired immune-evasion mechanism that allows cancer cells to overcome the IFN-γ mediated growth arrest, T cell attraction and the increased antigen-presenting machinery expression[23].

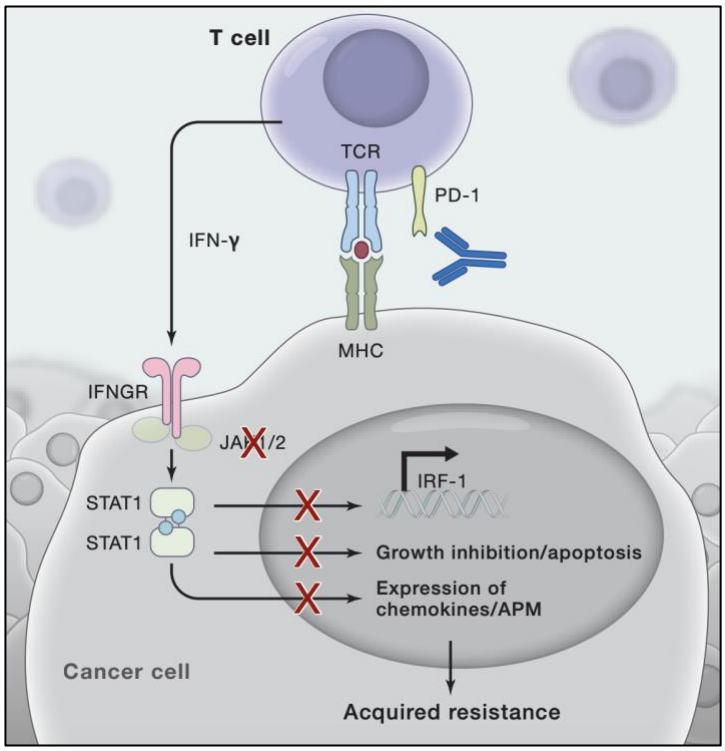

Figure 3. Acquired resistance to checkpoint blockade by loss of sensitivity to IFN- γ. Reprinted from Abril-Rodriguez and Ribas 2017.

3.3.- Oncogenic signaling pathways in immune evasion and resistance

In the recent years, it has become clearer that tumor intrinsic oncogenic signaling pathways play a key role in the outcome of cancer immunotherapies by actively influencing immune cell infiltration[24,25]. The WNT/β-catenin signaling pathway has been extensively associated with lack of T cell infiltration and resistance to PD-1 blockade resistance[26–28]. It has been proposed that active β-catenin could lead to decreased CCL4 expression, resulting in the absence of $CD103^+$ dendritic cells in the tumor and the lack of primed and activated T cells[29]. Other oncogenic signaling pathways include the MAPK pathway which increases VEGF and IL-8 expression, resulting in poor T cell recruitment and function[30]. Also, PTEN loss, which increases PI3K signaling, is associated with decreased T cell recruitment and resistance to PD-1 blockade[31]. In the context of oncogenic KRAS mutant, the loss of LKB1 increases IL-6 production which augments neutrophil recruitment while reducing T cell infiltration[32]. Furthermore, inactivating mutations in p53 have also been associated with poor immune infiltration[33]. These are just few examples of how cancer cells could alter the cancer-immunity cycle. Ideally, these pathways could be targeted pharmacologically to reverse immune resistance and use in combination with checkpoint blockade therapies.

4.- Overcoming resistance to PD-1 blockade immunotherapy

Huge efforts are currently underway to discover novel treatment strategies that improve and overcome resistance to PD-1 blockade therapy. Thousands of clinical trials are investigating the potential synergistic effect of new compounds in combination with anti-PD-1 therapy. For instance, as of September 2019, there are 2261 active trials testing combination regimens of PD-1/PD-L1 mAbs with other cancer therapies[34]. Unfortunately, the majority of these trials will not increase the efficacy of checkpoint blockade therapies. The incorporation of robust scientific rationales into the design of clinical trials will be key to improve and accelerate the finding of novel potent and effective treatment strategies. The following chapters will navigate towards this purpose. We characterized the transcriptomic profile of melanoma patients treated with anti-PD-1 to understand and unveil a new mechanism of resistance. Our analyses

identified PAK4 as a novel actionable target that improves PD-1 blockade efficacy and established the scientific foundation to combine a PAK4 inhibitor with PD-1/PD-L1 mAbs.

References

1. Ribas, A. & Wolchok, J. D. Cancer immunotherapy using checkpoint blockade. *Science* **359**, (2018).
2. Walker, L. S. K. & Sansom, D. M. The emerging role of CTLA4 as a cell-extrinsic regulator of T cell responses. *Nat. Rev. Immunol.* **11**, 852–863 (2011).
3. Zou, W., Wolchok, J. D. & Chen, L. PD-L1 (B7-H1) and PD-1 pathway blockade for cancer therapy : Mechanisms , response biomarkers , and combinations. *Sci. Transl. Med.* **8**, (2016).
4. Platanias, L. C. Mechanisms of type-I- and type-II-interferon-mediated signalling. *Nat. Rev. Immunol.* **5**, 375–86 (2005).
5. Lastwika, K. J. *et al.* Control of PD-L1 expression by oncogenic activation of the AKT-mTOR pathway in non-small cell lung cancer. *Cancer Res.* **76**, (2016).
6. Kataoka, K. *et al.* Aberrant PD-L1 expression through 3′-UTR disruption in multiple cancers. *Nature* **534**, (2016).
7. Dorand, R. D. *et al.* Cdk5 disruption attenuates tumor PD-L1 expression and promotes antitumor immunity. *Science (80-.).* **353**, (2016).
8. Tumeh, P. C. *et al.* PD-1 blockade induces responses by inhibiting adaptive immune resistance. *Nature* **515**, 568–571 (2014).
9. Garcia-Diaz, A. *et al.* Interferon Receptor Signaling Pathways Regulating PD-L1 and PD-L2 Expression. *Cell Rep.* **19**, 1189–1201 (2017).
10. Chen, D. S. & Mellman, I. Oncology meets immunology: The cancer-immunity cycle. *Immunity* **39**, 1–10 (2013).
11. Jenkins, R. W., Barbie, D. A. & Flaherty, K. T. Mechanisms of resistance to immune checkpoint inhibitors. *Br. J. Cancer* **118**, (2018).
12. Jhunjhunwala, S., Hammer, C. & Delamarre, L. Antigen presentation in cancer:

insights into tumour immunogenicity and immune evasion. *Nature Reviews Cancer* **21**, (2021).

13. Sucker, A. *et al.* Genetic evolution of T-cell resistance in the course of melanoma progression. *Clin. Cancer Res.* **20**, (2014).
14. Aptsiauri, N., Ruiz-Cabello, F. & Garrido, F. The transition from HLA-I positive to HLA-I negative primary tumors: the road to escape from T-cell responses. *Current Opinion in Immunology* **51**, (2018).
15. Seliger, B., Cabrera, T., Garrido, F. & Ferrone, S. HLA class I antigen abnormalities and immune escape by malignant cells. *Semin. Cancer Biol.* **12**, (2002).
16. Marincola, F. M., Jaffee, E. M., Hicklјn, D. J. & Ferrone, S. Escape of human solid tumors from t-cell recognition: molecular mechanisms and functional significance. *Adv. Immunol.* (2000). doi:10.1016/s0065-2776(08)60911-6
17. Gubin, M. M. *et al.* Checkpoint blockade cancer immunotherapy targets tumour-specific mutant antigens. *Nature* **515**, (2014).
18. Mehta, A. *et al.* Immunotherapy resistance by inflammation-induced dedifferentiation. *Cancer Discov.* **8**, (2018).
19. Landsberg, J. *et al.* Melanomas resist T-cell therapy through inflammation-induced reversible dedifferentiation. *Nature* **490**, 412–416 (2012).
20. Kim, Y. J. *et al.* Melanoma dedifferentiation induced by IFN-γ epigenetic remodeling in response to anti–PD-1 therapy. *J. Clin. Invest.* **131**, (2021).
21. Shin, D. S. *et al.* Primary Resistance to PD-1 Blockade Mediated by JAK½ Mutations. *Cancer Discov.* (2016). doi:10.1158/2159-8290.CD-16-1223
22. Parker, B. S., Rautela, J. & Hertzog, P. J. Antitumour actions of interferons: implications for cancer therapy. *Nat. Rev. Cancer* **16**, 131–144 (2016).
23. Zaretsky, J. M. *et al.* Mutations Associated with Acquired Resistance to PD-1 Blockade in Melanoma. *N. Engl. J. Med.* **375**, 819–29 (2016).
24. Kalbasi, A. & Ribas, A. Tumour-intrinsic resistance to immune checkpoint blockade. *Nature Reviews Immunology* **20**, (2020).

25. Spranger, S. & Gajewski, T. F. Impact of oncogenic pathways on evasion of antitumour immune responses. *Nat. Rev. Cancer* **18**, 139–147 (2018).

26. Grasso, C. S. *et al.* Genetic mechanisms of immune evasion in colorectal cancer. *Cancer Discov.* CD-17-1327 (2018). doi:10.1158/2159-8290.CD-17-1327

27. Spranger, S., Dai, D., Horton, B. & Gajewski, T. F. Tumor-Residing Batf3 Dendritic Cells Are Required for Effector T Cell Trafficking and Adoptive T Cell Therapy. *Cancer Cell* **31**, (2017).

28. Luke, J. J., Bao, R., Sweis, R. F., Spranger, S. & Gajewski, T. F. WNT/b-catenin pathway activation correlates with immune exclusion across human cancers. *Clin. Cancer Res.* **25**, (2019).

29. Spranger, S., Bao, R. & Gajewski, T. F. Melanoma-intrinsic β-catenin signalling prevents anti-tumour immunity. *Nature* **523**, 231–235 (2015).

30. Liu, C. *et al.* BRAF inhibition increases tumor infiltration by T cells and enhances the antitumor activity of adoptive immunotherapy in mice. *Clin. Cancer Res.* **19**, (2013).

31. Peng, W. *et al.* Loss of PTEN promotes resistance to T cell–mediated immunotherapy. *Cancer Discov.* **6**, (2016).

32. Koyama, S. *et al.* Adaptive resistance to therapeutic PD-1 blockade is associated with upregulation of alternative immune checkpoints. *Nat Commun* **7**, 1–9 (2016).

33. Xue, W. *et al.* Senescence and tumour clearance is triggered by p53 restoration in murine liver carcinomas. *Nature* **445**, (2007).

34. Xin Yu, J. *et al.* Trends in clinical development for PD-1/PD-L1 inhibitors. *Nature reviews. Drug discovery* **19**, (2020).

Chapter 2

PAK4 inhibition improves PD-1 blockade immunotherapy

ARTICLES
https://doi.org/10.1038/s43018-019-0003-0

nature cancer

Corrected: Publisher Correction

PAK4 inhibition improves PD-1 blockade immunotherapy

Gabriel Abril-Rodriguez[1,2], Davis Y. Torrejon[1], Wei Liu[3,4], Jesse M. Zaretsky[1], Theodore S. Nowicki[5], Jennifer Tsoi[1], Cristina Puig-Saus[1], Ignacio Baselga-Carretero[1], Egmidio Medina[1], Michael J. Quist[1], Alejandro J. Garcia[1], William Senapedis[6], Erkan Baloglu[6], Anusha Kalbasi[7,8,9], Gardenia Cheung-Lau[1], Beata Berent-Maoz[1], Begoña Comin-Anduix[8,9], Siwen Hu-Lieskovan[1,9], Cun-Yu Wang[3,4], Catherine S. Grasso[1,11] and Antoni Ribas[1,2,8,9,10,11]*

Lack of tumor infiltration by immune cells is the main mechanism of primary resistance to programmed cell death protein 1 (PD-1) blockade therapies for cancer. It has been postulated that cancer cell-intrinsic mechanisms may actively exclude T cells from tumors, suggesting that the finding of actionable molecules that could be inhibited to increase T cell infiltration may synergize with checkpoint inhibitor immunotherapy. Here, we show that p21-activated kinase 4 (PAK4) is enriched in non-responding tumor biopsies with low T cell and dendritic cell infiltration. In mouse models, genetic deletion of *PAK4* increased T cell infiltration and reversed resistance to PD-1 blockade in a CD8 T cell-dependent manner. Furthermore, combination of anti-PD-1 with the PAK4 inhibitor KPT-9274 improved anti-tumor response compared with anti-PD-1 alone. Therefore, high *PAK4* expression is correlated with low T cell and dendritic cell infiltration and a lack of response to PD-1 blockade, which could be reversed with PAK4 inhibition.

Immune checkpoint blockade therapies have significantly altered the current landscape of cancer treatment[1]. Programmed cell death protein 1 (PD-1) blockade induces major and durable anti-tumor response by releasing the PD-1/programmed death-ligand 1 checkpoint that blocks the effector functions of anti-tumor T cells[2]. However, this approach has limited activity in patients with cancers that lack pre-existing immune cell infiltration, which is the primary mechanism of resistance to PD-1 blockade therapy[3–6]. Exclusion of tumor infiltration by T cells could be mediated by several mechanisms that result in failure to attract or retain antigen-specific T cells in tumors, such as a lack of antigenic mutations, alterations in the antigen processing machinery, loss of human leukocyte antigen expression, and disruption of the interferon (IFN) signaling pathway that is needed to amplify the anti-tumor T cell response[7]. In addition, it has been proposed that cancer cell-intrinsic mechanisms such as oncogenic mitogen-activated protein kinase, phosphoinositide 3-kinase (PI3K) and WNT signaling pathways may actively exclude T cells from tumors[8–11]. In particular, it has been reported that alterations in the WNT/β-catenin signaling pathway are associated with impaired dendritic cell recruitment and immune cell exclusion in melanoma and other tumor types such as colorectal cancer[12–14]. These observations necessitate a clearer understanding of how WNT signaling causes immune evasion, as well as identification of actionable WNT-related targets that can be exploited to reverse T cell exclusion and overcome primary resistance to PD-1 blockade therapy.

To address this issue, we compared the transcriptional landscape of tumor biopsies from patients with advanced melanoma treated with anti-PD-1 immunotherapy. Here, we report on p21-activated kinase 4 (PAK4) as an actionable target that could be inhibited in combination with immune checkpoint blockade therapies to increase immune cell infiltration and overcome primary resistance to these therapies. PAK4 is a kinase known to be involved in tumorigenesis that directly binds and phosphorylates a specific site in β-catenin to activate WNT signaling[15–18]. Our work shows that: (1) *PAK4* expression is enriched in non-responding tumor biopsies with low immune cell infiltration; (2) genetic and pharmacologic PAK4 inhibition improve response to PD-1 blockade in vivo; and (3) this provides a novel therapeutic strategy that may improve the efficacy of immune checkpoint inhibitor therapies.

Results

Resistance to PD-1 blockade is associated with lack of immune cell infiltration. To identify drivers of resistance to immunotherapy, we generated transcriptome data from biopsies of 41 patients with advanced melanoma treated with PD-1-blocking antibody. We sequenced a total of 27 baseline and 33 on-treatment biopsies, including 14 non-responding and 13 responding samples (Fig. 1a and Supplementary Table 1). We removed two samples because *CD8A* gene expression did not agree with CD8 protein levels measured using immunohistochemistry (IHC) (Supplementary Fig. 1a–c), and four samples based on their outlier keratinocyte biomarker

[1]Department of Medicine, Division of Hematology and Oncology, University of California, Los Angeles, Los Angeles, CA, USA. [2]Department of Molecular and Medical Pharmacology, University of California, Los Angeles, Los Angeles, CA, USA. [3]Laboratory of Molecular Signaling, Division of Oral Biology and Medicine, School of Dentistry, University of California, Los Angeles, Los Angeles, CA, USA. [4]Department of Bioengineering, Henry Samueli School of Engineering and Applied Science, University of California, Los Angeles, Los Angeles, CA, USA. [5]Department of Pediatrics, Division of Pediatric Hematology and Oncology, University of California, Los Angeles, Los Angeles, USA. [6]Karyopharm Therapeutics, Newton, MA, USA. [7]Department of Radiation Oncology, University of California, Los Angeles, Los Angeles, CA, USA. [8]Department of Surgery, Division of Surgical Oncology, University of California, Los Angeles, Los Angeles, CA, USA. [9]Jonsson Comprehensive Cancer Center, Los Angeles, CA, USA. [10]Parker Institute for Cancer Immunotherapy, San Francisco, CA, USA. [11]These authors contributed equally: Catherine S. Grasso, Antoni Ribas. *e-mail: aribas@mednet.ucla.edu

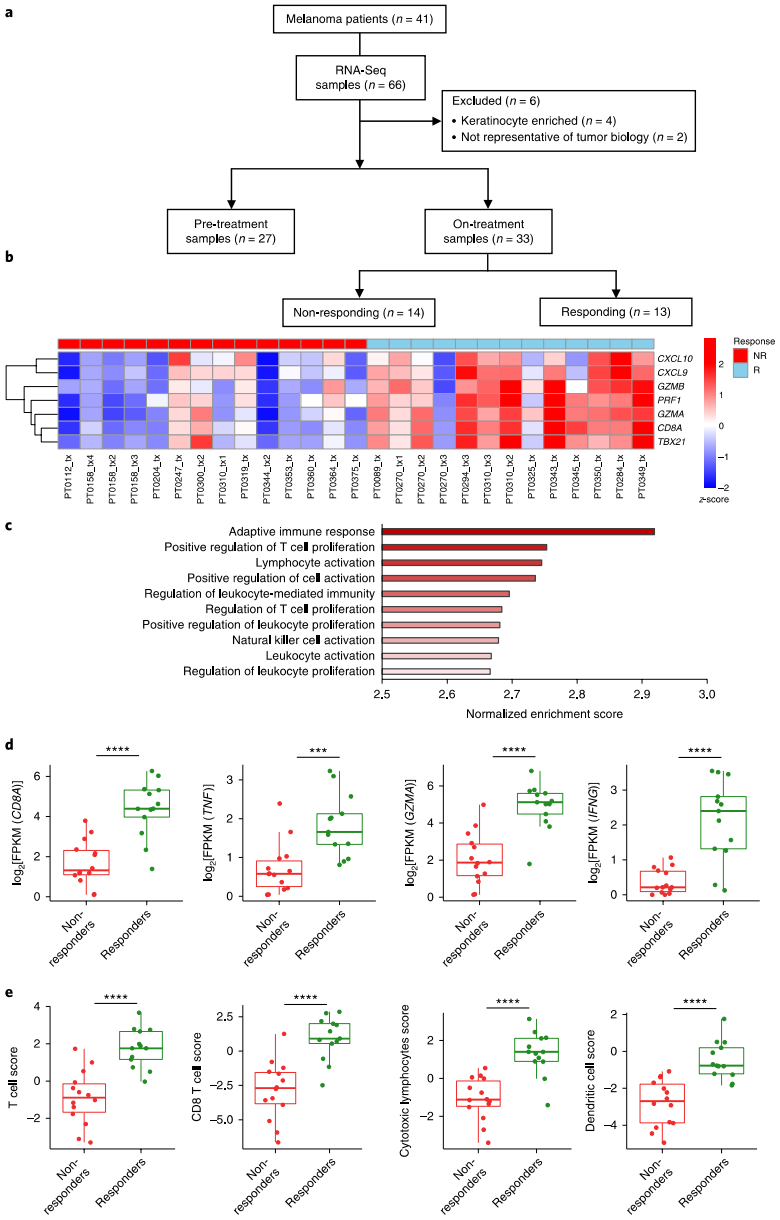

Fig. 1 | Responding biopsies present features of an adaptive immune response, while non-responding biopsies lack sufficient immune cell infiltration. **a**, Schematic of the analysis of tumor biopsies from patients with metastatic melanoma included in the RNA-Seq studies. **b**, Heatmap of a CD8 T cell effector signature for on-treatment biopsies (non-responding (NR; red; $n=14$) and responding (R; blue; $n=13$)). $P=1\times10^{-4}$. **c**, GSEA of on-treatment responding biopsies showing the top signatures for the Gene Ontology gene set. **d**, Differences in gene expression between non-responding ($n=14$) and responding biopsies ($n=13$) for *CD8A* ($P=1.45\times10^{-5}$), *TNF* ($P=6.04\times10^{-4}$), *GZMA* ($P=6.76\times10^{-6}$) and *IFNG* ($P=1.11\times10^{-4}$). **e**, Differences in immune population scores between non-responding and responding on-treatment biopsies ($n=13$), including T cell score ($P=1.21\times10^{-5}$), CD8 T cell score ($P=2.04\times10^{-5}$), cytotoxic lymphocytes score ($P=1.14\times10^{-5}$) and dendritic cell score ($P=1.90\times10^{-5}$). From top to bottom, box plots in **d** and **e** define the maximum, third quartile, median, first quartile and minimum values. *P* values were determined by two-sided Welch's *t*-test (***$P<0.001$; ****$P<0.0001$).

gene expression of *KRT15* and *KRT5*, which indicated that these biopsies mostly consisted of keratinocytes and did not have enough melanoma content[19] (Supplementary Fig. 1d,e). On-treatment biopsies taken from patients with a response to PD-1 blockade showed increased expression of a CD8 T cell effector signature including *CXCL9*, *CXCL10*, *GZMB*, *PRF1*, *GZMA*, *CD8A*, *TBX21*, *IFNG* and *TNF* (Fig. 1b; $P = 1 \times 10^{-4}$), consistent with previous data[2–5]. Paired *t*-tests with matched samples also confirmed that only biopsies from patients with a clinical response to PD-1 blockade exhibited significant increases in the expression of markers of immune response (Extended Data Fig. 1). We applied gene set enrichment analysis (GSEA) using the Gene Ontology gene sets to demonstrate that, unlike non-responding biopsies, the genes significantly increased in on-treatment responding biopsies were enriched in signatures associated with an adaptive immune response (Fig. 1c). We further identified immune genes that were upregulated in on-treatment responding biopsies relative to on-treatment non-responding biopsies. As expected, *CD8A*, *TNF*, *GZMA* and *IFNG*, among other immune genes, were expressed at higher levels in biopsies from patients who responded to PD-1 blockade therapy (Fig. 1d and Extended Data Fig. 1). To estimate the relative abundances and diversity of the different immune cells present in the tumor biopsies, we performed RNA sequencing (RNA-Seq)-based immune cell deconvolution using the microenvironment cell populations counter (MCP-counter)[20]. Responding biopsies were significantly infiltrated with T cells, CD8 T cells, myeloid dendritic cells and natural killer cells compared with non-responding tumor biopsies (Fig. 1e and Extended Data Fig. 1). Altogether, on-treatment biopsies from patients with a response to therapy present the characteristic features of an adaptive immune response, while on-treatment biopsies from patients without a response mostly lack T cell infiltration.

***PAK4* expression is enriched in poorly infiltrated tumor samples and constitutes a potential target to improve PD-1 blockade immunotherapies.** Because immune cell exclusion was a common factor among non-responding biopsies, we sought to determine tumor-intrinsic drivers of T cell exclusion by comparing immune-infiltrated tumor biopsies with immune-excluded ones. Differential gene expression analysis revealed that only 18 overlapping genes were enriched in biopsies with both a low dendritic cell score and a low T cell score ($\log_2$[fold change] > 1 and false discovery rate $< 5 \times 10^{-5}$; Supplementary Table 2c). Among these genes, we were interested in studying an actionable gene whose function could be blocked by a drug. *PAK4* stood out among the list of 18 genes as its expression was consistently higher in tumor biopsies with low infiltration with dendritic cells (adjusted *P* value (q) < 0.0001) and T cells ($q < 0.0001$) (Fig. 2a,c and Supplementary Table 2a), as well as in tumor biopsies with low expression of *CD8A*, *TNF* and *IFNG* (Fig. 2c and Supplementary Table 2b). The correlation with low intratumoral T cell and dendritic cell infiltration was validated in a published cohort of 99 biopsies analyzed by RNA-Seq[5] (Fig. 2b). Furthermore, tumors with high expression of *PAK4* were enriched and positively correlated with a signature of immune cell exclusion reported by Jerby-Arnon et al.[6], based on analysis of 33 melanoma biopsies using single-cell RNA-Seq (Extended Data Fig. 2a,b). PAK4 is a serine/threonine kinase that functions downstream of the small GTPases CDC42 and RAC, and plays an important role in several signaling pathways involved in tumorigenesis, including a known function of phosphorylating β-catenin, and shuttling with it into the nucleus to activate the WNT/β-catenin pathway[15–18,21]. This function of PAK4 seemed relevant based on previous work by Spranger et al.[11] showing that tumor-intrinsic β-catenin signaling can impair T cell infiltration in melanoma.

PAK4 negatively correlated with immune markers of an active CD8 T cell response, including *CD8A*, *TNF*, *GZMA* and *PRF1*, as well as with transcriptome signatures of different immune cell populations, such as T cells, CD8 T cells, cytotoxic T cells and dendritic cells, in both our cohort and the Riaz et al.[5] validation cohort (Fig. 2d and Extended Data Fig. 2c). To determine whether *PAK4* was expressed by melanoma cancer cells, we performed IHC on on-treatment tumor biopsies. Indeed, PAK4 co-localized with the melanoma marker S100 (Fig. 2e and Extended Data Fig. 2d). In addition, IHC analysis validated the inverse correlation between PAK4 and CD8 T cell infiltration observed by RNA-Seq (Fig. 2e). Overall, our data suggest that tumor-intrinsic PAK4 expression is associated with a lack of immune cell infiltration, and constitutes a potential target to overcome PD-1 blockade resistance.

***PAK4* expression correlates with WNT/β-catenin pathway activation in melanoma tumor biopsies and regulates its activation in vitro.** Given the evidence relating WNT signaling, immune infiltration and a lack of response to checkpoint blockade immunotherapies in melanoma and other solid tumors, and consistent with the known relationship between PAK4 and WNT signaling[15–18,21], we further investigated the role of PAK4 in the β-catenin pathway using clinical tumor samples. Tumor biopsies with high *PAK4* expression had increased levels of *MYC* and *CTNNB1* compared with tumor biopsies with low *PAK4* expression (Fig. 3a). Tumors with high expression of *PAK4* were also enriched for and positively correlated with a previously reported WNT signature that includes *APC*, *MYC*, *CTNNB1*, *DKK2* and *VEGFA*[12] (Fig. 3b). Furthermore, IHC analysis of the on-treatment tumor biopsies also showed that β-catenin co-localized with PAK4 (Fig. 3c). Of note, the PAK4 overlap with β-catenin was higher in the two tumor biopsies with low T cell infiltration, suggesting that there may be a dual requirement of β-catenin and PAK4 to induce a T cell-excluded phenotype (Extended Data Fig. 2e).

To directly investigate the impact of *PAK4* deletion on WNT signaling, we first generated PAK4 knockout (KO) sublines of the murine melanoma B16 using CRISPR–Cas9 (three sublines: B16 KO 6.2, B16 KO 8.1 and B16 KO 8.2; Extended Data Fig. 3a–d). To quantify WNT signaling activation, B16 PAK4 KO cells were

Fig. 2 | *PAK4* expression is enriched in non-infiltrated tumor biopsies and negatively correlates with immune markers in melanoma. a,**b**, Volcano plots derived from differential gene expression analysis between the upper and lower quartiles of the dendritic cell score, using both pre- and on-treatment samples. *PAK4* expression was enriched in the samples with low dendritic cell scores in our UCLA cohort (**a**; $n = 30$ biopsies; $q = 1.19 \times 10^{-5}$), as well as in the Riaz et al.[5] validation cohort (**b**; $n = 50$ biopsies; $q = 1.59 \times 10^{-11}$). **c**, *PAK4* expression was also enriched in samples with low T cell infiltration ($q = 2.74 \times 10^{-7}$), and low expression of *CD8A* ($q = 9.08 \times 10^{-9}$), *TNF* ($q = 6.67 \times 10^{-12}$) and *IFNG* ($q = 1.9 \times 10^{-6}$) ($n = 15$ biopsies per group for each comparison). In **a**–**c**, *P* values were calculated using the negative binomial generalized linear model fitting and Wald significance test, while q values were obtained by applying the Benjamini–Hochberg method. **d**, *PAK4* expression negatively correlates with $\log_2$[FPKM] expression of the known immune markers *CD8A* ($r = -0.54$; $P = 7.95 \times 10^{-6}$), *TNF* ($r = -0.69$; $P = 1.12 \times 10^{-9}$), *GZMA* ($r = -0.59$; $P = 7.95 \times 10^{-7}$) and *PRF1* ($r = -0.41$; $P = 6.20 \times 10^{-4}$), as well as the different immune populations assessed using MCP-counter: T cells ($r = -0.62$; $P = 1.04 \times 10^{-7}$), CD8 T cells ($r = -0.55$; $P = 5.25 \times 10^{-6}$), cytotoxic lymphocytes ($r = -0.46$; $P = 1.90 \times 10^{-4}$) and dendritic cells ($r = -0.49$; $P = 6.60 \times 10^{-5}$) ($n = 60$ biopsies for all correlations). Correlations were calculated applying Pearson's correlation coefficient test. **e**, Images from biopsies of two representative patients of non-responding/low T cell infiltration (top) and responding/high T cell infiltration (bottom). Slides were stained with S100, PAK4 and CD8. The results showed co-localization of PAK4 and S100, and validation of the exclusivity between PAK4 and CD8 expression. Scale bars: 100 μm.

transfected with the Topflash luciferase reporter, which is under the control of consensus T cell factor-binding sites[22,23]. Whereas Wnt-3a exposure induced the Topflash luciferase activity in B16 wild-type (WT) CRISPR control cells, the induction of Topflash luciferase activity by Wnt-3a was reduced in B16 PAK4 KO cells (Fig. 3d and Extended Data Fig. 4a). Rescuing WT *PAK4* expression

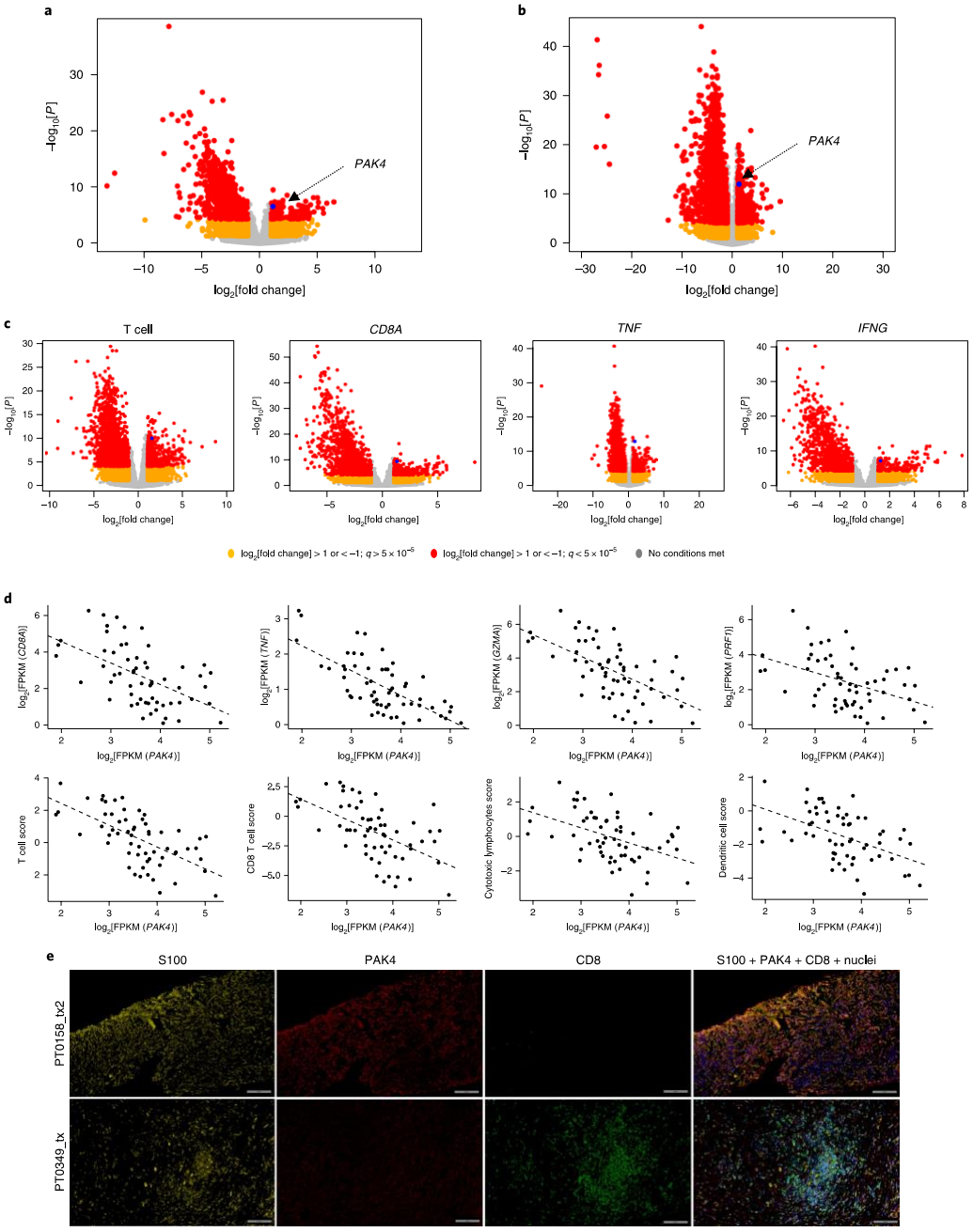

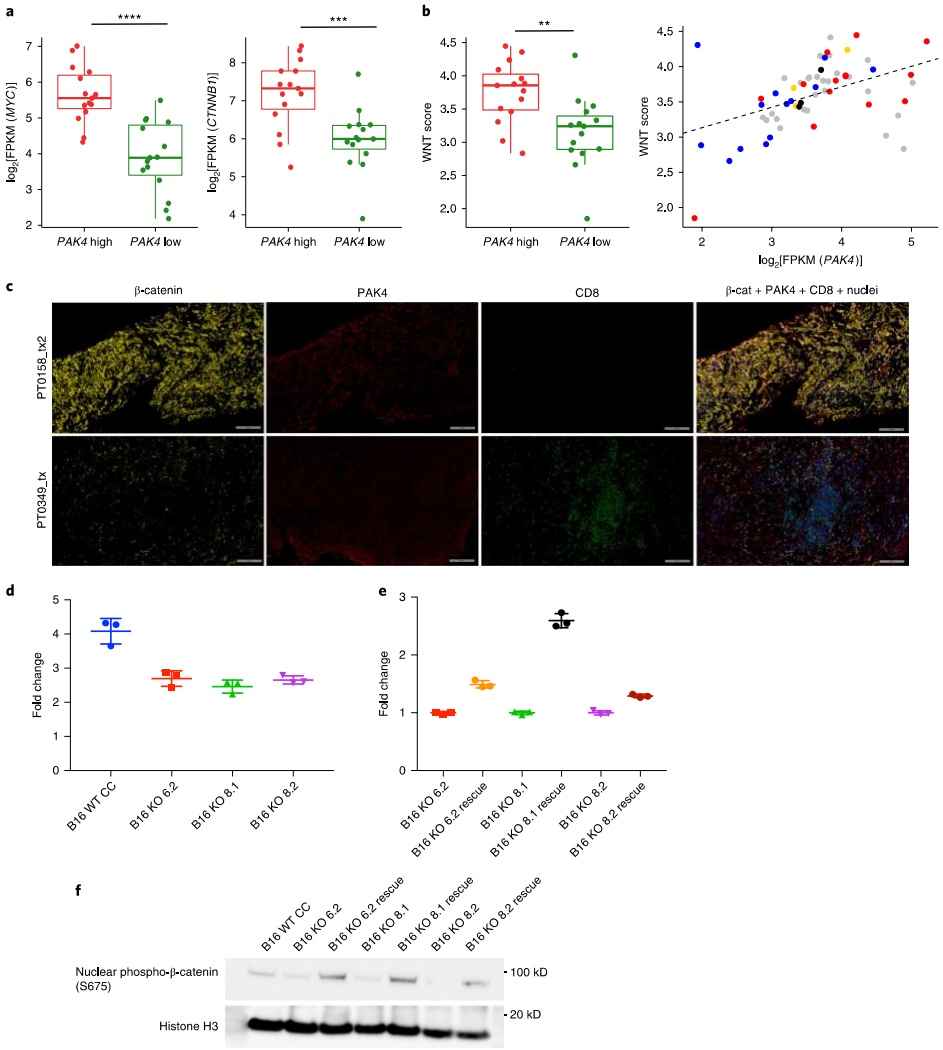

Fig. 3 | *PAK4* expression correlates with WNT genes in tumor biopsies and regulates WNT signaling activation in vitro. a, Comparison of *MYC* ($P = 1.32 \times 10^{-5}$) and β-catenin (*CTNNB1*; $P = 7.00 \times 10^{-4}$) $\log_2$[FPKM] expression values between tumor biopsies within the upper ($n = 15$) and lower ($n = 15$) quartile of *PAK4* expression using the UCLA cohort. **b**, Left: comparison of WNT scores ($P = 3 \times 10^{-3}$) between tumor biopsies within the upper ($n = 15$) and lower ($n = 15$) quartile of *PAK4* expression. Right: correlation ($n = 60$; $r = 0.45$; $P = 2.96 \times 10^{-4}$) between WNT scores and $\log_2$[FPKM] *PAK4* expression values (blue: responders; red: non-responders; yellow: stable disease; gray: pre-treatment). The WNT score was obtained based on the geometric mean of the following WNT-related genes: *APC*, *MYC*, *CTNNB1*, *DKK2* and *VEGFA*. In **a** and **b**, *P* values were determined by two-sided Welch's *t*-test (**a** and **b** (left)) and Pearson's correlation coefficient (**b** (right)) (**$P < 0.01$; ***$P < 0.001$; ****$P < 0.0001$). From top to bottom, box plots show the maximum, third quartile, median, first quartile and minimum values. **c**, Images from biopsies of two representative patients of non-responding/low T cell infiltration (top) and responding/high T cell infiltration (bottom). Slides were stained with β-catenin, PAK4 and CD8. Scale bars: 100 µm. **d**,**e**, Topflash WNT activity assays indicating that B16 PAK4 KO cells failed to upregulate WNT signaling as high as PAK4 CRISPR control WT cells (**d**; $P = 0.0054$ for B16 WT CRISPR control (CC) versus B16 KO 6.2; $P = 0.0026$ for B16 WT CC versus B16 KO 8.1; $P = 0.0033$ for B16 WT CC versus B16 KO 8.2), while rescuing PAK4 expression increased basal WNT activity (**e**; $P = 0.0002$ for B16 KO 6.2 versus B16 KO 6.2 rescue; $P < 0.0001$ for B16 KO 8.1 versus B16 KO 8.1 rescue; $P = 0.0004$ for B16 KO 8.2 versus B16 KO 8.2 rescue) ($n = 3$ technical replicates per group). The results are representative of three independent experiments. In **d** and **e**, data represent means ± s.e.m. and the results were compared by two-tailed unpaired *t*-test. **f**, Immunoblot for β-catenin S675 phosphorylation. Phosphorylation levels were decreased in B16 PAK4 KO cells compared with PAK4 WT cells and restored in PAK4 rescue cell lines. The results are representative of three independent experiments. Source data are available for **d**–**f**.

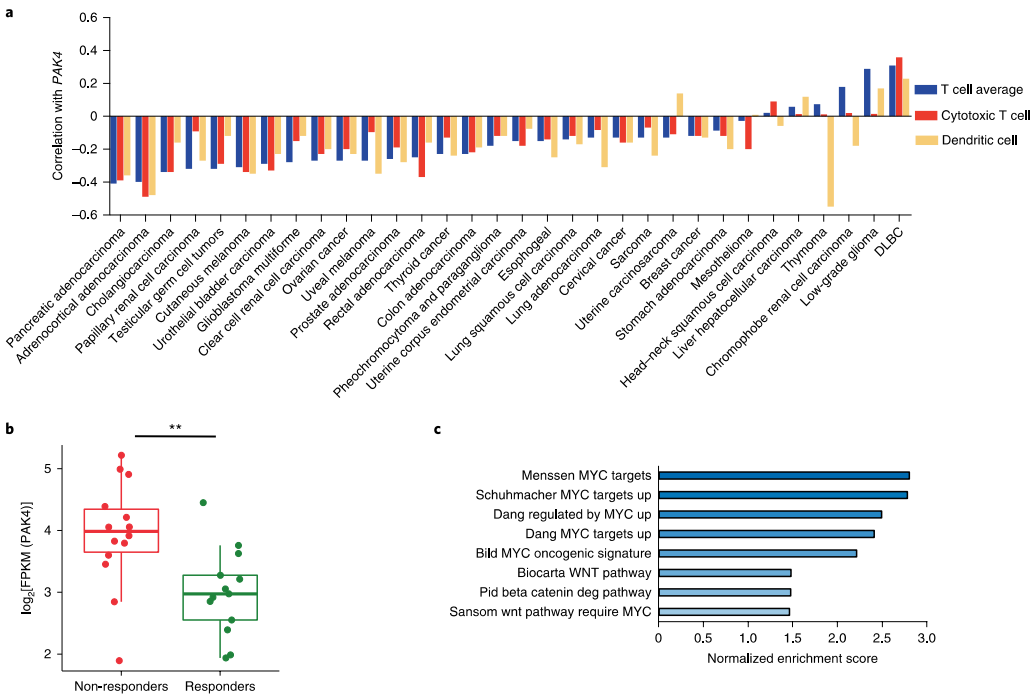

Fig. 4 | *PAK4* expression is enriched in non-responding tumor biopsies and negatively correlates with immune markers in multiple tumor types. **a**, Pan-cancer analysis using TCGA transcriptome data shows the negative correlation between *PAK4* expression and T cell (blue), cytotoxic T cell (red) and dendritic cell scores (yellow) across 32 tumor types (the sample size for each cancer type and the associated *P* value for each correlation can be found in Supplementary Table 3). Correlations were evaluated using Spearman's correlation coefficient. DLBC, diffuse large B-cell lymphoma. **b**,**c**, On-treatment non-responding biopsies ($n=14$) have higher levels of $\log_2$[FPKM] *PAK4* expression compared with responding biopsies (**b**; $n=13$; $P=4.72\times10^{-3}$), and are enriched in gene signatures related to known oncogenic signatures involved in immune cell exclusion, as observed by GSEA using Gene Ontology gene sets as targets (**c**). From top to bottom, box plots in **b** show the maximum, third quartile, median, first quartile and minimum values, and the *P* value was determined by two-sided Welch's *t*-test (**$P<0.01$).

in B16 PAK4 KO cells increased baseline WNT activity (Fig. 3e and Extended Data Fig. 3e), although *PAK4* deletion did not affect WNT activity at steady state (Extended Data Fig. 4b). In addition, *PAK4* deletion decreased nuclear β-catenin phosphorylation at serine 675 (S675), which was restored in *PAK4* rescue cell lines (Fig. 3f). Of note, neither *PAK4* deletion nor overexpression affected the levels of β-catenin nuclear protein (Extended Data Fig. 4c). Moreover, PAK4 inhibition with the dual PAK4 and nicotinamide phosphoribosyltransferase (NAMPT) inhibitor KPT-9274 (refs. [24–27]) recapitulated the results observed with the B16 PAK4 KO clones as it diminished nuclear S675 β-catenin phosphorylation and decreased sensitivity to Wnt-3a, while it did not affect WNT activity at steady state, nor nuclear β-catenin protein levels (Extended Data Fig. 5a–c). Furthermore, B16 PAK4 KO cell lines decreased tyrosinase expression (Extended Data Fig. 5d) and lost their pigmentation when cultured over time (Extended Data Fig. 5e)—a phenotype that is consistent with the suggested role of PAK4 in melanogenesis and the β-catenin/MITF (microphthalmia-associated transcription factor) pathway[17]. Taken together, our results validate the association between *PAK4* expression and WNT/β-catenin pathway activation, and provide evidence that genetic deletion and pharmacological inhibition of PAK4 impair Wnt/β-catenin pathway signaling in vitro.

***PAK4* negatively correlates with immune cell infiltration across human cancers.** We then investigated whether the association between *PAK4* expression and the lack of T cell infiltration in melanoma tumor biopsies could be expanded to other tumor types. To do so, we analyzed transcriptome data from 32 different cancer types in The Cancer Genome Atlas (TCGA), and calculated the correlation between *PAK4* expression and T cell, cytotoxic T cell and dendritic cell scores generated using MCP-counter[20] in all of the samples for each cancer type. In addition to cutaneous melanoma, we observed a negative correlation with T cell infiltration in the majority of cancer types (18 out of 32), including cancers that are notoriously resistant to anti-PD-1 therapy, such as prostate cancer, adrenocortical carcinoma, germ cell cancers and glioblastoma multiforme (Fig. 4a and Supplementary Table 3). In line with published data, one of the strongest negative correlations was in pancreatic cancer, where a pan-PAK inhibitor had previously been shown to enhance anti-tumor immune response in a preclinical model[28].

Lack of response to PD-1 blockade is associated with increased *PAK4* expression and is enriched in oncogenic pathways involved in immune cell exclusion. As *PAK4* showed a strong inverse correlation with both dendritic cells and T cells in melanoma, we reasoned

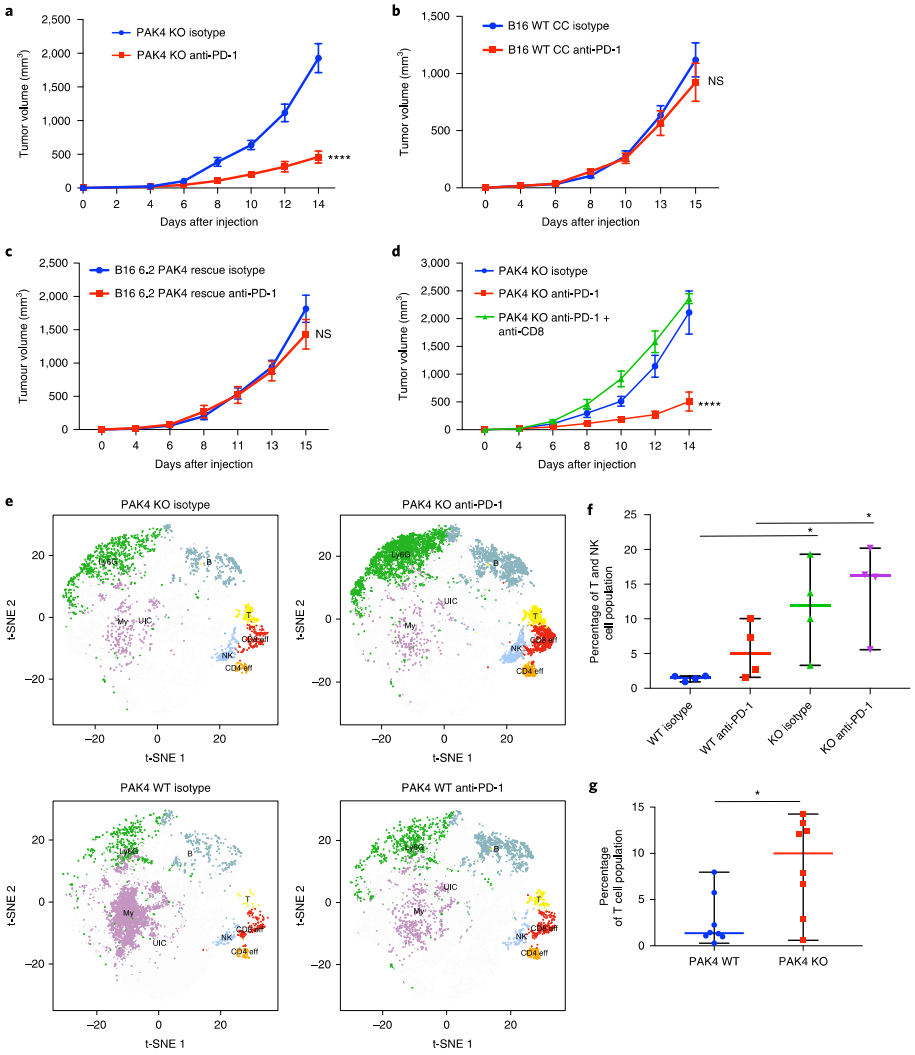

Fig. 5 | Inhibition of PAK4 reverses tumor-specific T cell exclusion and sensitizes tumors to PD-1 blockade. a, Tumor growth curves for B16 PAK4 KO 6.2 tumors ($n=16$ per group) treated with isotype (blue) or anti-PD-1 (red). Anti-PD-1-treated B16 PAK4 KO tumors showed decreased tumor growth compared with untreated B16 PAK4 KO tumors ($P=3.65\times10^{-6}$ at day 14). **b**, Tumor growth curves for B16 WT CC tumors treated with isotype (blue; $n=14$) or anti-PD-1 (red; $n=13$). No significant differences were observed in tumor growth ($P=0.91$ at day 14). **c**, Tumor growth curves for B16 6.2 PAK4 rescue tumors treated with isotype (blue; $n=5$) or anti-PD-1 (red; $n=5$). Anti-PD-1 treatment did not have significant anti-tumor efficacy when restoring PAK4 expression ($P=0.74$ at day 14). **d**, Tumor growth for B16 PAK4 KO 6.2 tumors with CD8 depletion ($n=5$) ($P=4.31\times10^{-5}$ at day 14 for B16 PAK4 KO anti-PD-1 versus B16 PAK4 KO anti-PD-1 + anti-CD8). **e**, T-distributed stochastic neighbor embedding plots for each of the following four groups: B16 PAK4 KO isotype; B16 PAK4 KO anti-PD-1; B16 WT isotype; and B16 WT anti-PD-1. The different immune populations were: myeloid cell (My); B cells (B); CD8 T cells (CD8 eff); CD4 T cells (CD4 eff); T cells (T); natural killer cells (NK); Ly6G$^+$ cluster (Ly6G) and unidentified cluster (UIC). **f**, Percentage of T cell and natural killer cell (NK cell) population from CD45$^+$ cells. PAK4 KO treated tumors had increased T and NK cell infiltration relative to WT treated tumors (median percentage: 16.18% for KO anti-PD-1; 4.99% for WT anti-PD-1; $P<0.05$). PAK4 KO untreated tumors also showed increased T and NK cell infiltration relative to WT untreated tumors (median percentage: 11.89% for KO anti-PD-1; 1.57% for WT anti-PD-1; $P=0.02$) ($n=4$ mice per group). **g**, Percentage of T cell population from CD45$^+$ cells. B16 PAK4 KO tumors presented increased T cell infiltration compared with B16 WT tumors (median percentage: 10% for KO; 1.37% for WT; $P=0.009$) ($n=8$ mice per group). In **a**–**d**, **f** and **g**, means ± s.e.m are shown. Statistical significance and corrections for multiple comparisons were determined using the Holm–Šidak method (**a**–**d**) or two-tailed unpaired *t*-test (**f** and **g**) (*$P<0.05$; ****$P<0.0001$). NS, not significant. Source data are available for **a**–**d**, **f** and **g**.

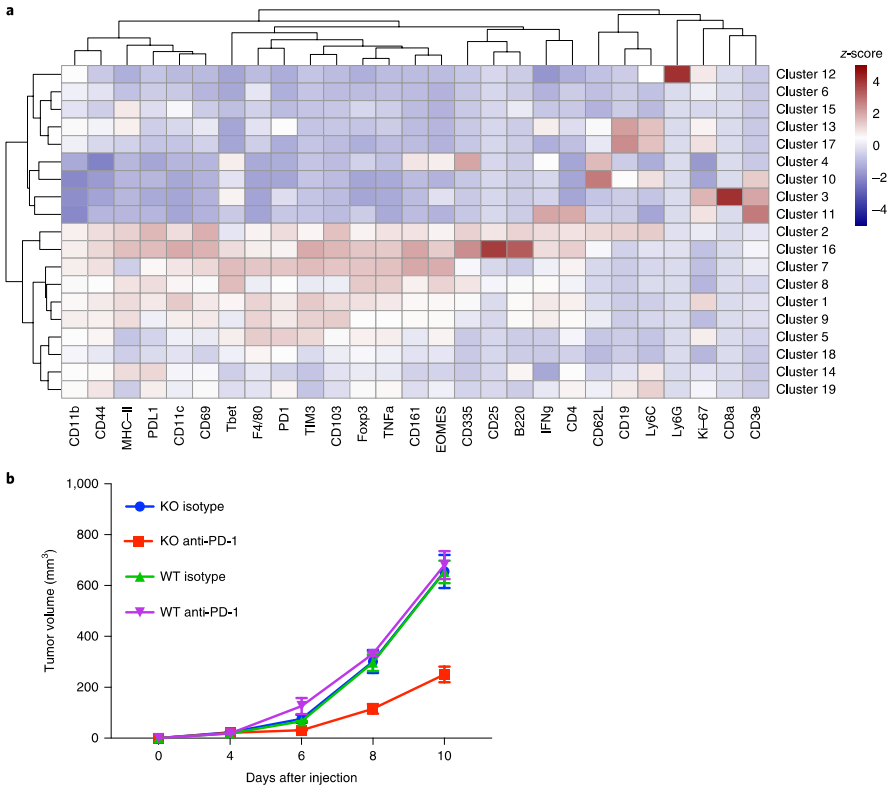

Fig. 6 | Analysis of tumor-infiltrating immune cells by CyTOF. a, Heatmap with the normalized median percentage for each of the immune markers in the different clusters obtained. Only clusters with a >0.5% frequency were analyzed. **b**, Tumor growth curves for the 16 samples ($n=4$ per group) used for the CyTOF analysis. Data represent means ± s.e.m.

that tumor biopsies from patients without a response to anti-PD-1 may have enriched *PAK4* expression. Indeed, non-responding biopsies had higher levels of *PAK4* transcripts ($P=0.004$; Fig. 4b). We also investigated whether our cohort of tumor biopsies non-responding to PD-1 blockade therapy recapitulated known oncogenic mechanisms of T cell exclusion[10]. To test this hypothesis, we compared on-treatment non-responding biopsies with responding biopsies, and applied GSEA using the curated gene sets. Signatures enriched in non-responding biopsies included gene sets related to WNT/β-catenin signaling and the WNT target gene *MYC* (Fig. 4c and Supplementary Table 4). Overall, biopsies from patients without a response to PD-1 blockade were enriched for *PAK4* expression and gene signatures related to known oncogenic pathways involved in T cell exclusion[10].

Genetic KO of *PAK4* sensitizes tumors to PD-1 blockade and increases immune cell infiltration. If PAK4 plays an active role in excluding tumor-specific T cells from the tumor microenvironment of melanoma biopsies, PAK4 inhibition would increase tumor-specific T cell infiltration and hence sensitize tumors to PD-1 blockade therapy. To test this hypothesis, we used the murine melanoma model B16, which exhibits primary resistance to PD-1 blockade[29], lacks previous infiltration by tumor-specific lymphocytes[30], and intrinsically expresses the immune resistance program defined by Jerby-Arnon[6]. To assess the anti-tumor efficacy of PD-1 blockade in the context of *PAK4* deletion, we treated syngeneic C57BL/6 mice bearing B16 PAK4 KO or B16 WT tumors with a murine anti-PD-1 antibody. We observed the anti-tumor activity of PD-1 blockade only in melanoma tumors lacking *PAK4* expression (Fig. 5a,b and Extended Data Fig. 6a,b). Of note, untreated B16 PAK4 KO tumors grew progressively, suggesting that although *PAK4* deletion provides sensitization to PD-1 blockade therapy, it is not sufficient by itself in the B16 model to trigger an anti-tumor immune response. In addition, restoring PAK4 protein levels in B16 PAK4 KO tumors resulted in the loss of PD-1 blockade anti-tumor efficacy (Fig. 5c and Extended Data Fig. 6c). To elucidate whether the observed response to anti-PD-1 was CD8 dependent, we depleted CD8 T cells in syngeneic C57BL/6 mice bearing B16 PAK4 KO tumors. CD8 depletion completely abrogated the anti-tumor activity of mouse anti-PD-1, showing that *PAK4* deletion sensitized melanoma B16 tumors to PD-1 blockade in a CD8 T cell-dependent manner (Fig. 5d and Extended Data Fig. 6d). These results suggest that genetic *PAK4* deletion allows the infiltration of tumor-specific T cells that confer anti-tumor efficacy on PD-1 blockade.

To validate whether *PAK4* deletion facilitates immune cell infiltration, we performed immune profiling of tumor-infiltrating

immune cells using cytometry by time of flight (CyTOF), and identified a total of 16 independent cell clusters (Fig. 6a). The T cell population was defined by three clusters, including a non-T regulatory CD4 T cell cluster positive for CD3e, CD4, IFN-γ and Ki-67, a CD8 T cell cluster positive for CD3e, CD8a, Tbet and Ki-67, and a general T cell cluster positive for CD3e. A natural killer cluster positive for CD335 and CD161 was also identified. B16 PAK4 KO anti-PD-1-treated tumors presented increased infiltration of T and natural killer cells compared with B16 WT anti-PD-1-treated tumors ($P=0.049$; Fig. 5e,f). Interestingly, untreated B16 PAK4 KO tumors already presented increased T and natural killer cell infiltration compared with B16 WT untreated tumors ($P=0.02$; Fig. 5e,f), although we did not observe anti-tumor efficacy in the B16 PAK4 KO group (Fig. 6b). Consistently, B16 PAK4 KO tumors had increased levels of T cells regardless of treatment with murine anti-PD-1 ($P=0.009$; Fig. 5g). Therefore, these data support the hypothesis that *PAK4* depletion increases tumor-specific T cell infiltration, which sensitizes tumors to PD-1 blockade.

Pharmacological inhibition of PAK4 synergizes with PD-1 blockade immunotherapy. KPT-9274 is a dual PAK4 and NAMPT inhibitor[24–27] currently in clinical trials. We tested whether treatment with KPT-9274 recapitulates the anti-tumor effects of genetic *PAK4* deletion to sensitize B16 melanoma to murine anti-PD-1 therapy. Indeed, B16 murine melanoma tumors treated with anti-PD-1 in combination with KPT-9274 showed a stronger anti-tumor effect compared with anti-PD-1 ($P=0.01$; Fig. 7a) and KPT-9274 monotherapy ($P=0.0007$; Fig. 7a). To expand the testing to other settings of partial anti-PD-1 therapy resistance, we used the MC38 mouse colon adenocarcinoma model, which is a model of a cancer with high tumor mutation burden and is partially sensitive to PD-1 blockade, but with ample margin for improvement as tumors grow progressively after a period of transient response[31,32]. Consistent with being an immunogenic tumor model, and with *PAK4* deletion per se facilitating T cell infiltration (Fig. 5f,g), both MC38 WT tumors, treated with either a combination of KPT-9274 and anti-PD-1 or KPT-9274 alone, showed decreased tumor growth compared with the anti-PD-1 monotherapy group (Fig. 7b). We generated a PAK4 KO subline of MC38 through CRISPR–Cas9 gene editing (Extended Data Fig. 7a,b), and consistent with the results with KPT-9274, MC38 PAK4 KO tumors achieved tumor regression even in the absence of anti-PD-1 therapy (Fig. 7c). Of note, MC38 PAK4 KO tumors only reached complete regression ($n=3$) when treated with anti-PD-1, suggesting that PD-1 blockade also improves anti-tumor T cell response in the setting of partial response to anti-PD-1 therapy. In addition, we found that MC38 PAK4 KO clones were more sensitive to the anti-proliferative effects of tumor necrosis factor (TNF), which is consistent with the current literature[33,34], and could contribute to the phenotype observed in this model (Extended Data Fig. 7c). Altogether, these data suggest that PAK4 inhibition synergizes with anti-PD-1 treatment.

Discussion

By studying the transcriptional landscape of biopsies of patients with melanoma treated with PD-1 blockade immunotherapy, we found that the expression of *PAK4* is associated with immune exclusion and lack of clinical response. Genetic and pharmacological PAK4 inhibition altered WNT/β-catenin signaling, increased intratumoral T cell infiltration and improved the response to checkpoint blockade therapy in two mouse models. The negative correlation between *PAK4* expression and T cell infiltration held true across several human cancers, including cancers notoriously resistant to PD-1 blockade, and hence expands the potential clinical applicability of the combined inhibition of PAK4 and PD-1.

Finding novel molecular targets that could improve and overcome resistance to PD-1 blockade therapy remains one of the main challenges that needs to be tackled to increase the efficacy rate of cancer immunotherapies[10]. Our current work validates and builds on the fundamental knowledge that PD-1 blockade works by unleashing the immune breaks of a pre-existent tumor-specific T cell population[2]. The transcriptional characterization of melanoma tumor samples highlighted the common denominator among biopsies of non-responding patients—the lack of a proper immune T cell infiltration of the tumor microenvironment. Therefore, interventions that increase the immunogenicity and the immune infiltration within the tumor microenvironment remain a top therapeutic priority[7].

The immune system exercises a selective pressure that shapes cancer evolution and results in the selection of malignant cells able to escape an immune cell attack. This has been termed cancer immunoediting[35]. Cancer cells can exploit and rewire oncogenic signaling pathways that alter the immunogenicity of the tumor and confer an advantage against the immune system[10]. Among the different oncogenic signaling pathways, there is compelling evidence from several studies that associate an active WNT/β-catenin signaling pathway with immune exclusion and resistance to immune checkpoint blockade therapy[11–13]. In this context, among the list of differentially expressed genes in non-immune-infiltrated biopsies, the appeal of focusing our studies on PAK4 became more relevant given its previously reported involvement in the WNT/β-catenin pathway[15,18]. PAK4 deletion disrupted WNT signaling activity without altering β-catenin protein levels, which suggests that PAK4 may be regulating WNT activity by means other than the number of molecules that translocate into the nucleus, such as alteration of the interaction of β-catenin with other proteins that are important in regulating β-catenin transcriptional activity. Overall, our findings provide novel insights into the mechanism by which PAK4 impacts WNT signaling activity. However, it still remains necessary to fully elucidate how PAK4-induced WNT inhibition contributes to overcoming PD-1 blockade resistance.

PAK4 overexpression or increased activity is associated with the development and progression of several tumor malignancies, including melanoma[36], pancreatic cancer[37] and prostate cancer[38]. In breast cancer, *PAK4* messenger RNA levels are also often overexpressed[39],

Fig. 7 | Pharmacological inhibition of PAK4 improves anti-PD-1 anti-tumor response. a, Tumor growth curves for B16 WT melanoma tumors treated with KPT-9274 in combination with anti-PD-1 ($n=6$; purple), KPT-9274 ($n=6$; green) or anti-PD-1 ($n=6$; red) versus controls ($n=6$; blue). The combination of KPT-9274 and anti-PD-1 showed decreased tumor growth compared with both anti-PD-1 monotherapy ($P=0.01$ at day 12) and KPT-9274 monotherapy ($P=0.0007$ at day 12). Data represent means ± s.e.m. **b**, Tumor growth curves for MC38 WT tumors treated with KPT-9274 and anti-PD-1 ($n=7$; purple), KPT-9274 ($n=5$; green), anti-PD-1 ($n=5$; red) and isotype ($n=3$; blue). The combination of KPT-9274 and anti-PD-1 or KPT-9274 monotherapy resulted in significantly decreased tumor growth compared with anti-PD-1 alone ($P=0.01$ for the combination group; $P=0.02$ for KPT-9274 monotherapy; both at day 10). KPT-9274 was given twice daily from days 4–7 and then discontinued due to KPT-9274-associated toxicity. **c**, Tumor growth curves for MC38 WT and MC38 PAK4 KO tumors treated with PD-1 blockade ($n=7$ for the MC38 PAK4 KO anti-PD-1 and MC38 PAK4 KO isotype groups; $n=4$ for the MC38 WT isotype and MC38 WT anti-PD-1 groups). Treated tumors received four doses of anti-PD-1 in total. Both MC38 PAK4 KO untreated and anti-PD-1-treated tumors showed decreased tumor growth compared with the MC38 WT anti-PD-1-treated group ($P=0.001$ for the WT isotype versus the KO isotype; $P=0.004$ for WT anti-PD-1 versus KO anti-PD-1; both at day 21). Statistical significance and correction for multiple comparisons were calculated using the Holm–Šidak method (*$P<0.05$; **$P<0.01$). Source data are available for **a**–**c**.

and its protein activity is required for oncogenic transformation[40,41]. In addition to regulating WNT/β-catenin signaling[15,18], PAK4 can promote tumorigenesis by altering different oncogenic pathways, including those that have been previously involved in immune cell exclusion[16]. For instance, PAK4 can increase PI3K/AKT signaling in different cancer malignancies by directly binding to PI3K

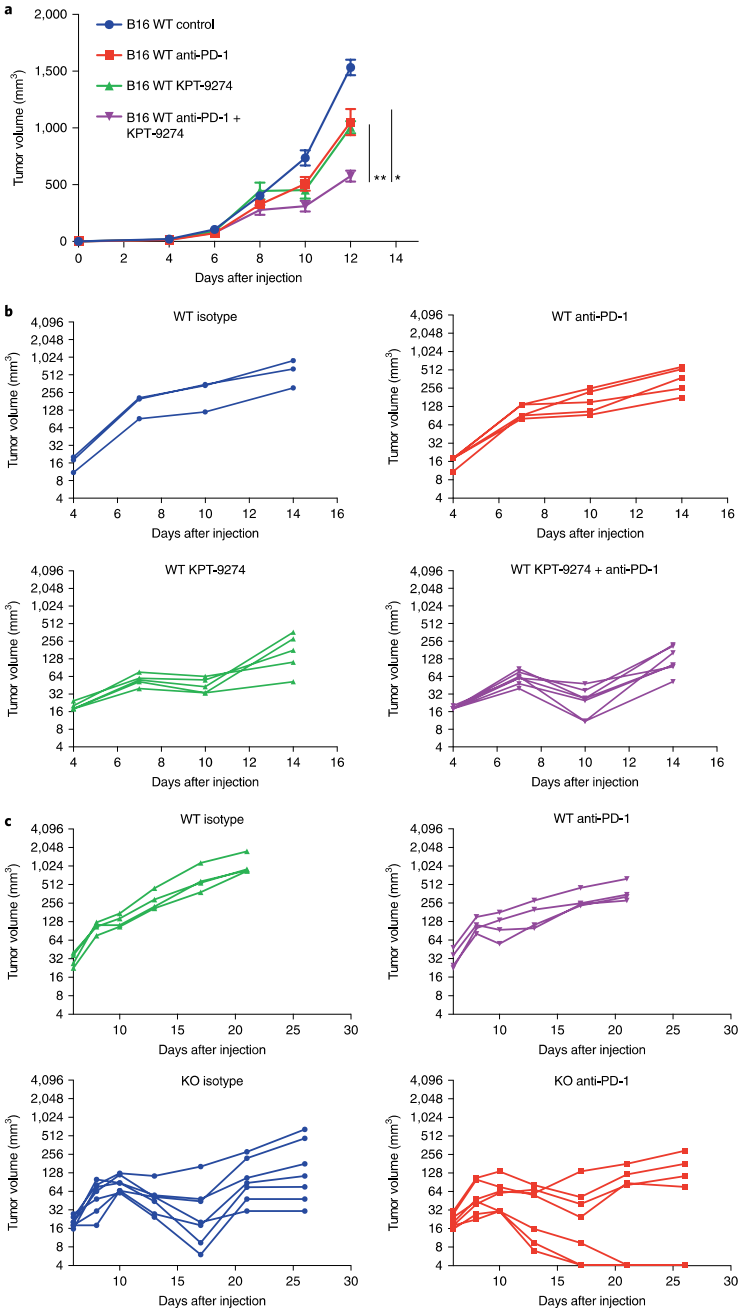

and increasing AKT phosphorylation[42–45]. Interestingly, PAK4 also presents kinase-independent functions. It has been reported that PAK4 acts as a scaffold to facilitate TNF receptor type 1-associated death domain (TRADD) protein binding to the TNF receptor to promote TNF survival activity[33]. Therefore, PAK4 protein inhibition increases TNF-induced apoptosis—an observation that is in line with our results seen in the MC38 model[34]. The role of PAK4 and TNF signaling in PD-1 blockade sensitivity necessitates a better understanding and will need to be explored further in the future.

In these studies, we primarily used the B16 murine melanoma model as it has previously been reported that it is poorly inflamed and resistant to checkpoint blockade[29]. Of note, we acknowledge that there may be additional mouse models that have not been used in this study and that could help expand our understanding of the role of PAK4 in immune cell exclusion, such as the *Braf*^{V600E}/*Pten*$^{-/-}$/*CAT-STA* mice used in the Spranger et. al. study[11]. This particular mouse model has been used to study WNT-induced T cell exclusion in melanoma, and has provided evidence that the oncogenic WNT/β-catenin pathway mediates dendritic cell exclusion, resulting in immune evasion. However, it is a model that relies on the in situ generation of multiple oncogene-driven primary skin cancers on induction of the driver oncogenes. This does not allow the genetic testing of *PAK4* inhibition, unless a new transgenic mouse with an inducible *PAK4* inhibition is created and cross-bred with the already *Braf*^{V600E}/*Pten*$^{-/-}$/*CAT-STA* triple genetically engineered mice.

In summary, this study presents a potential new therapeutic strategy to overcome PD-1 blockade resistance. Having analyzed three patient biopsy-derived RNA-Seq datasets, we conclude that *PAK4* expression is enriched in poorly infiltrated tumor samples and constitutes a target to reverse PD-1 blockade resistance. Our pan-cancer correlation analysis with multiple cancer histologies having an anti-correlation of *PAK4* expression and T cell infiltration suggests that patients with different cancers could potentially benefit from dual PAK4 and PD-1 inhibition. The results from this study have led to the planning of a phase 1 clinical trial combining the anti-PD-1 nivolumab with the dual PAK4 and NAMPT inhibitor KPT-9274 (NCT02702492).

Methods

Patients, tumor biopsies and response assessment. Tumor biopsies were collected under University of California, Los Angeles (UCLA) Institutional Review Board approvals 11-001918 and 11-003066 from 41 patients with metastatic melanoma treated with either pembrolizumab or nivolumab. All patients signed a written informed consent form. Samples were immediately stored in RNAlater (Ambion) or snap frozen in liquid nitrogen for subsequent RNA extraction. Response was assessed for each biopsy independently by A.R. Complete patient clinical information can be found in Supplementary Table 1.

RNA isolation and RNA-Seq analysis. We obtained a total of 66 tumor samples from which we extracted RNA using the AllPrep DNA/RNA Mini Kit (Qiagen) and mirVana miRNA Isolation Kit (Ambion). Poly-A selection was used for library construction, and samples were sequenced using the Illumina HiSeq 2500 platform with a read length of 2 × 100 at the UCLA Technology Center for Genomics and Bioinformatics. Raw FASTQ files were aligned to the hg19 genome using HISAT2 version 2.0.4 (ref. [46]) with the default parameters, and counted with HTSeq version 0.6.1 (ref. [47]) with the intersection-nonempty mode (ambiguous reads were counted if fully overlapping). Raw counts were then normalized to fragments per kilobase of transcript per million mapped reads (FPKM). Two tumor biopsies were excluded from the analysis due to discordancy with previous IHC analysis (Supplementary Fig. 1a–c). Four tumor biopsies were excluded based on the expression of *KRT15* and *KRT5* (Supplementary Fig. 1d,e). A total of 60 tumor biopsies were considered for transcriptomic analysis. RNA-Seq-based cell deconvolution of tissue-infiltrating and stromal populations was performed using MCP-counter[20] with the default settings, and immune cell infiltration was defined using the upper and lower quartile scores for each of the obtained immune cell populations. Differential gene expression was performed based on the negative binomial distribution with the DESeq2 package[48] using the default settings (Wald significance test). Principal component analyses were also performed, using the DESeq2 package[47], on prior normalization of raw reads using the variance-stabilizing transformation (vst) function. To identify enriched signaling pathways, we utilized GSEA with the following gene sets: C2 Curated Gene Sets and C5 Gene Ontology Gene Sets[49]. Pan-cancer correlation analysis between *PAK4* expression and immune cell infiltration (calculated using MCP-counter as described above) was performed using gene expression data from 32 tumor types from the TCGA Research Network (http://cancergenome.nih.gov/).

Cell lines and PAK4 CRISPR–Cas9 KO and rescue. Murine B16 and MC38 cells were maintained in DMEM and RPMI medium respectively, supplemented with 10% fetal bovine serum, 100 U ml^{-1} penicillin and 100 µg ml^{-1} streptomycin at 37 °C under a humidified atmosphere of 5% CO_2. The following single guide RNAs targeting PAK4 were used: forward: 5′-TTCGAGCACCGTGTACACAC-3′; reverse: 5′-GTGTGTACACGGTGCTCGAA-3′. These were cloned into the pSpCas9(BB)-2A-GFP vector (Addgene) as described in Zheng's protocol[50]. Cells were then transfected with PAK4-single guide RNA plasmid using lipofectamine 3000 (Thermo Fisher Scientific), and green fluorescent protein-positive cells were collected and single-cell sorted 48 h after transfection at the UCLA Flow Cytometry Core. Genomic DNA was isolated for each clone (NucleoSpin Tissue XS; Macherey Nagel), and after PCR amplifying the PAK4 sequence, we used the tracking of indels by decomposition (TIDE)[51] web tool to evaluate and confirm knockout efficiency (Extended Data Figs. 3a–c and 7a). PAK4 deletion was also validated by western blot, performed as described previously[52]. PAK4 antibody (Proteintech) immunoreactivity was assessed with an ECL-Plus Kit (Amersham Biosciences) and analyzed using the ChemiDoc MP system (Bio-Rad Laboratories) (Extended Data Figs. 3d and 7b). To restore PAK4 levels in PAK4 KO cells, we cloned the mouse PAK4 open reading frame into a lentiviral vector containing Thy1.1. 293T cells were used for lentiviral particle generation, and B16 PAK4 KO cells were transduced at 20% confluency. Then, 24 h after transduction, the media was changed and cells were expanded and sorted based on Thy1.1 expression. PAK4 expression was then validated by western blot (Extended Data Fig. 3e).

WNT activity assays. β-catenin protein levels and phosphorylation were investigated by western blot performed as described previously[51] using the following antibodies: β-catenin (catalog number: 9587); phospho-β-catenin (S675; catalog number: 9567) and phospho-β-catenin (S33/37/T41; catalog number: 9561) (all from Cell Signaling Technology). Cytoplasm and nuclear extraction were performed with NE-PER Nuclear and Cytoplasmic Extraction Reagents (Thermo Fisher Scientific) following the manufacturer's protocol.

For the Topflash WNT activity assay, cells were plated in 24-well plates and co-transfected with pSV-β-galactosidase control vector (PR-E1081; Promega) along with either pTopflash (Addgene; catalog number: 12456) or pFopflash (Addgene; catalog number: 12457). Then, 24 h after transfection, cells were treated with Wnt-3a (R&D Systems) at 200 ng ml^{-1}. After 8 h, cells were harvested using Reporter Lysis Buffer (Promega; catalog number: PR-E4030) and the luciferase activity was measured using a Bright-Glo Luciferase Assay System (Promega; catalog number: PR-E2610) and Beta-Glo Assay System (Promega; catalog number: PR-E4720). The luciferase activity was normalized to its corresponding Beta-Glo activity to account for transfection efficiency.

Tyrosinase expression was measured by reverse transcription PCR following manufacturer's protocol for the Power SYBR Green RNA-to-CT 1-Step Kit (Applied Biosystems) and using the following primers: 5′-GCACCTATCGGCCATAACAG-3′ and 5′-GCCAGATACGACTGGCTTGT-3′.

TNF proliferation assay. To assess the anti-proliferative effects of TNF, MC38 cells were plated into 96-well plates by triplicate with either media or media containing TNF (100 ng ml^{-1}; Peprotech). Cell confluency was measured using the IncuCyte S3 Live System. To determine the percentage of cell growth inhibition, we measured the area under the curve of each group and calculated the reduction in under the curve between the untreated and TNF-treated cells.

Mouse model studies. All mouse studies were performed under UCLA Animal Research Committee protocol number 2004-159-23. C57BL/6 mice were bred and kept under defined-flora pathogen-free conditions at the Association for Assessment and Accreditation of Laboratory Animal Care-approved animal facility of the Division of Experimental Radiation Oncology at UCLA. To study the in vivo effect of PD-1 blockade in anti-tumor response and immune cell infiltration, we injected 0.3 × 10^6 B16 PAK4 KO or PAK4 rescue melanoma cells or MC38 PAK4 KO cells subcutaneously into the flanks of C57BL/6 syngeneic mice. Then, 96 h after tumor injection, mice were randomly assigned to the different groups. Anti-PD-1 (catalog number: BE0146; clone RMP1-14; BioXCell) treatment was injected intraperitoneally three times per week at 200 µg per dose. For the CD8 depletion studies, we administered anti-CD8 (catalog number BE0117; clone YST 169.4; BioXCell) 1 d before anti-PD-1 treatment and then it was co-administered with anti-PD-1 for a total of four doses. Splenocytes from control and CD8-depleted mice were taken to validate CD8 depletion efficacy (Extended Data Fig. 6d). To study the combination effects of PAK4 inhibition with KPT-9274 and anti-PD-1 (catalog number: BE0146; clone RMP1-14; BioXCell) in immune cell infiltration and anti-tumor response, 0.3 × 10^6 B16 WT or 0.5 × 10^6 MC38 WT cells were injected subcutaneously into the flanks of C57BL/6 mice. Then, 96 h after tumor injection, mice were randomly assigned to the different groups. For B16 WT tumors, KPT-9274 was administered once a day by oral gavage at 300 mg kg^{-1} while

anti-PD-1 treatment was administered as described above. For MC38 WT tumors, KPT-9274 was administered twice a day by oral gavage at 150 mg kg^{-1}. Tumor progression was monitored three times per week by measuring two perpendicular dimensions with a calliper.

Mass cytometry. To study the different immune cell populations in the tumor microenvironment of melanoma B16 PAK4 KO and B16 WT tumors, we collected spleen and tumor samples from anti-PD-1-treated or untreated mice for each of the two conditions. Tumor samples were processed using the Tumor Dissociation Kit, mouse (Miltenyi Biotec) following the manufacturer's protocol. Spleens were manually disaggregated and filtered with a 70-µm strainer following digestion with ACK Lysing Buffer (Lonza). Samples were then stained and processed as described previously[53], with two deviations: (1) samples were not barcoded; and (2) 3% paraformaldehyde was used instead. Detailed information on the immune markers used for immune cell phenotyping can be found in Supplementary Table 5. Following staining, samples were analyzed using the Helios mass cytometer (Fluidigm) platform at the UCLA Flow Cytometry Core. Sample quality control was assessed by measuring the fluctuation/disruption over time. Calibration beads (Cs140) were also excluded. Samples were pre-gated for cells, singlets and double expression of the viable CD45 single-cell-positive population using FlowJo software (version 10.4.2) and used as the input for Cytofkit[54], which was analyzed in R (version 3.5.1). To identify and annotate each of the clusters obtained, cluster median data were normalized, and a threshold of >0.5 was used to define positive immune markers[53]. T-distributed stochastic neighbor embedding plots were generated by PhenoGraph clustering through cytofkiyShinyAPP from Cytofkit[54].

IHC. We re-analyzed IHC samples used in our previous work[2] with matching RNA-Seq data to correlate immune cell infiltration between IHC and RNA-Seq. We generated new slides for two representative patients and stained them with hematoxylin and eosin, S100, CD8, PAK4 and CTNNB1 at the UCLA Anatomic Pathology IHC Laboratory. Leica Bond-III autostainers (Leica Biosystems) were used for immunostaining as previously described[2]. Cell density (cells mm^{-2}) and quantification of PAK4 co-localization with S100 and CTNNB1 were calculated using the Indica Labs HALO 2.

Statistics and reproducibility. GraphPad Prism 7 (GraphPad Software) and R software (version 3.5.1) were used for graphic representation and statistical analysis. Gene expression comparisons were performed using two-sided Welch's *t*-test unless matching pre- and on-treatment samples were used, in which case a two-sided paired *t*-test was performed. Correlation analysis was performed using the Pearson correlation coefficient unless otherwise specified. Differential gene expression was performed using the R package DeSeq2 in which *P* values were calculated using the negative binomial generalized linear model fitting and Wald significance test, while *q* values were obtained by applying the Benjamini–Hochberg method. For in vivo studies, statistical significance and correction for multiple comparisons were calculated using the Holm–Šidak method. Differences were considered statistically significant if $P < 0.05$. Functional data are representative of at least three experiments unless otherwise specified.

Reporting Summary. Further information on research design is available in the Nature Research Reporting Summary linked to this article.

Data availability

RNA-Seq data supporting the findings of this study have been deposited in the National Center for Biotechnology Information database of Genotypes and Phenotypes (https://www.ncbi.nlm.nih.gov/gap/) with accession number phs001919. The data for the pan-cancer correlation analysis were derived from the TCGA Research Network (http://cancergenome.nih.gov/). Source data on unprocessed blots in Fig. 3 and Extended Data Figs. 3–5 and 7, as well as numerical raw data for Figs. 3, 5 and 7 and Extended Data Figs. 4–6 are provided with the paper. All other data supporting the findings of this study are available from the corresponding author on reasonable request.

Received: 26 August 2019; Accepted: 18 October 2019;
Published online: 9 December 2019

References

1. Ribas, A. & Wolchok, J. D. Cancer immunotherapy using checkpoint blockade. *Science* **359**, 1350–1355 (2018).
2. Tumeh, P. C. et al. PD-1 blockade induces responses by inhibiting adaptive immune resistance. *Nature* **515**, 568–571 (2014).
3. Chen, P. L. et al. Analysis of immune signatures in longitudinal tumor samples yields insight into biomarkers of response and mechanisms of resistance to immune checkpoint blockade. *Cancer Discov.* **6**, 827–837 (2016).
4. Ayers, M. et al. IFN-γ-related mRNA profile predicts clinical response to PD-1 blockade. *J. Clin. Invest.* **127**, 2930–2940 (2017).
5. Riaz, N. et al. Tumor and microenvironment evolution during immunotherapy with nivolumab. *Cell* **171**, 934–949.e15 (2017).
6. Jerby-Arnon, L. et al. A cancer cell program promotes T cell exclusion and resistance to checkpoint blockade. *Cell* **175**, 984–997.e24 (2018).
7. Sharma, P., Hu-Lieskovan, S., Wargo, J. A. & Ribas, A. Primary, adaptive, and acquired resistance to cancer immunotherapy. *Cell* **168**, 707–723 (2017).
8. Liu, C. et al. BRAF inhibition increases tumor infiltration by T cells and enhances the antitumor activity of adoptive immunotherapy in mice. *Clin. Cancer Res.* **19**, 393–403 (2013).
9. Peng, W. et al. Loss of PTEN promotes resistance to T cell-mediated immunotherapy. *Cancer Discov.* **6**, 202–216 (2016).
10. Spranger, S. & Gajewski, T. F. Impact of oncogenic pathways on evasion of antitumour immune responses. *Nat. Rev. Cancer* **18**, 139–147 (2018).
11. Spranger, S., Bao, R. & Gajewski, T. F. Melanoma-intrinsic β-catenin signalling prevents anti-tumour immunity. *Nature* **523**, 231–235 (2015).
12. Nsengimana, J. et al. β-Catenin-mediated immune evasion pathway frequently operates in primary cutaneous melanomas. *J. Clin. Invest.* **128**, 2048–2063 (2018).
13. Grasso, C. S. et al. Genetic mechanisms of immune evasion in colorectal cancer. *Cancer Discov.* **8**, 730–749 (2018).
14. Luke, J. J., Bao, R., Sweis, R. F., Spranger, S. & Gajewski, T. F. WNT/β-catenin pathway activation correlates with immune exclusion across human cancers. *Clin. Cancer Res.* **25**, 3074–3083 (2019).
15. Li, Y. et al. Nucleo-cytoplasmic shuttling of PAK4 modulates β-catenin intracellular translocation and signaling. *Biochim. Biophys. Acta* **1823**, 465–475 (2012).
16. Rane, C. K. & Minden, A. P21 activated kinase signaling in cancer. *Semin. Cancer Biol.* **54**, 40–49 (2019).
17. Yun, C. Y. et al. p21-activated kinase 4 critically regulates melanogenesis via activation of the CREB/MITF and β-catenin/MITF pathways. *J. Invest. Dermatol.* **135**, 1385–1394 (2015).
18. Vershinin, Z., Feldman, M., Chen, A. & Levy, D. PAK4 methylation by SETD6 promotes the activation of the Wnt/β-catenin pathway. *J. Biol. Chem.* **291**, 6786–6795 (2016).
19. Moll, R., Divo, M. & Langbein, L. The human keratins: biology and pathology. *Histochem. Cell Biol.* **129**, 705–733 (2008).
20. Becht, E. et al. Estimating the population abundance of tissue-infiltrating immune and stromal cell populations using gene expression. *Genome Biol.* **17**, 218 (2016).
21. Radu, M., Semenova, G., Kosoff, R. & Chernoff, J. PAK signalling during the development and progression of cancer. *Nat. Rev. Cancer* **14**, 13–25 (2014).
22. Chen, S. et al. Wnt-1 signaling inhibits apoptosis by activating β-catenin/T cell factor-mediated transcription. *J. Cell Biol.* **152**, 87–96 (2001).
23. Li, J. et al. LATS2 suppresses oncogenic Wnt signaling by disrupting β-catenin/BCL9 interaction. *Cell Rep.* **5**, 1650–1663 (2013).
24. Aboukameel, A. et al. Novel p21-activated kinase 4 (PAK4) allosteric modulators overcome drug resistance and stemness in pancreatic ductal adenocarcinoma. *Mol. Cancer Ther.* **16**, 76–87 (2017).
25. Takao, S. et al. Targeting the vulnerability to NAD^+ depletion in B-cell acute lymphoblastic leukemia. *Leukemia* **32**, 616–625 (2018).
26. Abu Aboud, O. et al. Dual and specific inhibition of NAMPT and PAK4 by KPT-9274 decreases kidney cancer growth. *Mol. Cancer Ther.* **15**, 2119–2129 (2016).
27. Rane, C. et al. A novel orally bioavailable compound KPT-9274 inhibits PAK4, and blocks triple negative breast cancer tumor growth. *Sci. Rep.* **7**, 42555 (2017).
28. Wang, K. et al. Inhibition of p21 activated kinase enhances tumour immune response and sensitizes pancreatic cancer to gemcitabine. *Int. J. Oncol.* **52**, 261–269 (2018).
29. Mosely, S. I. et al. Rational selection of syngeneic preclinical tumor models for immunotherapeutic drug discovery. *Cancer Immunol. Res.* **5**, 29–41 (2017).
30. Ueha, S. et al. Robust antitumor effects of combined anti-CD4-depleting antibody and anti-PD-1/PD-L1 immune checkpoint antibody treatment in mice. *Cancer Immunol. Res.* **3**, 631–640 (2015).
31. Homet Moreno, B. et al. Response to programmed cell death-1 blockade in a murine melanoma syngeneic model requires costimulation, CD4, and CD8 T cells. *Cancer Immunol. Res.* **4**, 845–857 (2016).
32. Yadav, M. et al. Predicting immunogenic tumour mutations by combining mass spectrometry and exome sequencing. *Nature* **515**, 572–576 (2014).
33. Li, X. & Minden, A. PAK4 functions in tumor necrosis factor (TNF) α-induced survival pathways by facilitating TRADD binding to the TNF receptor. *J. Biol. Chem.* **280**, 41192–41200 (2005).
34. Li, Q. et al. p21-activated kinase 4 as a switch between caspase-8 apoptosis and NF-κB survival signals in response to TNF-α in hepatocarcinoma cells. *Biochem. Biophys. Res. Commun.* **503**, 3003–3010 (2018).
35. Dunn, G. P., Old, L. J. & Schreiber, R. D. The three Es of cancer immunoediting. *Annu. Rev. Immunol.* **22**, 329–360 (2004).
36. Nicholas, N. S. et al. PAK4 suppresses PDZ-RhoGEF activity to drive invadopodia maturation in melanoma cells. *Oncotarget* **7**, 70881–70897 (2016).

37. Chen, S. et al. Copy number alterations in pancreatic cancer identify recurrent PAK4 amplification. *Cancer Biol. Ther.* **7**, 1793–1802 (2008).
38. Wells, C. M., Whale, A. D., Parsons, M., Masters, J. R. & Jones, G. E. PAK4: a pluripotent kinase that regulates prostate cancer cell adhesion. *J. Cell Sci.* **123**, 1663–1673 (2010).
39. Bi, Y. et al. Study on the expression of PAK4 and P54 protein in breast cancer. *World J. Surg. Oncol.* **14**, 160 (2016).
40. Rane, C. K. et al. Decrypting the PAK4 transcriptome profile in mammary tumor forming cells using next generation sequencing. *Genomics* **110**, 248–256 (2018).
41. Wong, L. E., Chen, N., Karantza, V. & Minden, A. The Pak4 protein kinase is required for oncogenic transformation of MDA-MB-231 breast cancer cells. *Oncogenesis* **2**, e50 (2013).
42. Kim, H., Woo, D. J., Kim, S. Y. & Yang, E. G. p21-activated kinase 4 regulates HIF-1α translation in cancer cells. *Biochem. Biophys. Res. Commun.* **486**, 270–276 (2017).
43. King, H. et al. PAK4 interacts with p85 alpha: implications for pancreatic cancer cell migration. *Sci. Rep.* **7**, 42575 (2017).
44. Fu, X. et al. PAK4 confers cisplatin resistance in gastric cancer cells via PI3K/Akt- and MEK/ERK-dependent pathways. *Biosci. Rep.* **34**, e00094 (2014).
45. He, L. F. et al. Activated-PAK4 predicts worse prognosis in breast cancer and promotes tumorigenesis through activation of PI3K/AKT signaling. *Oncotarget* **8**, 17573–17585 (2017).
46. Kim, D., Langmead, B. & Salzberg, S. L. HISAT: a fast spliced aligner with low memory requirements. *Nat. Methods* **12**, 357–360 (2015).
47. Anders, S., Pyl, P. T. & Huber, W. HTSeq—a Python framework to work with high-throughput sequencing data. *Bioinformatics* **31**, 166–169 (2015).
48. Love, M. I., Huber, W. & Anders, S. Moderated estimation of fold change and dispersion for RNA-Seq data with DESeq2. *Genome Biol.* **15**, 550 (2014).
49. Subramanian, A. et al. Gene set enrichment analysis: a knowledge-based approach for interpreting genome-wide expression profiles. *Proc. Natl Acad. Sci. USA* **102**, 15545–15550 (2005).
50. Ran, F. A. et al. Genome engineering using the CRISPR–Cas9 system. *Nat. Protoc.* **8**, 2281–2308 (2013).
51. Brinkman, E. K., Chen, T., Amendola, M. & van Steensel, B. Easy quantitative assessment of genome editing by sequence trace decomposition. *Nucleic Acids Res.* **42**, e168 (2014).
52. Escuin-Ordinas, H. et al. COX-2 inhibition prevents the appearance of cutaneous squamous cell carcinomas accelerated by BRAF inhibitors. *Mol. Oncol.* **8**, 250–260 (2014).
53. Wei, S. C. et al. Distinct cellular mechanisms underlie anti-CTLA-4 and anti-PD-1 checkpoint blockade. *Cell* **170**, 1120–1133 e1117 (2017).
54. Chen, H. et al. Cytofkit: a bioconductor package for an integrated mass cytometry data analysis pipeline. *PLoS Comput. Biol.* **12**, e1005112 (2016).

Acknowledgements

This study was funded in part by the Parker Institute for Cancer Immunotherapy, NIH grants R35 CA197633 and P01 CA168585, the Ressler Family Foundation, and support from K. Schultz and D. Schultz (to A.R.). G.A.-R. was supported by the Isabel and Harvey Kibel Fellowship award and Alan Ghitis Fellowship Award for Melanoma Research. D.Y.T. was supported by a Young Investigator Award from the American Society of Clinical Oncology, a grant from the Spanish Society of Medical Oncology for Translational Research in Reference Centers and the V Foundation–Gil Nickel Family Endowed Fellowship in Melanoma Research. J.M.Z. was part of the UCLA Medical Scientist Training Program supported by NIH training grant GM08042. T.S.N. was supported by NIH/NICHD grant K12-HD000850 (Pediatric Scientist Development Program). S.H.-L. was supported by a Young Investigator Award and a Career Development Award from the American Society of Clinical Oncology, a Tower Cancer Research Foundation Grant and a Dr. Charles A. Coltman Fellowship Award from the Hope Foundation. C.-Y.W. was supported by NIH/NIDCR grant R01DE15964. We acknowledge X. Li, L. Dong, J. Yoshizawa and J. Zhou from the UCLA Clinical Microarray Core for sequencing expertise, and J. Min Chen and J. Trent from the Parker Institute for Cancer Immunotherapy Center at UCLA for administrative support. Flow and mass cytometry were performed in the UCLA Jonsson Comprehensive Cancer Center and the Center for AIDS Research Flow Cytometry Core Facility (supported by NIH awards P30 CA016042 and 5P30 AI028697), as well as by the Jonsson Comprehensive Cancer Center, UCLA AIDS Institute and David Geffen School of Medicine at UCLA. The authors thank A. Minden from Rutgers, the State University of New Jersey, for helpful comments.

Author contributions

G.A.-R., C.S.G. and A.R. conceived and designed the study. G.A.-R., D.Y.T., W.L., J.M.Z., C.P.-S., T.S.N., A.K., A.J.G., G.C.-L., B.C.-A., S.H.-L., C.-Y.W., C.S.G. and A.R. developed the methodology. B.B.-M., I.B.C., S.H.-L., C-Y.W. and A.R. acquired the data (provided animals, acquired and managed patients, provided facilities, and so on). G.A.-R., D.Y.T., W.L., J.T., E.M., M.J.Q., W.S., E.B., B.C.-A., C-Y.W., C.S.G. and A.R. analyzed and interpreted the data (including statistical analysis, biostatistics and computational analysis). G.A.-R. and A.R. wrote the manuscript. All authors reviewed the manuscript.

Competing interests

G.A.-R. has received honoraria for consulting with Arcus Biosciences. W.S. and E.B. were employees of Karyopharm Therapeutics when this study was conducted. A.R. has received honoraria for consulting with Amgen, Bristol-Myers Squibb, Chugai, Genentech, Merck, Novartis, Roche and Sanofi, is or has been a member of the scientific advisory board, and holds stock in Advaxis, Arcus Biosciences, Bioncotech Therapeutics, Compugen, CytomX, Five Prime, FLX Bio, ImaginAb, IsoPlexis, Gilead Kite, Lutris Pharma, Merus, PACT Pharma, Rgenix and Tango Therapeutics. G.A.-R., D.Y.T., C.S.G. and A.R. are inventors in a patent application covering the use of PAK4 inhibitors for cancer immunotherapy.

Additional information

Extended data is available for this paper at https://doi.org/10.1038/s43018-019-0003-0.

Supplementary information is available for this paper at https://doi.org/10.1038/s43018-019-0003-0.

Correspondence and requests for materials should be addressed to A.R.

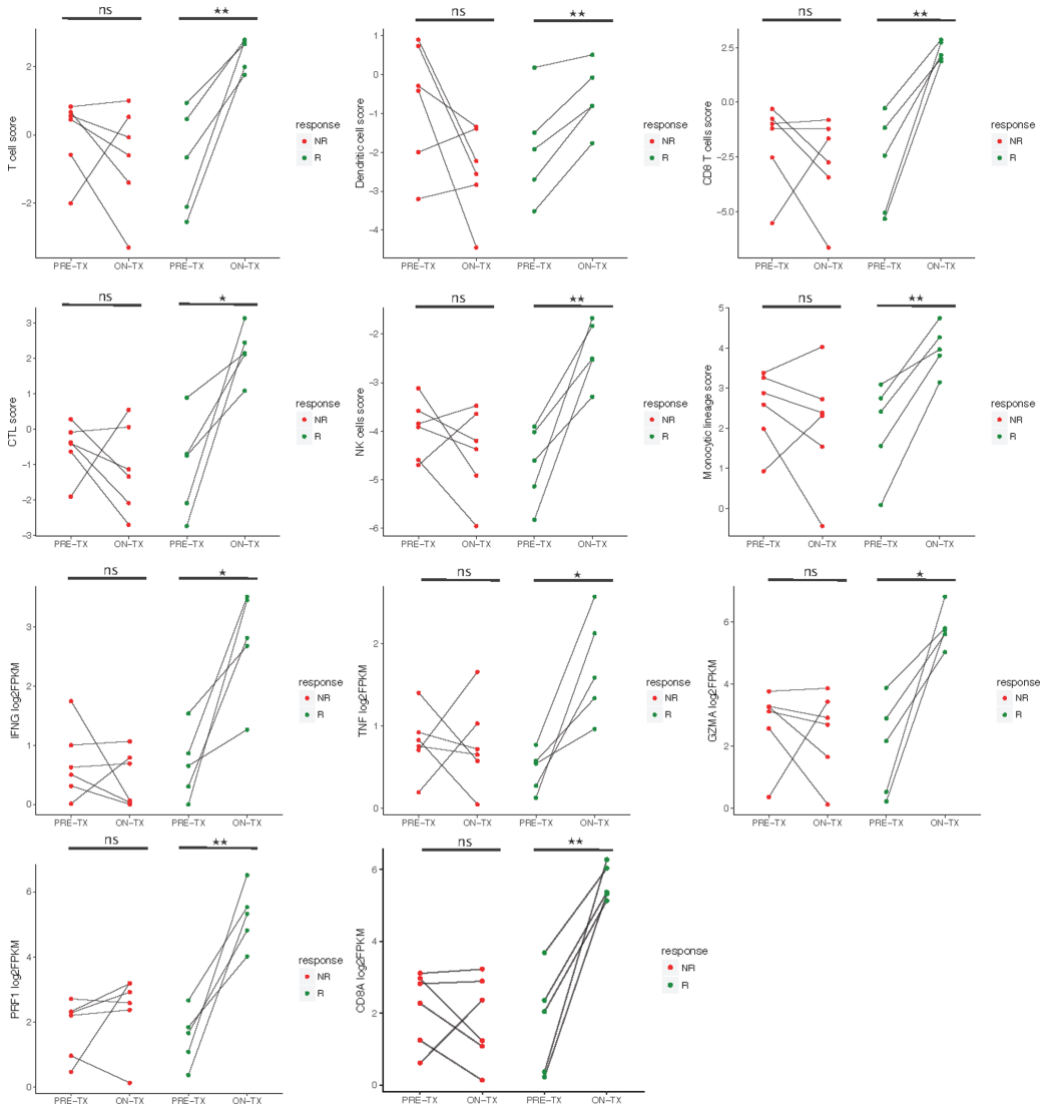

Extended Data Fig. 1 | Differential change in immune populations between non-responding and responding biopsies during anti-PD-1 therapy. Comparison (two-sided, paired T-test) of each of the immune populations and immune markers between baseline and on-treatment tumour samples for responding (n= 5) and non-responding (n= 6) biopsies. From left to right: T cell score (R P= 0.007, NR P= 0.44), Dendritic cell score (R P= 0.009, NR P= 0.08), CD8 T cell score (R P= 0.006, NR P= 0.48), CTL score (R P= 0.01, NR P= 0.43), NK cell score (R P= 0.006, NR P= 0.32), Monocyte lineage score (R P= 0.004, NR P= 0.48), IFNg (R P= 0.01, NR P= 0.47), TNF (R P= 0.01, NR P= 0.9), GZMA (R P= 0.01, NR P= 0.73), PRF1 (R P= 0.004, NR P= 0.29) and CD8A (R P= 0.004, NR P= 0.52) expression. Increase in all immune populations and markers was significant ($P < 0.05$) only in responding biopsies. *P <0.05, **$P < 0.01$; ns, not significant

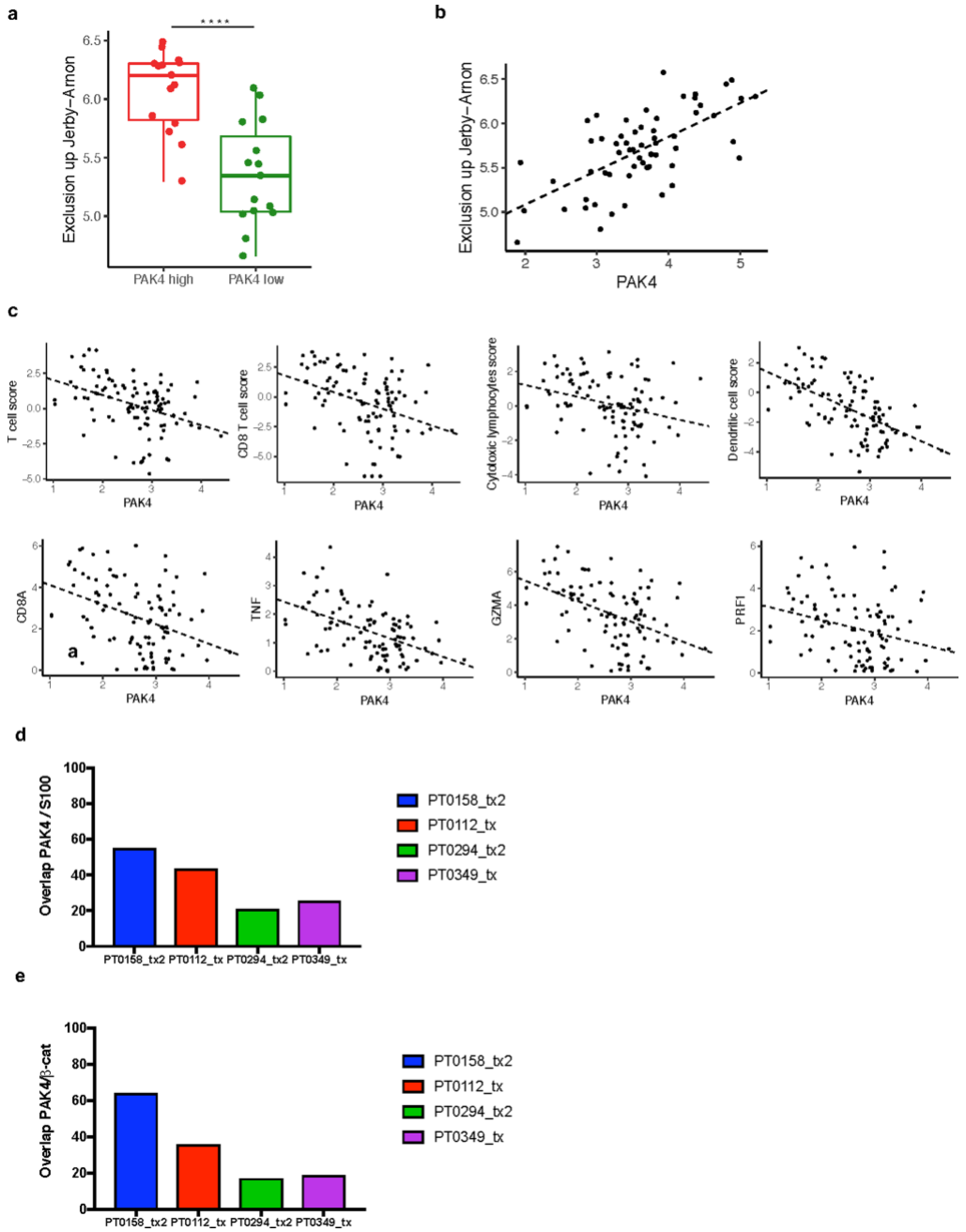

Extended Data Fig. 2 | See next page for caption.

Extended Data Fig. 2 | PAK4 expression analysis with immune infiltration and overlap with S100 and β-catenin staining. a, Comparison of exclusion up Jerby-Arnon score expression (P = 3.28e-05) between tumour biopsies within the upper (n = 15) and lower (n = 15) quartile of PAK4 expression. **b**, PAK4 correlation with Jerby-Arnon score expression (n = 60) (R = 0.65, P = 1.78e-08). Exclusion up Jerby-Arnon was obtained based on the geometric mean of the 302 gene from Jerby-Arnon et al. **c**, CD8A (R = -0.39, P = 6.07e-05), TNF (R = -0.49, P = 1.89e-07), GZMA (R = -0.45, P = 2.47e-06), PRF1 (R = -0.28, P = 4e-03) and the different immune populations assessed using MCP-Counter: T cells (R = -0.39, P = 4.41e-05), CD8 T cells (R = -0.36, P = 1.71e-04), cytotoxic lymphocytes (R = -0.28, P = 4.9e-03) and dendritic cells (R = -0.57, P = 3.95e-10). n= 99 for all plots. **d**, Quantification of PAK4 positive cells out of S100 total positive cells. PT0158_tx2 and PT0112_tx are two biopsies with low T cell infiltration and high PAK4 expression while PT0294_tx2 and PT0349_tx have low PAK4 and high T cell infiltrate as determined by RNAseq. **e**, Quantification of PAK4 positive cells out of β-catenin total positive cells. From top to bottom box-plots define the maximum, 3rd quartile, median, 1st quartile and minimum values a. P values obtained using two-sided Welch's t-test **a**. Correlations were calculated applying Pearson's correlation coefficient test **b**, **c**

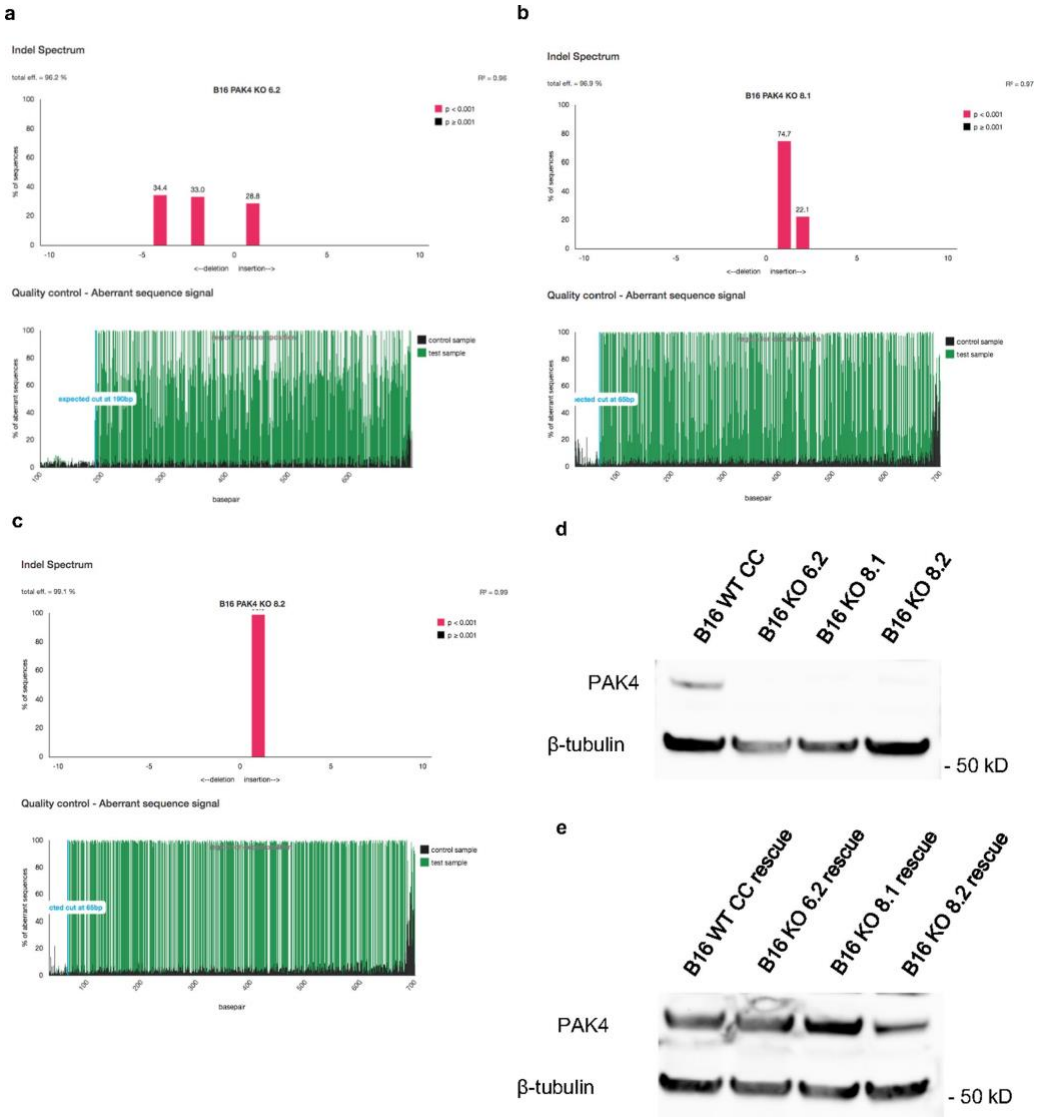

Extended Data Fig. 3 | Validation of the generation of a PAK4 KO B16 cell line. a, b, c TIDE analysis of the B16 PAK4 KO clones: 6.2, 8.1 and 8.2 respectively. **d, e**, Analysis of PAK4 protein expression in the three B16 PAK4 KO clones, B16 WT CRISPR control and rescue cell lines by Western blot. Results are representative from three independent experiments. Unprocessed blot images are provided as a Source Data file **d**, **e**.

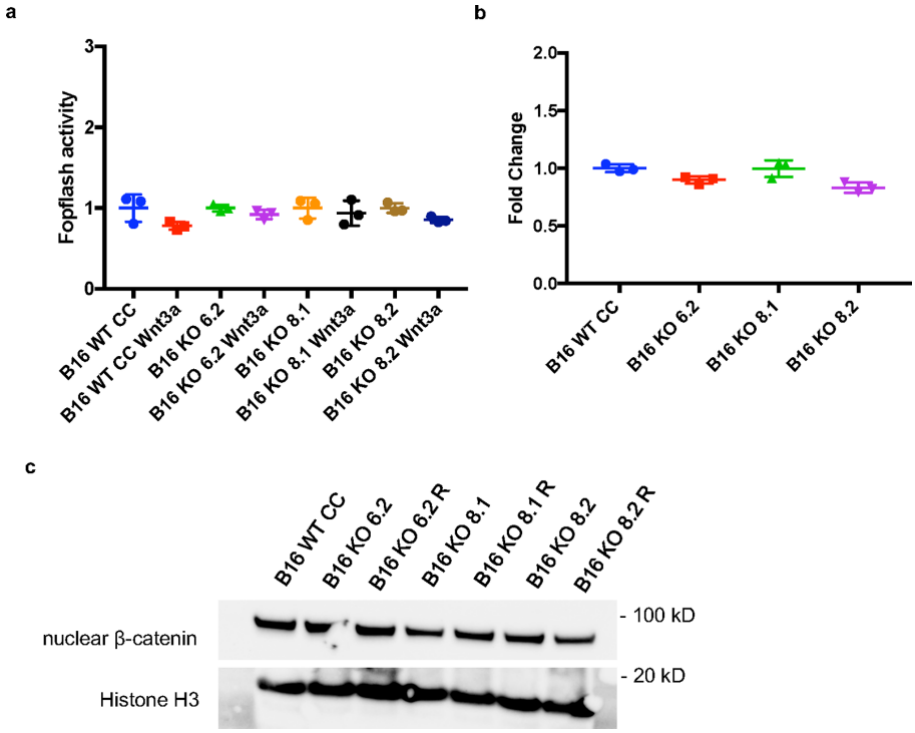

Extended Data Fig. 4 | PAK4 depletion impact on nuclear protein β-catenin and WNT signalling activity. a, Negative control for the Topflash experiment using the Fopflash luciferase vector which contains a mutated version of the TCF/LEF binding motifs. There are no changes in Fopflash activity upon stimulation with Wnt-3a ligand for 8 hours in any of the tested cell lines (n= 3 per group) ($P > 0.05$ for all comparisons). **b**, Baseline WNT activity levels assessed by Topflash assay (n= 3 per group). Values were normalized to B16 WT CC cell lines and no significant WNT activity changes were observed between PAK4 WT and KO cell. **c**, Immunoblots for nuclear β-catenin protein levels show no differences between B16 WT CRISPR control, PAK4 KO and PAK4 rescue cells. Results are representative from three independent experiments. Means +/- SEM two-tailed unpaired t-test **a, b.** Unprocessed blot images and raw data are provided as a Source Data file **a-c.**

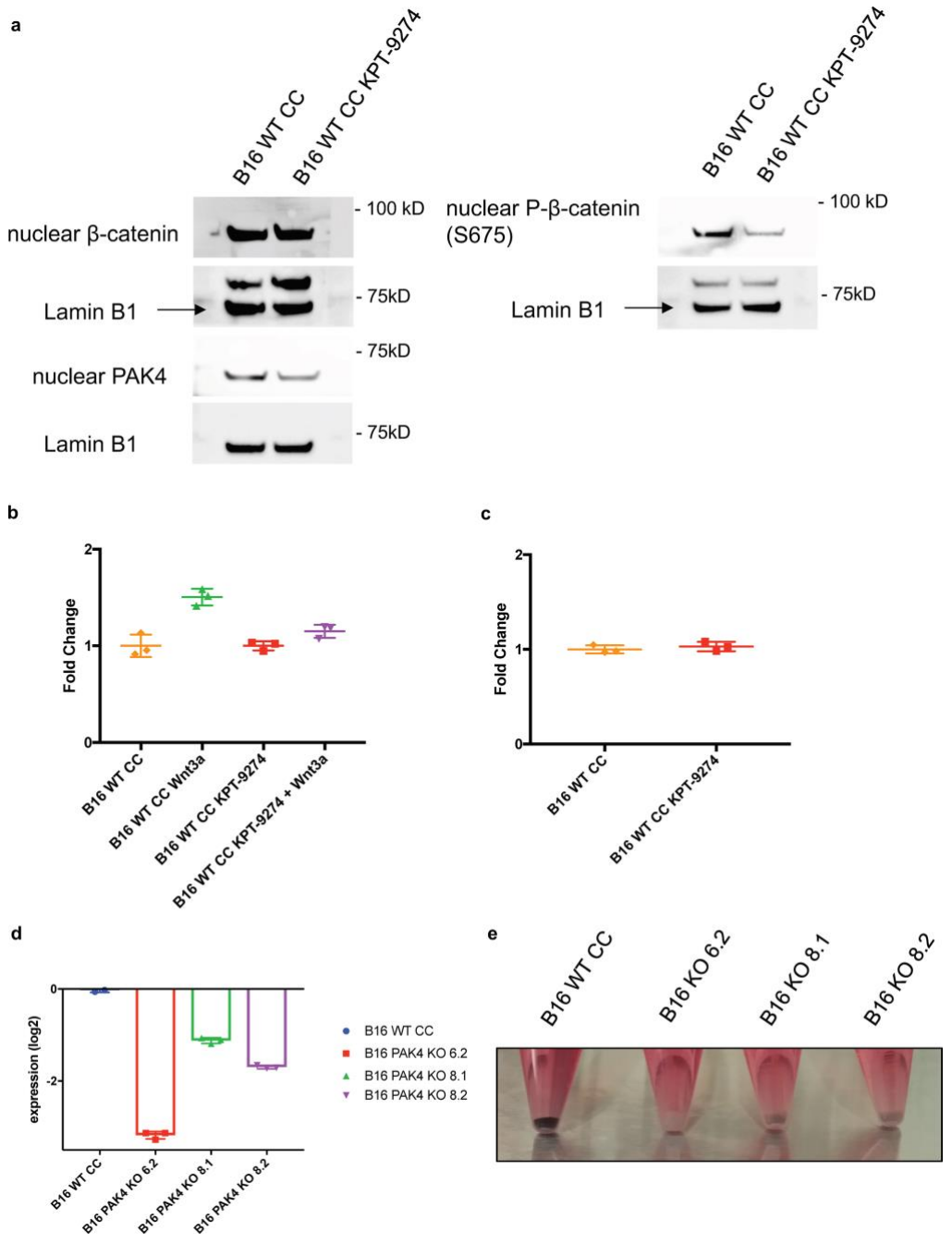

Extended Data Fig. 5 | See next page for caption.

Extended Data Fig. 5 | PAK4 inhibition disrupts WNT signalling and melanogenesis. a, Cells were cultured with 2μM KPT-9274 for 72 hours before nuclear protein isolation. Showing immunoblots for nuclear β-catenin, nuclear phosphor-β-catenin (S675) and nuclear PAK4 protein levels. Results are representative from two independent experiments. **b**, Cells were cultured with 2μM KPT-9274 for 72 hours and Wnt-3a for 8 hours prior to Topflash assay (n= 3 per group). Pharmacological inhibition of PAK4 significantly decreases sensitivity to Wnt-3a stimulation (P= 0.005 for WT Wnt3a vs WT KPT-9274 + Wnt3a comparison). **c**, Baseline WNT activity levels assessed by Topflash assay of cell treated with 2μM KPT-9274 for 72 hours (n= 3 per group) ($P > 0.05$). Values were normalized to untreated B16 WT CC cells. **d**, RT-PCR for *tyrosinase* expression show that PAK4 depletion reduces the expression levels of this gene. Showing means +/- SEM. Results are normalized to B16 WT CRISPR control levels and then log2 transformed (n= 3). **e**, For image, cells were cultured and harvest upon reaching 80% confluency. B16 WT CRISPR Control cell line maintains melanin production over time while PAK4 KO clones lose their pigmentation. Results are representative from three independent experiments. Means +/- SEM two-tailed unpaired t-test **b, c**. Unprocessed blots and raw data are provided as a Source Data file **a-c**.

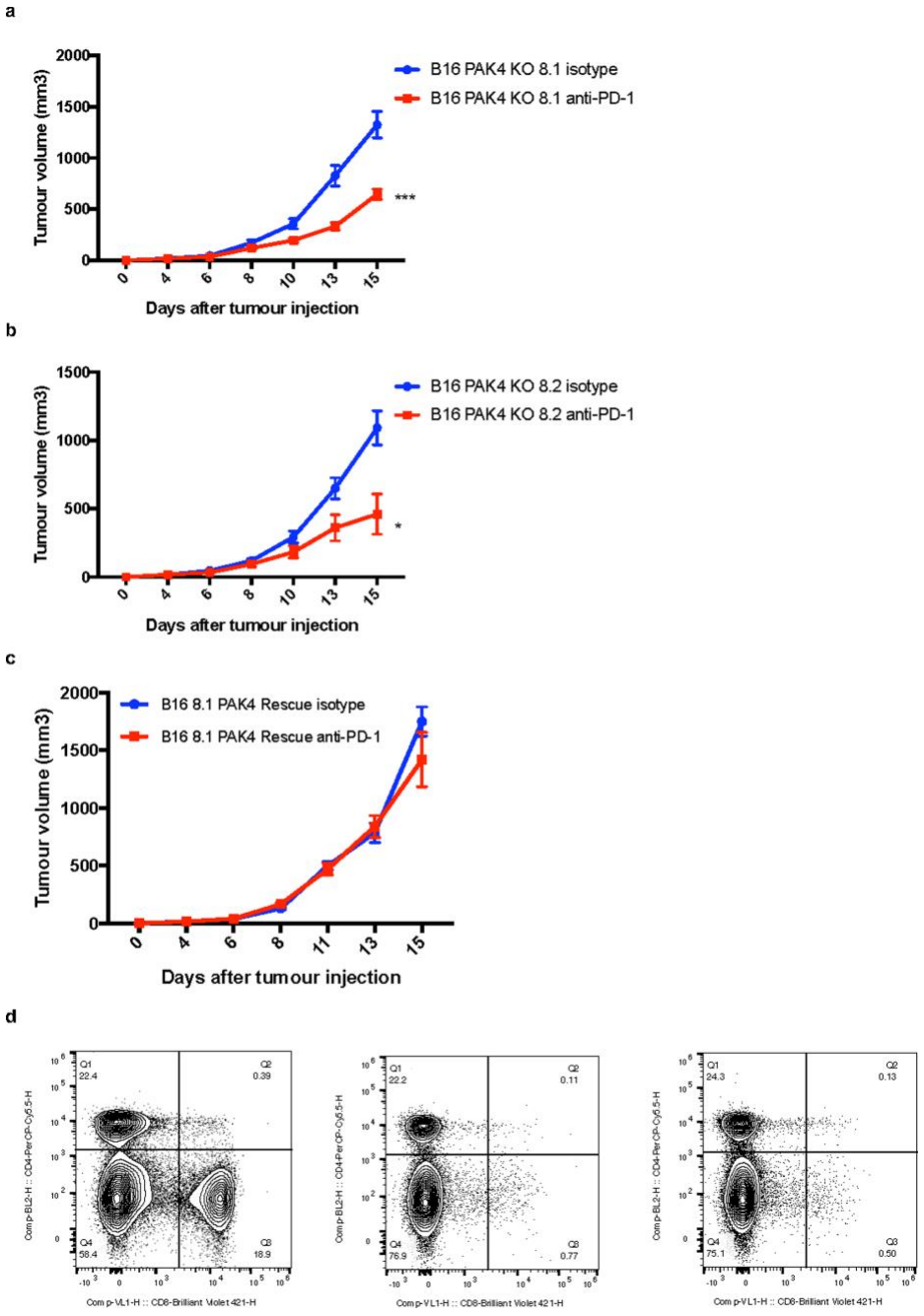

Extended Data Fig. 6 | See next page for caption.

Extended Data Fig. 6 | *In vivo* experiments with additional B16 PAK4 KO and rescue clones and CD8 depletion validation. a, Tumour growth curves for B16 PAK4 KO 8.1 tumours treated with isotype (blue, n = 10) or anti-PD-1 (red, n = 12) (P= 0.00024, day 15). **b**, Tumour growth curves for B16 PAK4 KO 8.2 tumours treated with isotype (blue, n = 10) or anti-PD-1 (red, n = 10) (P= 0.02, day 15). In both PAK4 KO cell lines anti-PD-1 treated tumours showed decreased tumour growth compared to untreated tumours. **c**, Tumour growth curves for B16 8.1 PAK4 rescue tumours treated with isotype (blue, n = 5) or anti-PD-1 (red, n = 5). Anti-PD-1 treatment did not result in any significant anti-tumour efficacy (P= 0.80, day 15). **d**, Flow cytometry analysis of CD8 positive splenocytes after CD8 depletion. Left panel show splenocytes pattern without anti-CD8 treatment (CD8 population = 18.9%) while middle and right panel show splenocytes derived from two independent mice treated with anti-CD8 antibody (CD8 population = 0.77% and 0.50% respectively). Plotting the mean +/- s.e.m **a-c**. Statistical significance and correction for multiple comparisons was calculated using Holm-Sidak method **a-c**. Raw data is provided as a Source Data file **a-c**. *P <0.05, **P < 0.01, ***P <0.001, ****P < 0.0001. ns, not significant.

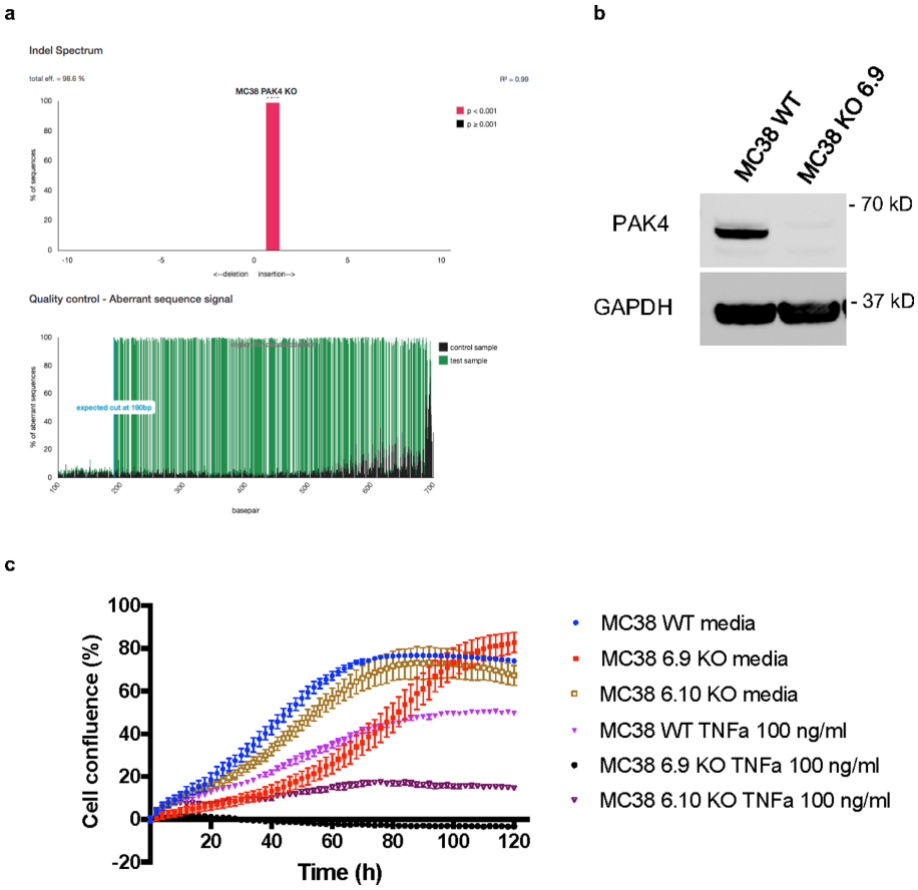

Extended Data Fig. 7 | PAK4 KO validation and sensitivity to TNF in MC38 cells. a, TIDE analysis of the MC38 PAK4 KO 6.9 clone. **b**, Analysis of PAK4 protein expression in MC38 PAK4 KO 6.9 clone and MC38 WT by Western blot. Results are representative from two independent experiments. **c**, Cells were plated by triplicate into 96 well plates and then treated with TNF at 100ng/mL. Cell proliferation was measured by cell confluence using the IncuCyte S3 Live Cell Analysis System. TNF treatment decreased proliferation of MC38 WT, MC38 PAK4 KO 6.9 and MC38 PAK4 KO 6.10 cells by 41%, 95% and 74% respectively compared to untreated cells (means +/- SEM). Results are representative from three biologically independent experiments. Unprocessed blots are provided as a Source Data file **b**.

nature research

Corresponding author(s): Antoni Ribas

Last updated by author(s): Oct 14, 2019

Reporting Summary

Nature Research wishes to improve the reproducibility of the work that we publish. This form provides structure for consistency and transparency in reporting. For further information on Nature Research policies, see Authors & Referees and the Editorial Policy Checklist.

Statistics

For all statistical analyses, confirm that the following items are present in the figure legend, table legend, main text, or Methods section.

n/a	Confirmed
☐	☒ The exact sample size (*n*) for each experimental group/condition, given as a discrete number and unit of measurement
☐	☒ A statement on whether measurements were taken from distinct samples or whether the same sample was measured repeatedly
☐	☒ The statistical test(s) used AND whether they are one- or two-sided *Only common tests should be described solely by name; describe more complex techniques in the Methods section.*
☐	☒ A description of all covariates tested
☐	☒ A description of any assumptions or corrections, such as tests of normality and adjustment for multiple comparisons
☐	☒ A full description of the statistical parameters including central tendency (e.g. means) or other basic estimates (e.g. regression coefficient) AND variation (e.g. standard deviation) or associated estimates of uncertainty (e.g. confidence intervals)
☐	☒ For null hypothesis testing, the test statistic (e.g. *F*, *t*, *r*) with confidence intervals, effect sizes, degrees of freedom and *P* value noted *Give P values as exact values whenever suitable.*
☒	☐ For Bayesian analysis, information on the choice of priors and Markov chain Monte Carlo settings
☒	☐ For hierarchical and complex designs, identification of the appropriate level for tests and full reporting of outcomes
☐	☒ Estimates of effect sizes (e.g. Cohen's *d*, Pearson's *r*), indicating how they were calculated

Our web collection on statistics for biologists contains articles on many of the points above.

Software and code

Policy information about availability of computer code

Data collection	Transcriptome data from TCGA Research Network was collected from: http://cancergenome.nih.gov/
Data analysis	The softwares used to analyze the data include: HISAT2 version 2.0.4, HTseq version 0.6.1, R version 3.5.1, DESeq 2 version 1.20.0, MCP-counter version 1.0.0, Cytofkit version 1.12.0 and FlowJo version 10.4.2

For manuscripts utilizing custom algorithms or software that are central to the research but not yet described in published literature, software must be made available to editors/reviewers. We strongly encourage code deposition in a community repository (e.g. GitHub). See the Nature Research guidelines for submitting code & software for further information.

Data

Policy information about availability of data

All manuscripts must include a data availability statement. This statement should provide the following information, where applicable:

- Accession codes, unique identifiers, or web links for publicly available datasets
- A list of figures that have associated raw data
- A description of any restrictions on data availability

Raw sequencing data derived from tumor biopsies collected under UCLA Institutional Review Board approvals 11-001918 and 11-003066 are deposited to dbGAP under accession number: phs001919

Field-specific reporting

Please select the one below that is the best fit for your research. If you are not sure, read the appropriate sections before making your selection.

☒ Life sciences ☐ Behavioural & social sciences ☐ Ecological, evolutionary & environmental sciences

For a reference copy of the document with all sections, see nature.com/documents/nr-reporting-summary-flat.pdf

Life sciences study design

All studies must disclose on these points even when the disclosure is negative.

Sample size	-No statistical method was used to determine the patient sample as they were collected upon availability of samples obtained in a clinical trial for PD-1 blockade in melanoma. We used a total of 27 baseline and 33 on-treatment biopsies from 41 metastatic melanoma patients (Fig. 1a). In any case, potential limitations of our sample size were tackle by validating our finding in several available clinical datasets. -For mice studies we used a sample size of >5 mice per group unless otherwise specified. This n is a standard sample size for these experiments and was sufficient to evaluate the effects of genetic and pharmacological inhibition of PAK4 on anti-tumor activity when combined with anti-PD-1.
Data exclusions	A total of 6 patient-derived RNA-seq samples were excluded from this study. We removed two samples because CD8A gene expression did not agree with CD8 protein levels measured using immunohistochemistry (Supplementary Fig. 1a-c) and four samples based on an outlier keratinocyte biomarker gene expression of KRT15 and KRT5 (Supplementary Fig. 1d-e).
Replication	-B16 PAK4 KO in vivo studies with the 6.2 clone were repeated and successfully replicated a total of 4 times (Fig. 5a shows the combination of replicate studies. Total of 16 mice per group). As for in vivo studies with the two additional PAK4 KO clones (8.1 and 8.2) in vivo studies were repeated and successfully replicated twice and the n for each of the groups is equal or higher than 10 (Extended Data Fig. 6a, b). As for the B16 PAK4 KO treated with anti-PD-1 + CD8 depletion (figure 5d) was repeated and successfully replicated once. -B16 WT CRISPR control studies (figures 5b) were repeated and successfully replicated twice and results are consistent with published data on this model. In the original submission, we had use a B16 WT cell line (not CRISPR control) and we performed the experiment once with the same results as in the B16 WT CRISPR control model. Nevertheless, we have just included the in vivo results with the B16 WT CRISPR control cell line. -In addition, both B16 PAK4 KO and WT in vivo studies were repeated for the main purpose of CyTOF, however, tumor growth was also measured (Figure 6b) and it recapitulated the results shown in Figure 5). -B16 WT studies with the PAK4 inhibitor, KPT-9274 were performed one time with a total of 24 mice (6 mice per group). -MC38 PAK4 KO studies were performed one time -MC38 WT studies with KPT-9274 were performed one time -B16 PAK4 Rescue in vivo studies with the 6.2 clone were repeated and successfully replicated a total of 2 times (Fig. 5c, n= 12). We also performed the experiment using the B16 PAK4 Rescue 8.1 cell line one time (n = 5) (Extended Data Fig. 6c).
Randomization	Mice were evenly distributed by tumor size four days after tumor injection.
Blinding	Blinding was not possible due to the treatment schedule.

Reporting for specific materials, systems and methods

We require information from authors about some types of materials, experimental systems and methods used in many studies. Here, indicate whether each material, system or method listed is relevant to your study. If you are not sure if a list item applies to your research, read the appropriate section before selecting a response.

Materials & experimental systems

n/a	Involved in the study
☐	☒ Antibodies
☐	☒ Eukaryotic cell lines
☒	☐ Palaeontology
☐	☒ Animals and other organisms
☐	☒ Human research participants
☒	☐ Clinical data

Methods

n/a	Involved in the study
☒	☐ ChIP-seq
☐	☒ Flow cytometry
☒	☐ MRI-based neuroimaging

Antibodies

Antibodies used	-PAK4 antibody for Western Blot (Cat. No. 3242, Cell Signaling Technology, Danvers, MA). Dilution 1/1000 -PAK4 antibody for Western Blot (Cat. No. 14685-1-AP, Proteintech, Rosemont, IL). Dilution 1/800 - B-catenin antibody for Western Blot (Cat. No. 9587,Cell Signaling Technology, Danvers, MA). Dilution 1/1000 -Phospho B-catenin (S675) for Western Blot (Cat. No. 9567, Cell Signaling Technology, Danvers, MA). Dilution 1/1000 -Phospho B-catenin (S33/37/T41) for Western Blot (Cat. No. 9561, Cell Signaling Technology, Danvers, MA). Dilution 1/1000

-Lamin B1 antibody for Western Blot (Cat. No. 12987-1-AP, Proteintech, Rosemont, IL). Dilution 1/3000
-Histone H3 for Western Blot (Cat. No. 4499, Cell Signaling Technology, Danvers, MA). Dilution 1/1000
-B-tubulin for Western Blot (Cat. No. 2128, Cell Signaling Technology, Danvers, MA). Dilution 1/1000
-Anti PD-1 for in vivo experiments (Cat. No. BE0146, clone RMP1-14, BioXCell, West Lebanon, NH). Concentration: 200ug.
-Anti-CD8 for in vivo experiments (Cat.No.BE0117, clone YST 169.4, BioXCell). Concentration: 200ug
-CD8 antibody for IHC (Cat.No. M7103, clone C8/144B, Dako, Santa Claro, CA). Dilution 1/100
-S100 antibody for IHC (Cat.No. Z0311, Dako, Santa Claro, CA). Dilution 1/10000
-B-catenin antibody for IHC (Cat.No. 9562, Cell Signaling Technology, Danvers, MA). Dilution 1/500
-PAK4 antibody for IHC (Cat. No. ab62509, Abcam, Cambridge, UK). Dilution 1/2000
-Detailed list of conjugated antibodies (including clone and company) used for CyTOF can be found in Supplementary Table 5.

Validation

-Validations statements and relevant references for the used antibodies can be found on manufacture's website.
-Validation of CD8 antibody (Cat.No.BE0117, clone YST 169.4, BioXCell) was also assessed by flow cytometry (Extended Data Figure 9)

Eukaryotic cell lines

Policy information about cell lines

Cell line source(s)

-B16 from ATCC
-MC38 from Steve Rosenberg's lab

Authentication

None of these cell lines were authenticated

Mycoplasma contamination

B16 WT and PAK4 KO cells were negative for mycoplasma contamination. MC38 WT and PAK4 KO cell lines have been not tested for contamination yet.

Commonly misidentified lines
(See ICLAC register)

None of the cell lines are listed in the ICLAC database

Animals and other organisms

Policy information about studies involving animals; ARRIVE guidelines recommended for reporting animal research

Laboratory animals

We used female 8-10 weeks old C57BL/6 mice, bred and kept under defined-flora pathogen-free conditions at the Association for Assessment and Accreditation of Laboratory Animal Care approved animal facility of the Division of Experimental Radiation Oncology, UCLA.

Wild animals

Study did not involved wild animals

Field-collected samples

Study did not involved samples collected from the field

Ethics oversight

All mouse studies were performed and approved under UCLA Animal Research Committee protocol #2004-159-23

Note that full information on the approval of the study protocol must also be provided in the manuscript.

Human research participants

Policy information about studies involving human research participants

Population characteristics

Covariant-relevant population characteristics, including sex, age, date of biopsy, anatomical location, response, cycle 1 day 1, overall survival, disease status, study, prior treatment regimens, histological subtype are provided in Supplemental Table 1.

Recruitment

Patients with metastatic melanoma treated with either pembrolizumab or nivolumab with metastasis amenable for biopsy were asked to consider signing a consent for tissue and blood collection for analyses under UCLA Institutional Review Board approvals 11-001918 and 11-003066

Ethics oversight

This study was approved by UCLA Institutional Review Board: approvals 11-001918 and 11-003066. Written informed consent was obtained from all participants.

Note that full information on the approval of the study protocol must also be provided in the manuscript.

Flow Cytometry

Plots

Confirm that:

☒ The axis labels state the marker and fluorochrome used (e.g. CD4-FITC).

☒ The axis scales are clearly visible. Include numbers along axes only for bottom left plot of group (a 'group' is an analysis of identical markers).

☒ All plots are contour plots with outliers or pseudocolor plots.

☒ A numerical value for number of cells or percentage (with statistics) is provided.

Methodology

Sample preparation	Tumor samples were processed using the tumor dissociation kit, mouse (Miltenyi, Bergisch Gladbach, Germany) following manufacture's protocol. Spleens were manually disaggregated and filtered with a 70 µm strainer following digestion with the ACK lysis buffer (Lonza, Basel, Switzerland). Samples were then stained and processed as previously described (ref 29 from article) with two deviations: samples were not barcoded and 3% paraformaldehyde was used instead.
Instrument	-For CyTOF experiment (Figure 5e-f and Figure 6a) we used Helios mass cytometer (Fluidigm, South San Francisco, CA) -Flow cytometry for CD8 depletion validation (Extended Data Figure 6d): Attune Nxt Acoustic Focusing Cytometer
Software	FlowJo software (v10.4.2, Ashland, OR) and Cytofkit (version 1.20.0).
Cell population abundance	We didn't perform any sorting. Not applicable.
Gating strategy	Gating strategy can be found on Supplementary Figure 2: a, Gating strategy for CD8 depletion validation. Splenocytes were first gated based on physical parameters (FSC-H vs SSC-H). Then, we excluded doublets using FSC-H vs FSC-A. Singlets were selected for viable cells (LiveDead vs SSC-H) and then gated for CD45 positive cells (CD45-Brilliant Violet vs SSC-H). We then gate CD4 vs CD8 to quantify the number of CD8 positive cells. b, Gating strategy for CD45+ cells. First, we checked the stability over time (data not shown) and excluded the beads (140Ce vs 193Ir). Singlets were gated based on 193Ir and CD45 cells were selected and used as an input for CyTOF analysis using Cytofkit.

☒ Tick this box to confirm that a figure exemplifying the gating strategy is provided in the Supplementary Information.

nature cancer

SUPPLEMENTARY INFORMATION

https://doi.org/10.1038/s43018-019-0003-0

In the format provided by the authors and unedited.

PAK4 inhibition improves PD-1 blockade immunotherapy

**Gabriel Abril-Rodriguez[1,2], Davis Y. Torrejon[1], Wei Liu[3,4], Jesse M. Zaretsky[1], Theodore S. Nowicki[5], Jennifer Tsoi[1], Cristina Puig-Saus[1], Ignacio Baselga-Carretero[1], Egmidio Medina[1], Michael J. Quist[1], Alejandro J. Garcia[1], William Senapedis[6], Erkan Baloglu[6], Anusha Kalbasi[7,8,9], Gardenia Cheung-Lau[1], Beata Berent-Maoz[1], Begoña Comin-Anduix[8,9], Siwen Hu-Lieskovan[1,9], Cun-Yu Wang[3,4], Catherine S. Grasso[1,11] and Antoni Ribas[1,2,8,9,10,11]*

[1]Department of Medicine, Division of Hematology and Oncology, University of California, Los Angeles, Los Angeles, CA, USA. [2]Department of Molecular and Medical Pharmacology, University of California, Los Angeles, Los Angeles, CA, USA. [3]Laboratory of Molecular Signaling, Division of Oral Biology and Medicine, School of Dentistry, University of California, Los Angeles, Los Angeles, CA, USA. [4]Department of Bioengineering, Henry Samueli School of Engineering and Applied Science, University of California, Los Angeles, Los Angeles, CA, USA. [5]Department of Pediatrics, Division of Pediatric Hematology and Oncology, University of California, Los Angeles, Los Angeles, USA. [6]Karyopharm Therapeutics, Newton, MA, USA. [7]Department of Radiation Oncology, University of California, Los Angeles, Los Angeles, CA, USA. [8]Department of Surgery, Division of Surgical Oncology, University of California, Los Angeles, Los Angeles, CA, USA. [9]Jonsson Comprehensive Cancer Center, Los Angeles, CA, USA. [10]Parker Institute for Cancer Immunotherapy, San Francisco, CA, USA. [11]These authors contributed equally: Catherine S. Grasso, Antoni Ribas. *e-mail: aribas@mednet.ucla.edu

Supplementary Figure 1

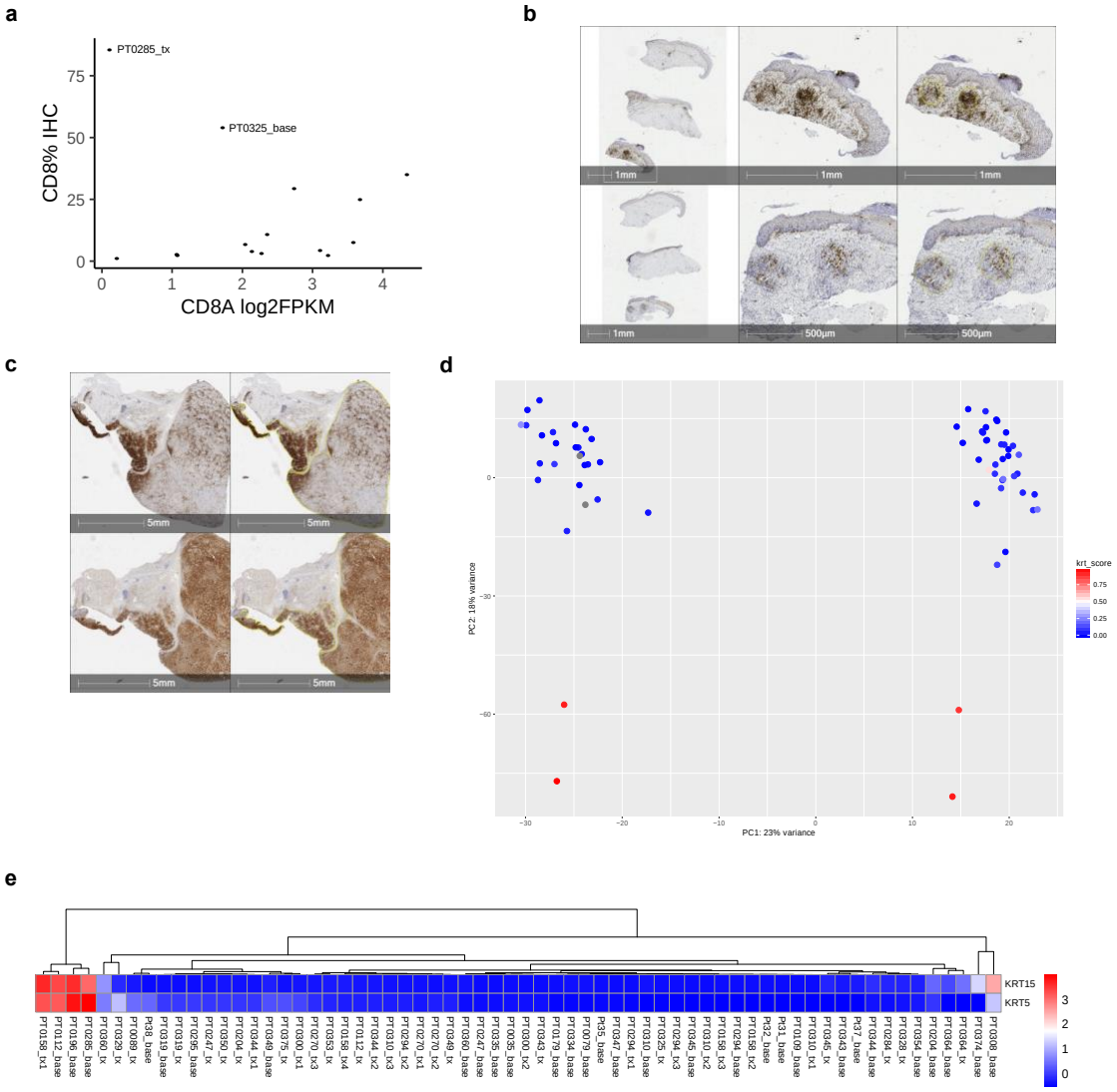

Supplementary Figure 1: Biopsy sample exclusion criteria. a, Scatterplot between percentage of CD8 T cells by immunohistochemistry and *CD8A* gene expression by RNA-seq. PT0285_tx and PT0325_base show high T cell infiltration by immunohistochemistry and was not captured by RNA-seq and therefore they were excluded from the analysis. **b, c,** Immunohistochemistry images for PT0285_tx (**b**) and PT0325_base (**c**). Slides were stained with CD8 (top) and S100 (bottom). **d**, Principal component analysis revealed four outlier samples (n = 64)**. e**, Heatmap showing that these samples are outliers with respect to overexpression of keratinocyte biomarkers *KRT15* and *KRT5*, flagging them for exclusion from further analysis (n= 64).

Supplementary Figure 2

a

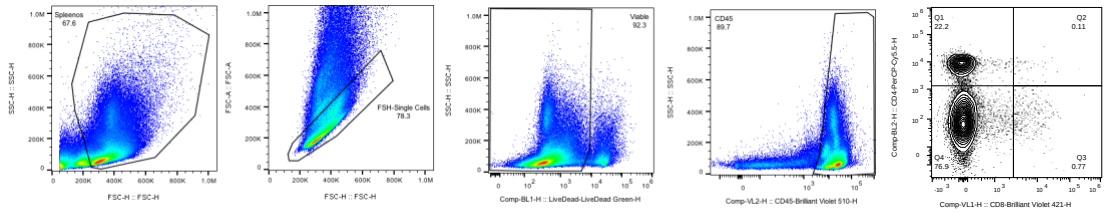

b

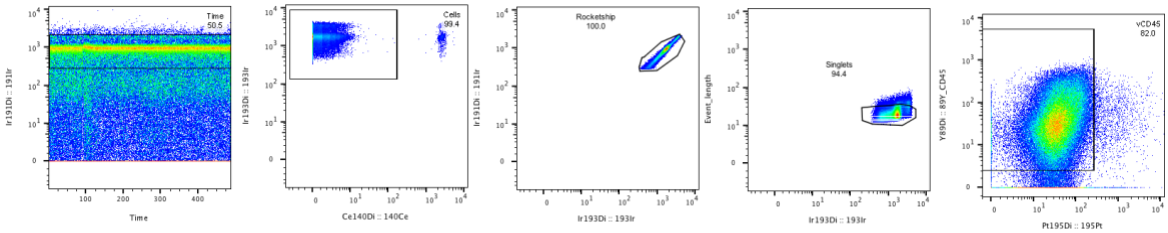

Supplementary Figure 2: **Gating strategy for CD8 depletion validation**. Splenocytes were first gated based on physical parameters (FSC-H vs SSC-H). Then, we excluded doublets using FSC-H vs FSC-A. Singlets were selected for viable cells (LiveDead vs SSC-H) and then gated for CD45 positive cells (CD45-Brilliant Violet vs SSC-H). We then gate CD4 vs CD8 to quantify the number of CD8 positive cells. b, Gating strategy for CD45+ cells. First, we checked the stability over time (data not shown) and excluded the beads (140Ce vs 193Ir). Singlets were gated based on 193Ir and CD45 cells were selected and used as an input for CyTOF analysis using Cytofkit.

Supplementary information

Supplementary tables for: Abril-Rodriguez G, Torrejon DY, Liu W, et al. PAK4 inhibition improves PD-1 blockade immunotherapy. Nat Cancer. 2020;1(1):46-58. doi:10.1038/s43018-019-0003-0

Supplementary table 1. Detailed description of the clinical information of the 60 patients used for analysis.

unique patient ID	scenario	response_biopsy	response_irRECIST
Pt31_base	base		PD
Pt32_base	base		PD
Pt35_base	base		PR
Pt37_base	base		PR
Pt38_base	base		PR
PT0035_base	base		PD
PT0079_base	base		PD
PT0089_tx	tx	PR	PR
PT0109_base	base		CR
PT0112_tx	tx	PD	PD
PT0158_tx4	tx	PD	PR
PT0158_tx2	tx	PD	PR
PT0158_tx3	tx	PD	PR
PT0179_base	base		PD
PT0204_base	base		PD
PT0204_tx	tx	PD	PD
PT0247_base	base		PD
PT0247_tx	tx	PD	PD
PT0270_tx1	tx	PR	PD
PT0270_tx2	tx	PR	PD
PT0270_tx3	tx	PR	PD
PT0284_tx	tx	CR	CR
PT0294_tx2	tx	SD	PD
PT0294_base	base		PD
PT0294_tx3	tx	PR	PD
PT0294_tx1	tx	SD	PD
PT0295_base	base		PD
PT0300_tx2	tx	PD	SD
PT0300_tx1	tx	NE	SD
PT0308_base	base		CR
PT0310_tx3	tx	PR	PR
PT0310_base	base		PR
PT0310_tx2	tx	PR	PR
PT0310_tx1	tx	PD	PR
PT0319_base	base		PD
PT0319_tx	tx	PD	PD
PT0325_tx	tx	PR	PR
PT0328_tx	tx	NE	PD
PT0329_tx	tx	NE	PD
PT0334_base	base		PD
PT0335_base	base		PD
PT0343_base	base		PR
PT0343_tx	tx	PR	PR
PT0344_tx2	tx	PD	PD
PT0344_tx1	tx	SD	PD
PT0344_base	base		PD
PT0345_base	base		PR
PT0345_tx	tx	PR	PR
PT0347_base	base		PR
PT0349_base	base		CR
PT0349_tx	tx	CR	CR
PT0350_tx	tx	PR	PR
PT0353_tx	tx	PD	PD
PT0354_base	base		PD
PT0360_base	base		PD
PT0360_tx	tx	PD	PD
PT0364_base	base		PD
PT0364_tx	tx	PD	PD
PT0374_base	base		PD
PT0375_tx	tx	PD	PD

age start of	sex	disease_sta	OS	OS_SOR	Date of biop	Cycle 1 day	Anatomical	BRAF	NRAS	NF1
47	M	M1c	704	Alive	2/22/13	1/13/14	Sigmoid colo	V600E		
47	M	M1c	171	Dead	4/16/14	9/29/14	Abdominal w	V600E		
65	F	M1c	427	Alive	8/1/14	11/3/14	Flank	V600E		
70	F	M1c	364	Alive	6/12/12	9/13/13	Small bowel	K483T, D594N		
57	F	M1c	448	Alive	9/11/13	10/16/14	Cervical, LN	-		
59	M	M1c	327	Dead	12/7/12	1/4/13	L lower abdo	V600E		
84	M	M1c	269	Dead	2/13/12	9/27/12	Lung	-		
60	M	M1b	945	Dead	6/28/12	3/5/12	Lung			
69	M	M1a	NA	Alive	5/19/14	NA	R leg, SC	V600R		
85	M	M1c	282	Dead	6/20/12	4/20/12	Left arm			
64	M	M1c	1328	Dead	12/11/13	1/22/13	Left groin	Base is V600E		
64	M	M1c	1328	Dead	7/18/13	1/22/13	L inguinal LN	Base is V600E		
64	M	M1c	1328	Dead	8/15/13	1/22/13	R flank	Base is V600E		
65	M	M1c	666	Dead	7/24/13	7/31/13	Lung	V600E		
66	F	M1b	607	Dead	1/27/12	2/13/12	L posterior th	WT	Q61L	
66	F	M1b	607	Dead	3/12/12	2/13/12	Back of left lo	WT		
55	M	M1c	182	Dead	1/3/13	1/8/13	L Flank	V600E		
55	M	M1c	182	Dead	3/13/13	1/8/13	Axillary LN			
58	M	M1c	503	Dead	4/25/12	1/4/12	R axillary LN	Base is V600E		
58	M	M1c	503	Dead	7/20/12	1/4/12	Tumor 1	Base is V600E		
58	M	M1c	503	Dead	7/20/12	1/4/12	Tumor 2	Base is V600E		
71	M	M1c	2008	Alive	7/10/12	4/17/12	L inguinal	Base is WT		R440*
70	M	M1b	980	Dead	3/26/14	10/15/12	R supraclavicular			
70	M	M1b	980	Dead	10/4/12	10/15/12	R claviculae	WT	G13D	Q1255*
70	M	M1b	980	Dead	10/30/14	10/15/12	R chest			
70	M	M1b	980	Dead	11/7/12	10/15/12	R supraclavicular			
77	M	M1b	282	Dead	9/24/12	9/27/12	Lung			
45	M	M1c	684	Dead	1/17/13	5/3/12	right groin LN	Base is WT		
45	M	M1c	684	Dead	6/5/12	5/3/12	Groin	Base is WT		
68	M	M0	1809	Alive	9/5/12	9/24/12	L upper arm	V600K		
61	M	M1c	1875	Alive	4/8/13	10/3/12	L flank			
61	M	M1c	1875	Alive	9/5/12	10/3/12	L Chestwall,	V600E		
61	M	M1c	1875	Alive	1/14/13	10/3/12	L flank			
61	M	M1c	1875	Alive	10/23/12	10/3/12	L Chestwall			
59	F	M1c	203	Dead	1/8/13	1/10/13	R armpit	WT	NRAS mut	
59	F	M1c	203	Dead	2/20/13	1/10/13	No annotated in care connect			
45	M	M1c	1456	Alive	3/11/14	2/1/13	Chest			
76	M	M1c	199	Dead	4/17/13	6/2/13	Leg	Base is WT		
81	M	M1b	168	Dead	3/20/13	2/27/13	Scalp	Base is WT		
55	F	M1c	662	Dead	8/8/13	8/15/13	Crown/scalp	WT	-	-
63	F	M1c	337	Dead	8/29/14	9/4/13	L clavicle	-	Q61R	K615K Splice
51	M	M1c	1579	Alive	6/6/13	6/7/13	L forearm, S	V600E	-	-
51	M	M1c	1579	Alive	8/5/13	6/7/13	L forearm			
44	F	M1c	317	Dead	2/6/14	10/9/13	Inner thigh			
44	F	M1c	317	Dead	10/30/13	10/9/13	R infrapubic			
44	F	M1c	317	Dead	10/7/13	10/9/13	R upper leg/	V600E		
62	M	M1c	1489	Alive	6/3/13	6/7/13	Adrenal	L331F	-	S2597*
62	M	M1c	1489	Alive	7/22/13	6/7/13	Adrenal			
55	M	M1c	1570	Alive	6/4/13	6/21/13	Lung	WT	-	Frame_Shift
53	F	M1c	1456	Alive	6/6/13	6/14/13	Lower back,	V600E	-	-
53	F	M1c	1456	Alive	8/23/13	6/14/13	L scapula			
38	M	M1c	1580	Alive	8/26/13	6/17/13	Liver	V600E		
45	F	M1c	149	Dead	8/12/13	7/2/13	R armpit	WT		
74	M	M1c	262	Dead	7/30/13	7/31/13	L Outer Ingui	-	-	-
63	M	M1c	103	Dead	10/4/13	10/8/13	L leg	V600K	-	-
63	M	M1c	103	Dead	10/30/13	10/8/13	L leg			
58	M	M1c	401	Dead	11/5/13	11/20/13	Chest			
58	M	M1c	401	Dead	12/17/13	11/20/13	Chest			
27	F	M1c	115	Dead	1/17/14	1/17/14	R neck, SC	V600E	-	R2349C
19	M	M1b	186	Dead	4/30/14	2/10/14	Lung	V600E	-	-

Study	Treatment	disease_ori	previous therapies
	Pembrolizumab		
	Pembrolizumab		
	Pembrolizumab		
	Pembrolizumab		
	Pembrolizumab		
Merck MK-3	Pembrolizum	Cutaneous	Surgery, Ipilimumab, peginterferon alfa-2b, vemurafenib, vemurafenib + combimetinib
Merck MK-3	Pembrolizum	Cutaneous	Surgery, RT, Ipi, MORAb-004
Merck MK-3	Pembrolizum	Cutaneous	Surgery, BCG injections
Merck MK-3	Pembrolizumab		
Merck MK-3	Pembrolizum	Cutaneous	Surgery, RT
Merck MK-3	Pembrolizum	Unknown pry	Surgery, RT, F5 TCR vaccination, ipilimumab, Vemurafenib, E7080
Merck MK-3	Pembrolizum	Unknown pry	Surgery, RT, F5 TCR vaccination, ipilimumab, Vemurafenib, E7080
Merck MK-3	Pembrolizum	Unknown pry	Surgery, RT, F5 TCR vaccination, ipilimumab, Vemurafenib, E7080
Merck MK-3	Pembrolizum	Cutaneous	RT to brain met, ipi, braf or mek inhibitor
Merck MK-3	Pembrolizum	Cutaneous	Surgery, ipi, temozolamide + sunitinib,
Merck MK-3	Pembrolizum	Cutaneous	Surgery, ipi, temozolamide + sunitinib,
Merck MK-3	Pembrolizum	Cutaneous	Surgery, RT, ipi, interferon alpha-2b, vemurafenib
Merck MK-3	Pembrolizum	Cutaneous	Surgery, RT, ipi, interferon alpha-2b, vemurafenib
Merck MK-3	Pembrolizum	Unknown pry	BRAF and or MEK
Merck MK-3	Pembrolizum	Unknown pry	BRAF and or MEK
Merck MK-3	Pembrolizum	Unknown pry	BRAF and or MEK
Merck MK-3	Pembrolizum	Cutaneous	Surgery, RT, cisplatin + vinblastine + temozolomide + interferon + interleukin-2, high dose IL-2, ipilimumab
Merck MK-3	Pembrolizum	Cutaneous	Surgery, GM-CSF
Merck MK-3	Pembrolizum	Cutaneous	Surgery, GM-CSF
Merck MK-3	Pembrolizum	Cutaneous	Surgery, GM-CSF
Merck MK-3	Pembrolizum	Cutaneous	Surgery, GM-CSF
Merck MK-3	Pembrolizum	Mucosal	Surgery, RT
Merck MK-3	Pembrolizum	Cutaneous	Surgery
Merck MK-3	Pembrolizum	Cutaneous	Surgery
Merck MK-3	Pembrolizum	Cutaneous	Surgery, RT, vemurafenib
Merck MK-3	Pembrolizum	Cutaneous	Surgery, ipilimumab, TIL tx, chemo for TIL tx, vemurafenib
Merck MK-3	Pembrolizum	Cutaneous	Surgery, ipilimumab, TIL tx, chemo for TIL tx, vemurafenib
Merck MK-3	Pembrolizum	Cutaneous	Surgery, ipilimumab, TIL tx, chemo for TIL tx, vemurafenib
Merck MK-3	Pembrolizum	Cutaneous	Surgery, ipilimumab, TIL tx, chemo for TIL tx, vemurafenib
Merck MK-3	Pembrolizum	Unknown Pri	RT, NIH ACT x2 (TIL, MAGE-A3 modified), ipilimumab, IL-2
Merck MK-3	Pembrolizum	Unknown Pri	RT, NIH ACT x2 (TIL, MAGE-A3 modified), ipilimumab, IL-2
Merck MK-3	Pembrolizum	Cutaneous	Surgery, RT, ipi
Merck MK-3	Pembrolizum	Cutaneous; s	Surgery, RT, ipi, carboplatin + taxol, temozolamide
Merck MK-3	Pembrolizum	Cutaneous;d	Surgery, ipi
Merck MK-3	Pembrolizum	Cutaneous	Surgery, ipi, caboplatinum + taxol
Merck MK-3	Pembrolizum	Cutaneous	Surgery, ipi
Merck MK-3	Pembrolizum	Cutaneous	ipi, vemurafenib
Merck MK-3	Pembrolizum	Cutaneous	ipi, vemurafenib
Merck MK-3	Pembrolizum	Acral; R plan	Surgery, ipilimumab (alongside vemurafenib), vemurafenib, vemurafenib + PLX3397
Merck MK-3	Pembrolizum	Acral; R plan	Surgery, ipilimumab (alongside vemurafenib), vemurafenib, vemurafenib + PLX3397
Merck MK-3	Pembrolizum	Acral; R plan	Surgery, ipilimumab (alongside vemurafenib), vemurafenib, vemurafenib + PLX3397
Merck MK-3	Pembrolizum	Unclear; disc	Surgery, RT
Merck MK-3	Pembrolizum	Unclear; disc	Surgery, RT
Merck MK-3	Pembrolizum	Unclear; pres	RT
Merck MK-3	Pembrolizum	Cutaneous	Surgery
Merck MK-3	Pembrolizum	Cutaneous	Surgery
Merck MK-3	Pembrolizum	Cutaneous	Surgery
Merck MK-3	Pembrolizum	Mucosal	RT to brain, ipi, Gleevec, Temodar
Merck MK-3	Pembrolizum	Cutaneous	Surgery, ipi
Merck MK-3	Pembrolizum	Cutaneous	Surgery, RT, ipi, vemurafenib, temozolamide + cisplatin + vinblastine + interferon + IL2
Merck MK-3	Pembrolizum	Cutaneous	Surgery, RT, ipi, vemurafenib, temozolamide + cisplatin + vinblastine + interferon + IL2
BMS CA209-	Nivolumab	Cutaneous	Surgery, RT, ipi, temozolamide
BMS CA209-	Nivolumab	Cutaneous	Surgery, RT, ipi, temozolamide
Merck MK34	Pembrolizum	Cutaneous; s	Surgery, RT, TIL infusion w/ prior chemo and RT conditioning, vemurafenib, Cytoxan + fludarabine as condi
Merck MK34	Pembrolizum	Cutaneous	BRAF and or MEK

Supplementary table 2A: Differential gene expression analysis between upper and lower quartile of dendritic cell score. Showing genes enriched in the low dendritic cell group.

gene	baseMean	log2FoldChange	lfcSE	stat	pvalue	padj
GPI	20437.101	1.170261859	0.1862642	6.2828058	3.33E-10	3.06E-08
CNKSR3	1644.8013	2.378900208	0.4002603	5.9433832	2.79E-09	2.07E-07
ITPKA	153.51751	3.075361448	0.528283	5.8214282	5.83E-09	3.83E-07
PTPRN	911.82116	4.993903696	0.8645681	5.7761831	7.64E-09	4.87E-07
APCDD1	9064.8585	4.64203725	0.8036121	5.7764652	7.63E-09	4.87E-07
RNFT2	199.57573	2.014865933	0.360327	5.5917701	2.25E-08	1.31E-06
NKD1	2251.4788	3.977099531	0.7199402	5.5242082	3.31E-08	1.83E-06
TOMM34	3237.1728	1.316061365	0.239685	5.4907962	4.00E-08	2.15E-06
SLC38A8	53.293317	6.398504956	1.1686737	5.4750139	4.37E-08	2.34E-06
NRAP	46.524662	5.078605187	0.9325576	5.4458888	5.15E-08	2.68E-06
SLC35E4	824.17447	1.650105941	0.3036186	5.4347981	5.49E-08	2.83E-06
DPF1	113.23191	1.973894066	0.3647733	5.4112891	6.26E-08	3.18E-06
RFNG	2148.4631	1.028814301	0.1904282	5.4026368	6.57E-08	3.31E-06
SP5	571.0496	5.795877324	1.0766251	5.3833755	7.31E-08	3.62E-06
GPR39	738.55297	4.397509507	0.8352613	5.2648312	1.40E-07	6.42E-06
TMEM189	2739.2461	1.093817557	0.2079348	5.260388	1.44E-07	6.54E-06
ACO2	9642.5629	1.299972989	0.2474086	5.2543572	1.49E-07	6.73E-06
GPC1	13648.157	3.37613282	0.643728	5.2446576	1.57E-07	7.08E-06
DNAJB1	11730.605	1.205152626	0.2316165	5.203224	1.96E-07	8.61E-06
ONECUT2	396.14645	3.626152888	0.6985857	5.1907058	2.09E-07	9.11E-06
SLC1A5	14325.666	1.939282721	0.3741058	5.1837816	2.17E-07	9.37E-06
PAK4	3208.4323	1.155104701	0.2249118	5.1358123	2.81E-07	1.19E-05
ESPN	274.88854	3.811009485	0.7429295	5.1297054	2.90E-07	1.22E-05
CIT	2712.7044	1.471022033	0.2869754	5.125951	2.96E-07	1.24E-05
TRIB3	4980.3364	2.049526016	0.400997	5.1110752	3.20E-07	1.33E-05
KLHDC8A	156.86839	4.115646907	0.8082856	5.0918228	3.55E-07	1.46E-05
MSX1	437.76175	1.603963591	0.3150909	5.0904796	3.57E-07	1.46E-05
GAP43	2447.5338	5.02900688	0.9900466	5.079566	3.78E-07	1.54E-05
FAM19A5	1721.3673	3.790628082	0.7546784	5.0228393	5.09E-07	2.00E-05
HES6	2054.2813	2.741225655	0.5462145	5.018588	5.21E-07	2.03E-05
ALDOA	61654.985	1.197328087	0.2391119	5.0073975	5.52E-07	2.13E-05
CCDC74B	30.333758	3.650335497	0.7293423	5.0049689	5.59E-07	2.15E-05
FNTB	2252.6564	2.676647629	0.53673	4.9869539	6.13E-07	2.33E-05
PMP2	2056.5516	5.450317291	1.0941381	4.9813799	6.31E-07	2.38E-05
ARC	701.37478	4.135708592	0.8302933	4.9810214	6.32E-07	2.38E-05
TTLL12	3565.1407	1.173545164	0.2363057	4.9662169	6.83E-07	2.54E-05
SWI5	1319.5175	1.097425315	0.2223851	4.9347968	8.02E-07	2.93E-05
PARVB	6234.7599	1.573390667	0.3189788	4.932587	8.11E-07	2.95E-05
SLAMF9	320.9587	4.045054078	0.822444	4.9183338	8.73E-07	3.14E-05
CFAP77	59.003119	3.672547953	0.7489731	4.9034442	9.42E-07	3.37E-05
DPH3P1	380.55472	1.857118097	0.3789108	4.9012013	9.53E-07	3.39E-05
BNIP3	973.52429	1.839562657	0.3788627	4.855486	1.20E-06	4.15E-05

HSPA1B	4211.4357	1.811004883	0.3741614	4.84017	1.30E-06	4.42E-05
NRTN	159.88092	3.468208592	0.7251011	4.7830687	1.73E-06	5.70E-05
ADCY2	401.7384	3.893884643	0.8166397	4.7681792	1.86E-06	6.08E-05
ISM2	9.6701889	2.917396875	0.6118384	4.7682475	1.86E-06	6.08E-05
BARX1	36.210624	3.99805859	0.8387246	4.7668311	1.87E-06	6.09E-05
ZNRF3	1367.4841	1.749771654	0.3680483	4.7541897	1.99E-06	6.43E-05
DHRS2	413.23059	3.856584873	0.8134868	4.7408084	2.13E-06	6.83E-05
NPW	64.666702	3.1793424	0.6709881	4.7382996	2.16E-06	6.91E-05
XPNPEP3	1533.9678	1.151996821	0.2431998	4.7368335	2.17E-06	6.94E-05
LRP1B	132.49839	4.692785991	0.9976362	4.7039052	2.55E-06	7.97E-05
HOXD11	31.09414	3.993306731	0.8501501	4.6971785	2.64E-06	8.19E-05
CFAP61	67.344985	3.196063611	0.6811037	4.692477	2.70E-06	8.36E-05
TUBA8	462.03548	2.714547412	0.5819071	4.6649156	3.09E-06	9.33E-05
SLC24A4	3996.0059	4.191110203	0.9013249	4.6499439	3.32E-06	9.96E-05
METAP1D	727.29294	1.284446564	0.2762721	4.6492091	3.33E-06	9.98E-05
LMF2	8515.0902	1.326191148	0.2865176	4.6286557	3.68E-06	0.0001092
FAT1	11852.878	1.396733531	0.301835	4.6274735	3.70E-06	0.0001097
COMT	13390.754	1.902958173	0.4116245	4.6230445	3.78E-06	0.0001117
EEF1A2	2184.7826	4.352885093	0.9462253	4.600263	4.22E-06	0.0001216
ZP1	67.702514	3.7316213	0.8118328	4.596539	4.30E-06	0.0001234
OPRK1	8.5193417	5.511059038	1.1997035	4.5936843	4.35E-06	0.0001248
OSGIN1	783.83022	1.648488187	0.3598138	4.5815039	4.62E-06	0.0001311
VIM	259294.04	1.007019024	0.2203631	4.5698164	4.88E-06	0.0001374
CHST10	1601.0363	1.042929066	0.2286553	4.5611418	5.09E-06	0.0001422
SOWAHC	1157.9932	1.102775106	0.2418336	4.5600569	5.11E-06	0.0001424
BAG3	3841.2672	1.131053291	0.2480931	4.558987	5.14E-06	0.0001428
SLC25A1	4072.4214	1.316695887	0.2900528	4.539504	5.64E-06	0.0001541
SCN5A	53.683901	2.857190526	0.6311799	4.5267449	5.99E-06	0.0001615
IL36RN	35.534126	3.90808958	0.8643943	4.5211886	6.15E-06	0.0001651
PFKFB4	1854.2354	1.794807439	0.3991178	4.4969365	6.89E-06	0.000183
C17orf53	290.00063	1.176251613	0.262107	4.487677	7.20E-06	0.0001896
CHPF	14441.323	1.417560397	0.3174955	4.4648211	8.01E-06	0.0002096
GSTT2B:2	5.1969872	3.097629354	0.6971643	4.4431845	8.86E-06	0.0002277
CRYM	193.23772	2.825922796	0.6362481	4.441542	8.93E-06	0.0002286
SLC7A4	175.74469	3.592944893	0.8107631	4.4315593	9.36E-06	0.0002375
ZNF462	2121.9123	1.118735805	0.2532013	4.4183645	9.95E-06	0.0002495
IL36B	14.647743	3.685988937	0.835008	4.414316	1.01E-05	0.0002536
FAM178B	1246.8067	3.930041667	0.8916574	4.4075694	1.05E-05	0.0002606
SCLY	955.93398	1.033345017	0.2345832	4.4050249	1.06E-05	0.0002626
TIMP2	72137.702	1.278892606	0.2908159	4.3976027	1.09E-05	0.00027
MIF	29574.444	1.405404701	0.3198843	4.3934781	1.12E-05	0.0002741
IGF1R	8236.9339	1.204750893	0.2752872	4.3763419	1.21E-05	0.0002947
SEMA3B	7609.4402	3.15841239	0.7227397	4.3700554	1.24E-05	0.0003029
TMPRSS9	246.54655	2.626197308	0.6015211	4.3659272	1.27E-05	0.0003075
HRAS	1632.6837	1.095273971	0.2509902	4.3638118	1.28E-05	0.0003101
MCAT	1147.9	1.051104174	0.24194	4.3444821	1.40E-05	0.0003332

DUSP14	1406.147	1.095946941	0.2527084	4.3368044	1.45E-05	0.000343
RTBDN	54.441555	4.265270178	0.9849348	4.3305103	1.49E-05	0.0003516
P4HA1	6382.9777	1.100975872	0.2544132	4.3275103	1.51E-05	0.0003551
MZT2A	690.79099	1.118477959	0.2588901	4.3202813	1.56E-05	0.0003665
ZNF771	409.48591	1.251083734	0.2897499	4.3178051	1.58E-05	0.0003688
ANO7	144.09598	1.319342004	0.306223	4.3084357	1.64E-05	0.0003811
SLC9A2	182.9201	4.202389169	0.9776139	4.2986186	1.72E-05	0.000395
LONP1	7252.1778	1.042675098	0.2430425	4.2900944	1.79E-05	0.0004071
TMEM249	49.418728	1.547288552	0.3609922	4.2862105	1.82E-05	0.0004123
RIPK4	3282.5848	2.912000571	0.6805942	4.2786153	1.88E-05	0.0004241
VAT1	33489.121	1.237135319	0.2899157	4.2672244	1.98E-05	0.0004422
LRRC45	1254.0453	1.026820142	0.2407442	4.2651923	2.00E-05	0.0004457
CLDN14	147.16379	2.983389749	0.700904	4.2564887	2.08E-05	0.0004607
WFS1	2599.0738	1.070411139	0.2516401	4.2537387	2.10E-05	0.0004648
PMEPA1	7864.3931	2.274002122	0.5360926	4.2418082	2.22E-05	0.0004863
FN3K	1876.0525	1.575678351	0.3715571	4.2407433	2.23E-05	0.000488
TTLL1	928.90262	1.312808503	0.3101118	4.23334	2.30E-05	0.0005032
PERM1	88.658962	1.947870625	0.4622242	4.2141248	2.51E-05	0.0005376
WDR54	894.44169	1.098231303	0.2607614	4.2116326	2.54E-05	0.0005424
DIP2C	5507.7257	1.312527339	0.3124696	4.2004962	2.66E-05	0.0005666
CA12	1879.0994	2.470623165	0.5897924	4.1889706	2.80E-05	0.0005929
OR51B5	11.807045	4.096189067	0.9794399	4.1821751	2.89E-05	0.0006079
AVPI1	1873.8409	1.994910664	0.4772846	4.1797085	2.92E-05	0.0006128
HSPA1A	5542.3525	1.391996718	0.3331789	4.1779261	2.94E-05	0.0006163
IGLON5	57.478059	2.624421389	0.6287996	4.1737006	3.00E-05	0.0006251
RNF182	864.17066	2.91545457	0.6988543	4.1717633	3.02E-05	0.0006277
SLC3A2	15983.118	1.192956254	0.2859536	4.1718526	3.02E-05	0.0006277
MEX3D	1440.2853	1.048568465	0.2514403	4.1702475	3.04E-05	0.0006285
ENO1	84443.236	1.190291567	0.2873851	4.1417998	3.45E-05	0.0006997
EME1	535.97661	1.515056821	0.3660256	4.1392098	3.49E-05	0.0007069
TM4SF19	364.35318	2.593986252	0.627086	4.136572	3.53E-05	0.0007136
LCN2	70.907614	3.780882617	0.9143579	4.1350138	3.55E-05	0.0007177
CHRND	11.669543	3.326273741	0.8070845	4.1213449	3.77E-05	0.0007544
WDR31	305.50162	1.049113449	0.25472	4.1186927	3.81E-05	0.0007605
DDIT3	2806.707	1.725518959	0.4190366	4.1178239	3.82E-05	0.0007621
PPFIA4	425.77571	1.806022366	0.4391817	4.1122438	3.92E-05	0.0007746
VPS37D	185.5173	1.220191837	0.2968274	4.1107786	3.94E-05	0.0007776
C9orf129	19.285589	4.214670633	1.0274186	4.1021942	4.09E-05	0.0008037
NUP93	5140.0525	1.213307713	0.2961292	4.0972247	4.18E-05	0.0008187
USP11	8410.8774	1.132343001	0.2765432	4.094633	4.23E-05	0.0008244
CYB5R2	1869.235	2.926508701	0.716504	4.0844273	4.42E-05	0.0008512
SLC2A1	5514.3482	1.264847714	0.309801	4.0827751	4.45E-05	0.0008556
P4HB	63685.449	1.129446454	0.277217	4.074233	4.62E-05	0.0008823
UCN2	1162.7535	3.2503279	0.7980423	4.0728768	4.64E-05	0.0008865
GAD1	272.80529	3.419546581	0.8400748	4.0705262	4.69E-05	0.0008927
DLX2	79.846436	2.68717152	0.6604959	4.0684151	4.73E-05	0.0008992

SRXN1	2995.0135	1.021349789	0.2511902	4.0660423	4.78E-05	0.0009056
CDT1	990.1377	1.214414694	0.298745	4.065054	4.80E-05	0.0009069
ESM1	793.79274	2.036746994	0.5026593	4.0519431	5.08E-05	0.000948
CCDC74A	143.88096	2.473492365	0.6121223	4.0408467	5.33E-05	0.0009863
MED15	9503.1924	1.01778666	0.2522705	4.0345046	5.47E-05	0.0010078
PEX10	1905.036	1.060431373	0.2630369	4.0314933	5.54E-05	0.0010186
NCAPH2	4700.5384	1.127244871	0.2796466	4.0309628	5.55E-05	0.0010199
UPK1A	47.026932	2.410475471	0.5999681	4.017673	5.88E-05	0.0010719
SOX12	2647.2796	1.164995388	0.2899676	4.0176739	5.88E-05	0.0010719
NAV2	8528.4872	1.436866388	0.3579658	4.0139771	5.97E-05	0.0010828
C10orf126	8.9940517	4.513233127	1.1259882	4.0082418	6.12E-05	0.0011041
PES1	7303.3271	1.05255145	0.2631184	4.0002954	6.33E-05	0.0011344
CHADL	172.35862	1.909863194	0.4782356	3.9935616	6.51E-05	0.0011595
OPRD1	53.834216	3.609001711	0.9046326	3.9894668	6.62E-05	0.0011721
CBARP	266.152	1.601704281	0.4017859	3.9864617	6.71E-05	0.0011841
GGA1	4923.0641	1.040729686	0.2615581	3.9789617	6.92E-05	0.0012128
MRPS2	2490.5426	1.049927879	0.2640516	3.9762229	7.00E-05	0.0012239
FASN	22708.036	1.592265809	0.400598	3.9747221	7.05E-05	0.0012289
PLPPR4	2492.7097	3.255142737	0.8195614	3.9718106	7.13E-05	0.0012384
CNP	14757.311	1.112855086	0.2801833	3.9718817	7.13E-05	0.0012384
ZNF703	4246.7894	1.67686507	0.4225674	3.9682785	7.24E-05	0.0012535
NR4A1	3299.0575	1.560724166	0.3944299	3.956911	7.59E-05	0.0013029
KDELR3	4107.2958	1.211894206	0.3063034	3.9565153	7.61E-05	0.0013039
MAFF	3077.8001	1.458547045	0.3694236	3.9481699	7.88E-05	0.001343
CEP170B	4896.2445	1.438705665	0.3648649	3.9431193	8.04E-05	0.0013655
CRMP1	1277.4458	1.500822632	0.3811953	3.9371483	8.25E-05	0.0013937
IFT27	1284.9323	1.22148135	0.3102965	3.9364977	8.27E-05	0.0013963
B3GNT7	1474.5555	2.086798946	0.5302002	3.9358694	8.29E-05	0.0013975
HM13	12767.533	1.022374716	0.2599399	3.9331196	8.39E-05	0.0014111
PNCK	85.03719	2.243695423	0.5705626	3.9324261	8.41E-05	0.0014139
ATAD3A	2025.4859	1.079997998	0.2754586	3.9207273	8.83E-05	0.001474
ACP7	20.115859	3.494275728	0.8914208	3.919895	8.86E-05	0.0014778
ARHGDIA	25164.21	1.041437661	0.2659387	3.9160823	9.00E-05	0.0014965
RNF144A	4425.0804	1.015095734	0.2593933	3.9133461	9.10E-05	0.0015093
SPHK1	2832.2818	1.64076608	0.4197165	3.9092247	9.26E-05	0.00153
MTCL1	991.20035	1.762604764	0.4511024	3.9073278	9.33E-05	0.0015392
KCNJ14	117.61043	1.045338615	0.2683146	3.8959434	9.78E-05	0.0015957
BAIAP2	3189.0974	1.01864035	0.2615303	3.8949222	9.82E-05	0.0016011
SH3BGR	155.12786	1.639291524	0.421276	3.8912533	9.97E-05	0.00162
UBE2S	2530.5834	1.23527285	0.317638	3.8889332	0.0001007	0.0016328
E2F1	1755.9538	1.264478505	0.3252899	3.887236	0.0001014	0.0016428
KCNG1	369.32723	2.544143815	0.6546772	3.886104	0.0001019	0.0016491
ANKRD37	447.0346	1.213243992	0.3127089	3.8797867	0.0001045	0.0016856
DCXR	2769.1204	1.321292311	0.3408993	3.8759017	0.0001062	0.0017056
ADM	2069.7808	1.893821156	0.4909469	3.8574866	0.0001146	0.0018193
TRIM62	1435.9328	1.557722436	0.4039807	3.8559328	0.0001153	0.0018278

SV2C	46.435351	2.948535024	0.76687	3.8448954	0.0001206	0.0018995
IRS2	5089.6779	1.054763194	0.2746993	3.8397014	0.0001232	0.0019259
NECAB2	44.940524	2.370066715	0.6175862	3.8376292	0.0001242	0.0019407
MAP6D1	235.77281	1.369879052	0.3586513	3.8195293	0.0001337	0.002052
LINGO1	3108.7904	2.232311301	0.5845596	3.8187917	0.0001341	0.0020548
SEC14L2	1469.3027	1.666969652	0.4365851	3.8182013	0.0001344	0.0020565
DHX33	4248.5782	1.393036197	0.3653148	3.8132491	0.0001372	0.0020881
CCND1	28237.76	1.485837504	0.3903632	3.8062953	0.0001411	0.002135
WNT7B	80.075461	3.053965917	0.8028134	3.8040795	0.0001423	0.0021516
SLC7A11	3122.1287	2.63324614	0.6925712	3.8021308	0.0001435	0.0021652
GNG4	568.82966	1.974717134	0.5194863	3.8012879	0.0001439	0.0021706
NOTUM	222.2643	3.286481705	0.865431	3.7975084	0.0001462	0.0021962
VSX1	7.7034419	2.803170882	0.7386233	3.7951294	0.0001476	0.002215
TTYH2	5586.1857	1.628962467	0.4292487	3.7949157	0.0001477	0.0022151
TRIML2	9.8797872	2.569193624	0.67725	3.7935678	0.0001485	0.00222
MYO1D	15510.619	1.999889958	0.5272023	3.7934018	0.0001486	0.00222
CHCHD10	3663.1736	1.987633561	0.5248959	3.7867192	0.0001526	0.00227
LOC101928841	79.509496	2.947425676	0.7784973	3.7860448	0.0001531	0.0022744
SPTB	548.6002	2.090004244	0.5523629	3.7837521	0.0001545	0.0022866
PRICKLE3	1226.3072	1.219845658	0.3224202	3.7834035	0.0001547	0.002288
PERP	5804.0176	1.6020532	0.4235901	3.7820841	0.0001555	0.0022966
RAB36	801.74529	1.897805828	0.5021285	3.7795225	0.0001571	0.002315
PAQR4	2984.6948	1.091877619	0.290185	3.7626952	0.0001681	0.0024483
PEX26	3327.9337	1.008127225	0.2680449	3.7610386	0.0001692	0.0024627
VGF	13763.392	3.66640495	0.9755027	3.7584775	0.000171	0.0024795
PSAT1	5593.5284	2.585429561	0.6880381	3.7576838	0.0001715	0.0024809
TMEM99	639.0198	1.290704923	0.3440243	3.7517841	0.0001756	0.0025305
BRINP2	40.83539	4.497929204	1.1998216	3.7488316	0.0001777	0.0025489
MZT2B	1785.6418	1.004789432	0.2681839	3.7466436	0.0001792	0.0025674
LYPD1	1660.5633	2.549757275	0.6810303	3.7439706	0.0001811	0.0025891
TK1	2136.1039	1.148252114	0.307163	3.7382504	0.0001853	0.0026408
TEKT5	84.515592	3.472186888	0.9293029	3.736335	0.0001867	0.0026531
NPTX2	4407.9347	3.305257255	0.8859822	3.7306137	0.000191	0.0027081
DHCR7	2463.9503	1.448782721	0.388405	3.7300829	0.0001914	0.0027099
MC1R	2962.8609	1.711677289	0.459171	3.7277554	0.0001932	0.0027309
POLR3H	5462.366	1.085322816	0.2912933	3.7258769	0.0001946	0.0027453
ENO2	6087.893	1.653476357	0.4438628	3.7251967	0.0001952	0.0027507
TLN2	1959.1331	1.284768819	0.3450897	3.7229992	0.0001969	0.0027666
FOXC1	875.20688	1.05075629	0.2822734	3.7224774	0.0001973	0.0027682
SLC5A4	240.06549	2.777652259	0.7466898	3.7199548	0.0001993	0.0027879
KNOP1	2259.4651	1.130973276	0.304322	3.7163703	0.0002021	0.0028154
NKAIN1	178.80669	2.619652382	0.7049334	3.7161702	0.0002023	0.0028156
PRSS3	19.46726	3.187419696	0.8589553	3.7108096	0.0002066	0.0028696
KCNU1	16.099172	3.704029885	0.9994281	3.7061494	0.0002104	0.0029145
GPR3	209.86184	1.286639813	0.3479762	3.6974941	0.0002177	0.0029968
SERINC2	1740.2227	1.192239963	0.3228833	3.6924792	0.0002221	0.0030386

SLC6A8	5243.2981	1.28343986	0.3479529	3.6885448	0.0002255	0.003077
STC2	814.36761	1.796576302	0.4887289	3.6760181	0.0002369	0.0032043
METTL9	13985.008	1.477247191	0.4032899	3.6629912	0.0002493	0.0033345
RRP7A	5719.2559	1.102086149	0.3011977	3.6590122	0.0002532	0.003382
TMEM52	33.351286	2.377983277	0.650091	3.6579238	0.0002543	0.0033916
ANKRD54	2427.415	1.107838667	0.3029932	3.6563154	0.0002559	0.0034082
FAHD1	2465.6899	1.082098372	0.2962025	3.6532384	0.000259	0.0034422
MARCH4	19.283207	2.119065083	0.5807524	3.6488273	0.0002634	0.0034945
PMAIP1	1559.9549	1.933933607	0.5300672	3.6484684	0.0002638	0.003497
HBG2	16.770212	2.967157373	0.8148447	3.6413776	0.0002712	0.0035824
HAGHL	1165.5677	1.279259549	0.3522185	3.6320056	0.0002812	0.0036796
CXCL8	1902.6457	2.602441743	0.7166337	3.6314811	0.0002818	0.003683
C4orf47	80.871531	1.568977889	0.4321051	3.6310098	0.0002823	0.0036862
RNASEH2A	1771.8497	1.105757861	0.3045612	3.6306596	0.0002827	0.0036887
HK2	6142.9265	1.017138972	0.2803229	3.6284551	0.0002851	0.0037103
NCS1	3013.5338	1.098621015	0.3028998	3.6270118	0.0002867	0.003726
ABCB6	2011.2311	1.071380031	0.2961404	3.6178116	0.0002971	0.003817
ANKRD18B	18.542026	3.87963561	1.0737719	3.613091	0.0003026	0.003869
KRT80	278.2721	2.982167019	0.826867	3.6065859	0.0003103	0.0039488
B4GALNT3	1563.9349	2.287832358	0.6349094	3.6033997	0.0003141	0.0039896
CRLF1	545.58224	2.976419903	0.8271461	3.5984209	0.0003202	0.0040543
SOGA3	543.58039	1.989343077	0.5529715	3.5975508	0.0003212	0.0040619
OLFM2	932.80248	1.77604423	0.493685	3.5975249	0.0003213	0.0040619
MAD1L1	3887.1148	1.289755662	0.3596269	3.5863717	0.0003353	0.0042008
TFRC	11120.433	1.219370051	0.3403319	3.5828854	0.0003398	0.004249
TCFL5	1824.5912	1.052310147	0.2939856	3.5794611	0.0003443	0.004291
GVQW2	31.362602	1.262363227	0.3530379	3.5757157	0.0003493	0.0043473
ACSL3	14105.799	1.053409189	0.2950269	3.5705527	0.0003562	0.0044195
IGF2BP2	3201.3166	1.387614491	0.3894524	3.5629884	0.0003667	0.0045168
RAB32	3758.6457	1.283957611	0.3604825	3.5617756	0.0003684	0.0045284
SPATC1L	586.84933	1.294834008	0.3636202	3.560952	0.0003695	0.004533
DDT	2072.8556	1.093241696	0.306994	3.5611178	0.0003693	0.004533
TMEM179	17.84129	3.324726558	0.9341541	3.5590772	0.0003722	0.0045539
CMTM8	571.47508	1.936138643	0.5443528	3.5567717	0.0003754	0.0045808
OSBPL5	2122.9255	1.166477728	0.3280364	3.5559396	0.0003766	0.0045924
PKMYT1	1192.1951	1.391278187	0.391377	3.5548288	0.0003782	0.0046031
PCLO	1199.3486	2.440139003	0.6880179	3.5466216	0.0003902	0.0047398
MYL10	26.391144	3.730697907	1.052119	3.5458898	0.0003913	0.004747
DNAAF5	2799.7945	1.003413543	0.2833668	3.541041	0.0003986	0.0048229
ATP2B2	149.58376	2.97953126	0.8416591	3.5400688	0.0004	0.0048315
IGFBP3	12658.816	1.660176142	0.4690326	3.5395755	0.0004008	0.0048357
CCDC140	87.856362	1.825694409	0.5158494	3.5392005	0.0004013	0.0048383
ANKRD39	817.82318	1.033398188	0.2924516	3.5335699	0.00041	0.004927
GSG1	6.5042475	2.559697918	0.7246771	3.5321912	0.0004121	0.0049466
HSPB1	23582.088	1.092461317	0.3093682	3.5312658	0.0004136	0.0049608
FMN2	276.98719	3.113459473	0.8828395	3.5266426	0.0004209	0.005042

CD3EAP	1023.2281	1.500437059	0.4265051	3.5179816	0.0004348	0.00519
SLC22A18AS	290.59429	1.615670901	0.4594227	3.5167416	0.0004369	0.005211
ATG4B	4347.6607	1.049530046	0.2984696	3.5163721	0.0004375	0.005215
FAM118A	1911.6056	1.196358398	0.3408463	3.5099641	0.0004482	0.0053192
GALE	2642.3385	1.052161034	0.2998048	3.5094868	0.000449	0.0053254
HPS4	10657.838	1.611908065	0.4619696	3.4892082	0.0004845	0.0056587
ASCL4	46.351822	4.995608352	1.4318654	3.4888812	0.000485	0.0056622
TDRD3	4234.0304	1.814915268	0.5203354	3.4879716	0.0004867	0.0056781
PRKAA2	188.28596	2.176064098	0.6239292	3.4876781	0.0004872	0.0056808
HES2	192.93525	2.87201478	0.8265522	3.4746925	0.0005114	0.0058968
HYAL3	235.60314	1.203710693	0.3465622	3.4732894	0.0005141	0.0059212
COL9A3	7501.3703	2.768116696	0.7973514	3.4716394	0.0005173	0.0059409
AHNAK2	9523.1572	2.123711904	0.6120181	3.470015	0.0005204	0.0059663
SLC16A3	6398.2371	1.469553337	0.4235975	3.4692209	0.000522	0.0059803
ADRA2C	728.88956	2.461901904	0.7106501	3.4642956	0.0005316	0.0060547
ARHGEF4	351.00296	2.309400352	0.6667601	3.4636152	0.000533	0.0060665
STEAP3	2702.6964	1.873929383	0.5417127	3.4592679	0.0005416	0.0061434
TMEM59L	204.44704	2.985073125	0.8630619	3.4587012	0.0005428	0.0061527
UBE2C	2324.963	1.298115455	0.3758974	3.4533771	0.0005536	0.0062495
TTYH3	18573.071	1.00957876	0.2925613	3.4508278	0.0005589	0.0062977
VEPH1	2080.4959	2.668312573	0.7733987	3.4501127	0.0005604	0.0063107
BACE2	22401.777	1.336249201	0.3877056	3.4465567	0.0005678	0.0063794
TSPAN11	1653.4268	2.148215325	0.6233524	3.4462295	0.0005685	0.0063834
COL7A1	2012.9493	2.17387762	0.6308322	3.4460472	0.0005689	0.0063839
TRIP13	1058.7741	1.191609897	0.3459254	3.4447018	0.0005717	0.0064045
PLCD3	1204.6592	1.322853037	0.3843279	3.4419903	0.0005775	0.0064577
HS3ST2	1060.7781	2.584144667	0.7512201	3.43993	0.0005819	0.0064995
DNER	940.06108	3.660383247	1.0645731	3.4383579	0.0005853	0.006529
RASGEF1C	109.2007	2.925005346	0.8522762	3.4319923	0.0005992	0.0066501
WIPF3	488.24816	2.042410585	0.5953215	3.4307689	0.0006019	0.0066763
MARCH10	30.402144	2.306961272	0.672504	3.4304054	0.0006027	0.0066814
TRIM7	216.29414	1.404548519	0.4108231	3.4188645	0.0006288	0.0069273
TLX3	27.703928	3.641384132	1.0654559	3.4176772	0.0006316	0.0069458
CRELD2	3385.8167	1.045949359	0.306313	3.4146421	0.0006387	0.0070073
ARMC5	1291.8236	1.017502165	0.2981555	3.4126557	0.0006433	0.0070505
OBSL1	4817.1109	1.270450412	0.3724522	3.4110427	0.0006472	0.0070778
SYT1	324.37422	2.493006562	0.73129	3.4090532	0.0006519	0.0071199
FAH	2506.4253	1.153750402	0.3384536	3.4088882	0.0006523	0.0071201
ABHD14A	715.29899	1.050670194	0.3083787	3.4070774	0.0006566	0.0071635
STXBP1	8786.8565	1.284089009	0.377804	3.3988231	0.0006768	0.0073331
PTPRU	2565.1987	2.115213343	0.6229207	3.3956381	0.0006847	0.0074064
PCBP4	3760.1449	1.200071165	0.3535753	3.3941039	0.0006885	0.0074361
ETV5	16686.446	1.395772745	0.4112812	3.393719	0.0006895	0.0074417
SS18L1	2168.5348	1.213995329	0.3579011	3.3919859	0.0006939	0.0074694
SDF2L1	2363.8743	1.029571349	0.3037175	3.3898977	0.0006992	0.0075208
PSMC3IP	722.66853	1.030346683	0.3049018	3.3792742	0.0007268	0.0077652

C16orf59	380.00127	1.110489349	0.3289364	3.3760006	0.0007355	0.0078495
RAC3	702.51449	1.398789641	0.4149143	3.3712739	0.0007482	0.007928
SLC1A4	7362.3175	1.611448308	0.4784642	3.3679598	0.0007573	0.0080062
GPSM1	2152.1491	1.103213456	0.3276282	3.3672725	0.0007592	0.0080129
FAM166A	16.121783	2.232620849	0.6631364	3.3667594	0.0007606	0.0080235
KCP	272.79915	1.83813281	0.5462525	3.3649876	0.0007655	0.0080707
BEGAIN	302.48512	2.205610832	0.655667	3.3639191	0.0007684	0.0080842
ACP6	1825.2568	1.700529735	0.5058228	3.3619078	0.0007741	0.0081255
IQCK	3507.6701	1.597960191	0.4753732	3.3614857	0.0007752	0.0081335
MAP1B	11747.991	1.793590078	0.5337712	3.3602224	0.0007788	0.0081663
PSEN2	3876.7357	1.338430233	0.3985182	3.3585172	0.0007836	0.0082124
TPPP	950.01136	1.86022394	0.5545863	3.3542553	0.0007958	0.0083217
RFPL2	48.878496	2.488270938	0.7438143	3.3452854	0.000822	0.008525
CTSV	238.8535	1.703700381	0.5094554	3.3441602	0.0008253	0.008542
ENTHD1	471.72397	2.288093767	0.6842967	3.3437158	0.0008266	0.0085464
NT5M	233.97824	1.162894676	0.3478051	3.3435239	0.0008272	0.0085477
KIAA0930	13679.224	1.104239771	0.3308012	3.3380762	0.0008436	0.008675
RTN4R	902.37536	1.916024131	0.5740294	3.3378503	0.0008443	0.0086774
IL17B	62.303349	2.619220073	0.7849033	3.3369971	0.0008469	0.0086948
PLOD1	22420.102	1.064448713	0.3191259	3.3355134	0.0008514	0.008734
TCERG1L	18.843864	3.038681936	0.9112589	3.3345979	0.0008542	0.0087514
CDC6	1553.7716	1.124441943	0.3379206	3.3275328	0.0008762	0.0089304
LUZP4	5.2241497	3.137160224	0.9430132	3.3267406	0.0008787	0.0089445
DAB1	77.86625	2.908836424	0.8752649	3.3233785	0.0008893	0.0090387
ARSE	457.36682	1.682240602	0.5062231	3.3231207	0.0008902	0.0090416
IGSF8	8242.9191	1.22446672	0.3694666	3.3141476	0.0009192	0.0092785
OLAH	6.590418	2.573250317	0.7764798	3.3139951	0.0009197	0.0092786
HES4	439.66564	1.776650084	0.5362927	3.3128368	0.0009235	0.0093036
BNC1	68.129378	2.511032502	0.7603537	3.3024531	0.0009584	0.0095983
GRAMD4	4657.8262	1.21449083	0.3681108	3.299253	0.0009694	0.0096932
SH3PXD2B	8197.2714	1.412018854	0.429222	3.2897168	0.0010029	0.0099345
ASB5	16.486179	4.231744739	1.286691	3.2888586	0.0010059	0.0099546
GPAT3	807.49101	1.81355059	0.5517474	3.2869216	0.0010129	0.009982
LKAAEAR1	16.740715	2.111909571	0.643063	3.2841412	0.0010229	0.0100552
SLC7A5	24019.027	1.514003153	0.4610543	3.2837848	0.0010242	0.010059
CIB2	459.79228	1.203928768	0.3667205	3.2829597	0.0010272	0.0100716
USP13	2651.9027	1.029154388	0.3136477	3.2812432	0.0010335	0.0101228
SLC12A1	15.177191	2.079927703	0.6355246	3.272773	0.001065	0.0103833
DAPL1	187.63949	3.392881522	1.0368302	3.2723599	0.0010665	0.0103932
FOXRED2	4447.9056	1.118480854	0.3422901	3.2676405	0.0010845	0.0105323
MT3	10.12554	2.227986085	0.682323	3.2652952	0.0010935	0.0105967
BSN	194.27121	1.172857995	0.3597291	3.2603922	0.0011126	0.0107459
HAPLN2	19.247583	2.048432595	0.6290004	3.2566475	0.0011274	0.0108548
EREG	49.586402	3.209097847	0.9880048	3.2480589	0.001162	0.0111195
C9orf116	103.81433	1.106472351	0.3426396	3.2292596	0.0012411	0.0117519
TCN1	746.49357	2.419773212	0.7505428	3.2240311	0.001264	0.0119137

ERFE	79.408661	1.626635855	0.504539	3.2240041	0.0012641	0.0119137
RDH8	598.72728	3.593144743	1.1159628	3.2197711	0.0012829	0.0120723
LGALS1	44157.638	1.135255507	0.3529956	3.2160616	0.0012996	0.0122054
HEY1	3235.0737	1.617720926	0.5034681	3.2131546	0.0013129	0.0122935
ZNF70	616.04552	1.094278002	0.340723	3.2116355	0.0013198	0.0123527
FAM86B2	7.7704836	1.633531792	0.510041	3.2027462	0.0013612	0.0126942
TUBB3	6615.8136	1.57110564	0.4911578	3.1987798	0.0013801	0.0128354
DHRS11	622.1543	1.212827618	0.379244	3.1980137	0.0013838	0.0128634
FERMT1	169.53555	2.67215818	0.8359994	3.1963636	0.0013917	0.0128999
LAYN	1069.2708	1.757589147	0.5500614	3.1952602	0.001397	0.012924
CDC20	1974.0838	1.179988528	0.3692933	3.1952613	0.001397	0.012924
ARVCF	757.55675	1.126837545	0.353048	3.1917406	0.0014142	0.0130636
TMEM240	83.312744	1.280365932	0.4016341	3.1878917	0.0014331	0.0131753
GYPC	9673.5001	1.472488631	0.4636449	3.1758971	0.0014937	0.0136084
SNCB	136.46023	2.873730679	0.9062344	3.1710679	0.0015188	0.0137648
DDTL	480.9208	1.538700255	0.4852313	3.1710655	0.0015188	0.0137648
NAGS	224.70229	1.208924255	0.381517	3.1687295	0.0015311	0.0138432
MELTF	11374.236	1.783774623	0.5635704	3.1651318	0.0015501	0.0139628
ADSSL1	434.53758	1.435406975	0.4549826	3.1548614	0.0016057	0.0143894
ABCG5	25.161678	2.269095192	0.7194936	3.1537394	0.0016119	0.0144381
NQO1	4333.1712	1.402966407	0.445372	3.1501001	0.0016321	0.0145987
PROSER2	396.57368	1.547283774	0.4918721	3.1457033	0.0016569	0.0147717
ACVR1C	188.50759	1.396718824	0.4445717	3.141718	0.0016796	0.0149395
ZNF697	3405.0793	1.012548635	0.3223623	3.1410273	0.0016836	0.0149608
LRRC8E	256.75683	1.431151376	0.4569394	3.1320373	0.001736	0.0153271
CKMT2	174.84853	1.802057497	0.5761167	3.1279384	0.0017604	0.0154839
TM7SF2	532.82154	1.021119407	0.3269169	3.1234832	0.0017872	0.015682
SLC22A18	1913.2923	1.089322878	0.3489682	3.1215533	0.001799	0.0157601
FAM131C	9.1442105	2.870976587	0.9201	3.1202875	0.0018067	0.0158136
RTN4RL1	723.3263	2.533857068	0.8124278	3.1188705	0.0018155	0.0158826
POU3F1	336.85242	2.017168643	0.6469008	3.1182041	0.0018196	0.015904
MAP1LC3B2	47.843198	1.070172311	0.3434024	3.1163798	0.0018309	0.0159591
FABP3	784.00193	1.387850759	0.4453737	3.1161486	0.0018323	0.0159643
PTX4	9.6856854	2.528908874	0.8119641	3.1145575	0.0018422	0.0160145
CDC42EP3	5907.1271	1.030322976	0.3309038	3.113663	0.0018478	0.0160338
GOLGA7B	1942.1497	1.936018483	0.6220765	3.112187	0.0018571	0.0160915
BFSP1	874.8083	1.91652954	0.6162768	3.1098516	0.0018718	0.0161835
OAF	5301.7081	1.609299219	0.5179104	3.1072925	0.0018881	0.0163023
CA8	304.64223	1.985011896	0.6391262	3.1058217	0.0018975	0.0163614
DHH	162.15347	1.950456924	0.6288109	3.101818	0.0019234	0.0165101
CCDC148	71.538471	1.663851111	0.5367796	3.0996913	0.0019372	0.0165993
ASIP	34.171777	1.315773199	0.4257938	3.0901656	0.0020004	0.0170194
PTTG1IP	40634.77	1.022672292	0.3310101	3.0895505	0.0020046	0.0170471
CDON	1289.1731	1.134095608	0.3687475	3.0755346	0.0021013	0.0176963
AATK	767.13163	1.471117412	0.4792365	3.0697105	0.0021427	0.0179661
GSTP1	18734.219	1.178497628	0.3841079	3.0681423	0.0021539	0.0180528

KLK4	25.838684	2.625384562	0.8559127	3.0673509	0.0021597	0.0180719
PRR7	717.09234	1.258177093	0.4102061	3.0671828	0.0021609	0.0180719
FAHD2B	378.87398	1.331795167	0.4354705	3.0582903	0.002226	0.0184953
LONRF3	385.48591	1.658571816	0.5424533	3.0575386	0.0022316	0.0185177
OR51B4	7.5400534	3.466220659	1.1339562	3.0567501	0.0022375	0.0185184
FSTL3	2342.797	1.45339859	0.4754553	3.0568566	0.0022367	0.0185184
CDK18	1644.2989	1.691615447	0.5534831	3.0563089	0.0022408	0.0185376
ENTPD2	222.74983	3.187706404	1.0432937	3.0554257	0.0022474	0.0185532
MAPK12	981.97769	1.270396138	0.416967	3.0467546	0.0023133	0.0189541
NACAD	330.6252	1.835352759	0.6033671	3.0418507	0.0023513	0.0192112
PAEP	2418.4621	3.268391039	1.0753049	3.0395016	0.0023697	0.0193205
BRSK1	884.6873	1.496020768	0.492258	3.0390993	0.0023729	0.0193298
BHMT	7.9425807	2.343083195	0.7717127	3.0362117	0.0023957	0.0194333
ASPHD1	469.40388	1.566156511	0.5164852	3.0323358	0.0024267	0.0196348
GPR137B	8525.5881	1.192894955	0.3935403	3.0311892	0.0024359	0.0196919
TMEM158	3027.1341	1.993896963	0.6590291	3.0255066	0.0024822	0.0199741
ABCD1	3432.9797	1.039285289	0.3438532	3.0224676	0.0025072	0.0201588
CYTH3	12093.36	1.302701636	0.43118	3.0212475	0.0025174	0.0202232
HBEGF	1679.2921	1.529605993	0.5068199	3.0180465	0.0025441	0.0204039
KLK6	247.45261	2.835643042	0.9413945	3.012173	0.0025938	0.0206989
MRPS24	1896.207	1.215630389	0.4037258	3.0110299	0.0026036	0.0207597
CDC42EP1	2771.6686	1.140070304	0.3788117	3.0095961	0.002616	0.020832
ANKRD13B	545.24578	1.204276757	0.4010056	3.0031423	0.0026721	0.0211384
SMOC1	230.81641	2.11697015	0.7059347	2.9988187	0.0027103	0.021335
KCNF1	51.710016	2.724839776	0.9088533	2.9981073	0.0027166	0.0213586
NAT16	33.350298	2.35753632	0.786808	2.9963301	0.0027325	0.0213957
HIST1H4B	4.6364878	1.752824462	0.5858502	2.9919328	0.0027722	0.0216465
SH3RF3	1073.5651	1.273349376	0.4256162	2.9917783	0.0027736	0.0216465
BEX1	134.3764	2.500270518	0.8369583	2.9873298	0.0028143	0.0218661
FAM57B	18.620908	2.120819169	0.7104688	2.9850984	0.0028349	0.0220174
CDC45	1044.2333	1.136752531	0.3813439	2.9809114	0.0028739	0.0222485
FGD1	1624.2323	1.062182662	0.3566065	2.978585	0.0028958	0.0224
P4HA2	5116.0745	1.324998649	0.4450372	2.9772765	0.0029082	0.0224596
SHROOM2	1667.5054	1.472022672	0.4944499	2.9770915	0.00291	0.0224641
SMIM1	150.4029	1.55019262	0.520901	2.9759831	0.0029205	0.0225364
CDR2L	1175.2829	1.266065072	0.4260387	2.9717139	0.0029614	0.0227787
LRAT	510.22573	2.497108825	0.8406018	2.9706203	0.002972	0.0228325
DMRT2	87.317224	1.920343048	0.6464909	2.97041	0.002974	0.022839
NID1	21523.545	1.675225322	0.5642095	2.9691549	0.0029862	0.022905
CAPN3	10380.003	1.724930369	0.5819393	2.9641071	0.0030356	0.023219
SLC22A14	7.7340013	2.213419945	0.7475024	2.9610874	0.0030655	0.0234105
FLRT1	181.16025	2.096609948	0.7081426	2.9607172	0.0030692	0.0234294
TMC7	344.40707	1.818515202	0.6154485	2.9547803	0.0031289	0.0237641
FAM135B	29.334657	1.772526494	0.5998479	2.9549599	0.0031271	0.0237641
GPRIN1	1410.6323	1.204837723	0.4084786	2.949574	0.0031821	0.0240896
PI3	114.23629	2.646972341	0.8986944	2.9453531	0.0032259	0.0243151

ERICH2	169.02937	1.714927133	0.5825022	2.9440696	0.0032393	0.0243778
DLGAP1	690.74617	1.873751382	0.6371538	2.9408149	0.0032735	0.0245872
HOMER2	675.33353	1.610848065	0.5488053	2.9351907	0.0033334	0.0249396
GP1BB	161.47065	1.481710404	0.5055115	2.9311109	0.0033775	0.0252006
KLK5	90.39318	3.757484547	1.2841344	2.9260836	0.0034326	0.0255319
MAFK	3516.9587	1.235472745	0.4227688	2.9223366	0.0034742	0.0257911
SPECC1	2067.0333	1.14633082	0.3925954	2.9198781	0.0035017	0.0259653
ODF3L2	18.298295	2.067273717	0.7083188	2.9185639	0.0035165	0.0259845
CELF5	33.696247	1.862338554	0.6387603	2.9155513	0.0035506	0.0261661
ZCCHC12	17.121589	1.491801272	0.5126867	2.9097717	0.0036169	0.0265274
IL19	6.7313529	2.786324832	0.9583673	2.9073665	0.0036449	0.0266761
CHST6	1805.0306	1.717695909	0.5909943	2.9064509	0.0036555	0.0267441
PHLDA2	1835.7657	1.644900084	0.5685729	2.8930328	0.0038154	0.0276708
RGS7	36.200108	2.817411434	0.9762256	2.8860249	0.0039014	0.0281772
PHF21B	178.53119	2.415921942	0.8380673	2.8827304	0.0039424	0.0283773
APOLD1	1449.1099	1.125880307	0.3907055	2.8816597	0.0039559	0.0284526
FSD1	110.86483	2.231103906	0.7747056	2.8799378	0.0039775	0.0285762
HIBCH	2474.9308	1.279740092	0.4449012	2.876459	0.0040216	0.028796
EPHA4	1693.3027	1.845909287	0.6437419	2.8674679	0.0041377	0.0293964
ADAM23	2533.5393	1.715476199	0.5982819	2.8673378	0.0041394	0.0293974
FOSL1	1060.4172	1.735975933	0.6062883	2.8632846	0.0041927	0.0296555
FUT3	30.124226	2.639911296	0.9226664	2.8611764	0.0042207	0.0297765
ITPR3	12752.178	1.270873774	0.4446415	2.8581985	0.0042605	0.0300022
TMEM229A	10.378348	3.091657582	1.0831877	2.8542216	0.0043142	0.0303358
ADD2	357.08551	1.852134671	0.6490026	2.8538169	0.0043197	0.0303633
SCUBE2	1092.8338	1.840322002	0.6460408	2.8486157	0.004391	0.0307401
COL9A1	207.31843	2.71544348	0.9534477	2.8480255	0.0043991	0.0307781
IQGAP3	1456.093	1.015563528	0.356604	2.8478744	0.0044012	0.0307781
TMEM184A	824.79292	2.489954573	0.8749758	2.8457409	0.0044308	0.0309625
BIRC5	2345.9448	1.035524432	0.364105	2.8440271	0.0044547	0.0310615
ANKRD9	1939.3786	1.406335385	0.4955319	2.8380319	0.0045393	0.0314565
ALDH1A2	178.39553	1.421297667	0.5008346	2.8378581	0.0045417	0.0314622
KIAA1549L	3949.7671	1.365175559	0.481325	2.8362863	0.0045642	0.0315719
QRFPR	12.590444	3.073130802	1.085016	2.8323368	0.0046209	0.0318518
SHB	981.99506	1.528017774	0.5394944	2.8323146	0.0046212	0.0318518
REP15	118.28856	1.11389392	0.3932458	2.8325638	0.0046176	0.0318518
FOXD1	374.51197	1.370522578	0.4848206	2.8268652	0.0047006	0.0322828
LRRIQ4	13.105708	2.376803721	0.841538	2.8243569	0.0047376	0.032477
ACY1	1110.673	1.415191027	0.5010845	2.8242561	0.0047391	0.032477
CATSPERZ	19.407378	1.697323731	0.6024422	2.8174052	0.0048413	0.033001
ITPRIP	3380.9492	1.074537278	0.3817739	2.8145908	0.0048839	0.0332087
EXO1	824.26479	1.003432115	0.3567182	2.8129546	0.0049089	0.0333545
UCP1	3.1404122	3.594438195	1.2809924	2.8059794	0.0050164	0.0339049
OTX1	132.34647	1.406783855	0.5016044	2.8045686	0.0050384	0.0340176
ERVMER34-1	197.88695	2.206667333	0.7873519	2.8026443	0.0050686	0.034149
PLXNC1	18024.423	1.578690809	0.5648796	2.7947386	0.0051942	0.0347997

SLC24A2	40.920172	1.874733536	0.672139	2.789205	0.0052838	0.0352153
PRELID2	432.52897	1.027270495	0.3688459	2.785094	0.0053512	0.0355797
FAM71D	6.9199316	1.94004044	0.6973784	2.7819049	0.0054041	0.0358304
HBE1	5.8834167	2.447954176	0.8802264	2.7810506	0.0054183	0.0358875
DRAXIN	141.70761	2.320608704	0.8352712	2.7782699	0.0054649	0.0361586
LTK	319.71698	1.72290768	0.6202976	2.7775504	0.005477	0.0361888
SLC7A8	6704.8166	1.258884989	0.4532853	2.7772464	0.0054822	0.0361977
PDF	488.29555	1.165983674	0.421131	2.7686956	0.0056281	0.0369072
MOCOS	1150.2372	1.492371963	0.5390548	2.7684977	0.0056315	0.036917
MSRB2	1983.9027	1.172859708	0.4239252	2.7666665	0.0056633	0.0370616
HHAT	1207.9313	1.131773221	0.4100718	2.7599389	0.0057812	0.0375965
RASAL1	134.43432	2.20169257	0.7978584	2.759503	0.0057889	0.0376143
PRR19	175.85868	1.243653777	0.4511195	2.7568169	0.0058367	0.0378862
TMEM233	60.012603	1.589708137	0.5768676	2.7557591	0.0058556	0.0379663
FAM71E1	96.648743	1.595619672	0.580239	2.7499354	0.0059607	0.0384504
PCDH20	81.146632	2.825565985	1.027783	2.7491855	0.0059744	0.03848
CCNA1	92.249098	2.087207097	0.7604534	2.7446878	0.0060569	0.0388417
CATSPER1	112.1516	1.642069931	0.5983501	2.7443295	0.0060635	0.0388423
SLC35G2	370.38631	1.489071619	0.5426175	2.7442383	0.0060651	0.0388423
TMEM151B	63.808755	2.073274431	0.755811	2.7431123	0.006086	0.0389113
FSCN1	13830.56	1.251992288	0.4566286	2.7418173	0.00611	0.039026
POPDC3	555.62021	1.737337563	0.6347238	2.7371552	0.0061973	0.0395045
KCNJ12	113.73032	1.818988394	0.6647499	2.7363502	0.0062125	0.0395881
MFSD12	12447.246	1.037445814	0.3791656	2.7361288	0.0062167	0.0396016
TGFA	690.06689	1.737200735	0.6350657	2.7354662	0.0062292	0.039655
PDZRN3	2279.2956	1.332935277	0.4884629	2.7288365	0.0063558	0.04027
RASEF	1462.2913	2.136711105	0.7833987	2.7274888	0.0063818	0.0403587
NR4A3	1035.1178	1.803508182	0.6617718	2.725272	0.0064249	0.0405618
ANKRD30B	55.838018	2.492154425	0.9155261	2.7221008	0.0064868	0.0408609
LHX9	9.9216383	2.561473783	0.941825	2.7196918	0.0065343	0.0411057
C9orf50	31.45324	1.9585035	0.7206436	2.7177145	0.0065735	0.0412979
RNF157	3029.7843	1.204825675	0.4434311	2.7170529	0.0065866	0.0413399
TANC2	4197.1891	1.069960729	0.3940448	2.7153275	0.006621	0.0415152
CRYBA2	3.8493998	4.7373828	1.7458794	2.713465	0.0066584	0.0417083
SBSN	101.54031	1.932046497	0.7120877	2.7132143	0.0066634	0.0417168
USH2A	29.226255	1.429616664	0.527051	2.7124826	0.0066781	0.0417639
PLEK2	308.59633	1.24589999	0.4595519	2.7111191	0.0067057	0.0418814
WIPI1	7027.555	1.21837756	0.4504109	2.7050358	0.0068297	0.04249
SLC19A3	413.43383	2.0357921	0.7528354	2.7041664	0.0068476	0.0425513
SLC38A3	42.387014	2.062911353	0.7635866	2.7016075	0.0069005	0.0427448
PLOD3	25277.654	1.094119522	0.4051032	2.7008412	0.0069164	0.0427851
MAGED4:1	5.976417	3.327139632	1.2324643	2.699583	0.0069426	0.0428726
MAGED4B:1	5.976417	3.327139632	1.2324643	2.699583	0.0069426	0.0428726
CREG2	13.611149	1.641479832	0.6082083	2.6988775	0.0069574	0.0429221
NHSL1	2967.6701	1.210774209	0.4486974	2.6984205	0.0069669	0.0429396
LDLR	3938.5023	1.663344806	0.6167376	2.6970058	0.0069966	0.0430809

NME2	13212.768	1.072176451	0.3979621	2.6941673	0.0070565	0.0433521
LUZP2	27.665484	2.810913647	1.0436106	2.6934507	0.0070717	0.0434112
GJB1	5598.2502	1.934377226	0.7205615	2.6845415	0.0072629	0.0442658
SLC26A10	240.04939	1.37709301	0.5129678	2.6845604	0.0072625	0.0442658
LRRN1	462.63699	2.338342585	0.8712367	2.6839349	0.0072761	0.0443039
FBLN7	665.42566	1.16296181	0.433409	2.6832896	0.0072902	0.0443754
FKBP10	18212.826	1.016031881	0.3791118	2.6800326	0.0073615	0.0447101
ARL14EPL	5.5278609	2.585878228	0.9654456	2.6784296	0.0073968	0.0448678
PDIA2	34.514264	2.284288804	0.8530663	2.6777387	0.0074121	0.0449248
SLC25A4	3783.0866	1.041216264	0.3891071	2.6759119	0.0074526	0.0450877
SLC35D3	1.8468921	2.530775876	0.9464178	2.6740578	0.007494	0.0451995
TMEM38A	113.09854	1.391114322	0.5204983	2.6726587	0.0075253	0.0453456
SPRR2D	16.894152	2.050920366	0.7675166	2.6721513	0.0075367	0.0453715
CDH3	5363.596	2.228999112	0.8345343	2.6709497	0.0075637	0.04549
ABLIM2	232.82328	1.412690825	0.5297135	2.6668961	0.0076555	0.045871
INHA	30.127707	1.528185419	0.5731945	2.6660851	0.007674	0.04591
NMUR2	7.0130969	2.72408579	1.0222127	2.6648915	0.0077013	0.0460446
MCF2L2	121.20782	1.058573694	0.3973778	2.6638972	0.0077241	0.0460946
EYA4	844.18065	1.646587979	0.6184752	2.6623346	0.0077601	0.0462659
PLAC4	117.6507	1.463726122	0.5498675	2.6619616	0.0077687	0.0463028
AXIN2	1090.069	1.563382731	0.5877824	2.6597984	0.0078187	0.0464856
GPER1	442.55968	1.400410664	0.5266371	2.659157	0.0078336	0.0465598
LARGE1	2865.7479	1.142802768	0.4303712	2.6553885	0.0079217	0.0469812
KAAG1	15.54188	2.261703557	0.8519461	2.6547495	0.0079367	0.0470412
TMEM255A	725.79612	1.670724492	0.6297945	2.6528089	0.0079825	0.0472541
NKX6-1	97.972757	2.196388234	0.8280309	2.6525438	0.0079888	0.0472766
ULBP2	108.7533	1.462598959	0.5516414	2.6513584	0.0080169	0.0473843
TGFBR3L	48.543801	1.540067203	0.581128	2.6501343	0.008046	0.0474539
CHRNA7	36.641191	2.238387016	0.8454674	2.6475143	0.0081086	0.0477204
HHIP	11.746102	1.661257865	0.6275841	2.647068	0.0081193	0.0477542
GRIK4	102.8037	1.970125393	0.7443085	2.6469203	0.0081228	0.0477604
TMEM163	3654.5809	2.408147435	0.9106339	2.6444736	0.0081818	0.0480039
FMN1	17521.063	1.234155513	0.4667313	2.6442528	0.0081872	0.0480206
GAMT	886.65826	1.175630487	0.4446809	2.6437618	0.008199	0.0480756
TGM3	11.053825	2.156805975	0.8161903	2.6425284	0.008229	0.0481743
EFCAB6	167.8661	1.753908812	0.6645191	2.6393655	0.0083061	0.0484811
RAB6B	2858.9785	1.402570118	0.5318417	2.6371946	0.0083595	0.0487463
MAP7D2	424.81304	2.068067285	0.7846803	2.6355538	0.0084	0.0488654
TMEM246	506.88922	1.62095804	0.6160626	2.6311579	0.0085094	0.0493075
NEFL	1569.1682	2.837738434	1.0788807	2.6302615	0.0085319	0.049378
WIF1	5.2991884	2.071627098	0.7881301	2.6285346	0.0085754	0.0495409
FAM227A	143.72209	1.053547737	0.4009932	2.6273457	0.0086054	0.0496383
TRABD2B	167.06901	1.71413951	0.652658	2.6263976	0.0086294	0.0497392

Supplementary table 2B: PAK4 expression analysis between upper and lower quartile of different immune markers of response.

Comparison	log2FC	FDR	Rank	Genes in comparison (FDR < 0.05)
Dendritic Cells	1.15	1.18E-05	23	1449
T cells	1.31	2.74E-07	61	3044
CD8A	1.3	9.08E-09	14	2635
TNF	1.55	6.67E-12	5	2859
IFNg	1.21	1.90E-06	35	2103
BATF3 DC score	1.52	2.25E-09	35	3752

Supplemental table 2C: Overlap of genes enriched in samples with low (lower quartile) T cells and dendritic cells (log2FC > 1 and FDR < 5e-05)

Genes	Kinase	Known inhibitor
CNKSR3	NO	
ITPKA	NO	
APCDD1	NO	
NKD1	NO	
TOMM34	NO	
SLC35E4	NO	
DPF1	NO	
SP5	NO	
TMEM189	NO	
SLC1A5	NO	
PAK4	**YES**	**KPT-9274, PF-03758309**
TRIB3	YES	
FAM19A5	NO	
HES6	NO	
PMP2	NO	
TTLL12	NO	
CFAP77	NO	
DPH3P1	NO	

Supplemental table 3: Pan-cancer analysis between PAK4 expression and T cell, cytotoxic T cell and Dendritic Cell scores

Cancer Type	Cytotoxic T-cell Spearman Rho	Cytotoxic T-cell Spearman P-value	Cytotoxic T-cell Q-value	Cytotoxic T-cell Q-value Rank Anti-Correlated	Cytotoxic T-cell Total Genes Significantly Anti-Corrrelated by Q-Value
Adrenocortical Adenocarcinoma [ACC]	-0.49	5.42E-06	8.50E-05	174	1974
Bladder Urothelial Carcinoma [BLCA]	-0.33	5.13E-12	2.89E-11	534	3788
Low Grade Glioma [LGG]	NA	NA	N.S	NA	NA
Breast Cancer [BRCA]	-0.12	4.00E-05	9.30E-05	1925	3259
Cervical Cancer [CESC]	NA	NA	N.S	NA	NA
Cholangiocarcinoma [CHOL]	NA	NA	N.S	NA	NA
Colon Adenocarcinoma [COAD]	-0.22	9.36E-07	2.80E-06	1294	3011
Esophageal Carcinoma [ESCA]	NA	NA	N.S	NA	NA
Glioblastoma multiforme [GBM]	NA	NA	N.S	NA	NA
Head and Neck Squamous Cell Carcinoma [HNSC]	NA	NA	N.S	NA	NA
Chromophobe Renal Cell Carcinoma [KICH]	NA	NA	N.S	NA	NA
Clear Cell Renel Cell carcinoma [KIRC]	-0.23	8.53E-08	4.83E-07	105	1141
Papillary Renal Cell Carcinoma [KIRP]	NA	NA	N.S	NA	NA
Liver Hepatocellular Carcinoma [LIHC]	NA	NA	N.S	NA	NA
Lung Adenocarcinoma [LUAD]	NA	NA	N.S	NA	NA
Lung Squamous Cell Carcinoma [LUSC]	NA	NA	N.S	NA	NA
DLBC [DLBC]	NA	NA	N.S	NA	NA
Mesothelioma [MESO]	NA	NA	N.S	NA	NA
Ovarian Cancer [OV]	-0.20	6.88E-05	4.44E-04	508	2062
Pancreatic adenocarcinoma [PAAD]	-0.39	1.20E-07	5.61E-07	151	1684
Pheochromocytoma and Paraganglioma [PCPG]	NA	NA	N.S	NA	NA
Prostate Adenocarcinoma [PRAD]	-0.19	1.77E-05	4.12E-05	846	1862
Rectum Adenocarcinoma [READ]	-0.37	1.01E-06	1.31E-05	22	988
Sarcoma [SARC]	NA	NA	N.S	NA	NA
Skin Cutaneous Melanoma [SKCM]	-0.34	6.61E-14	4.86E-13	17	1796
Stomach Adenocarcinoma [STAD]	NA	NA	N.S	NA	NA
Testicular Germ Cell Tumors [TGCT]	-0.29	3.89E-04	1.90E-03	821	2071
Thymoma [THYM]	NA	NA	N.S	NA	NA
Thyroid Cancer [THCA]	-0.13	3.33E-03	8.25E-03	1832	2261
Uterine Carcinosarcoma [UCS]	NA	NA	N.S	NA	NA
Uterine Corpus Endometrial Carcinoma [UCEC]	-0.18	1.91E-05	1.38E-04	255	1323
Uveal Melanoma [UVM]	NA	NA	N.S	NA	NA
N.S. - Not Significant					

Dendritic cell Spearman Rho	Dendritic cell Spearman P-value	Dendritic cell Q-value	Dendritic cell Q-value Rank Anti-Correlated	Dendritic cell Total Genes Significantly Anti-Correlated by Q-value
-0.48	1.03E-05	1.32E-04	344	2448
-0.23	3.03E-06	1.66E-05	484	2968
0.17	1.31E-04	3.48E-04	NA	NA
-0.13	1.72E-05	4.81E-05	1197	2762
NA	NA	N.S	NA	NA
NA	NA	N.S	NA	NA
-0.19	4.07E-05	1.27E-04	734	1808
-0.25	1.63E-03	7.44E-03	545	1119
NA	NA	N.S	NA	NA
NA	NA	N.S	NA	NA
NA	NA	N.S	NA	NA
-0.20	2.31E-06	1.65E-05	36	540
-0.27	2.43E-06	1.78E-05	105	1181
NA	NA	N.S	NA	NA
-0.31	1.44E-13	8.83E-13	619	4187
-0.17	1.37E-04	4.07E-04	1829	3403
NA	NA	N.S	NA	NA
NA	NA	N.S	NA	NA
-0.23	6.31E-06	5.26E-05	276	2433
-0.36	8.40E-07	4.39E-06	68	1211
NA	NA	N.S	NA	NA
-0.28	4.33E-10	1.40E-09	288	2167
NA	NA	N.S	NA	NA
-0.24	8.12E-05	5.79E-04	423	1943
-0.35	8.10E-15	6.70E-14	3	1736
-0.20	1.02E-04	3.02E-04	1407	2814
NA	NA	N.S	NA	NA
-0.55	5.15E-11	4.12E-10	517	5076
-0.24	2.88E-08	7.38E-08	2540	5247
NA	NA	N.S	NA	NA
NA	NA	N.S	NA	NA
-0.35	1.32E-03	3.86E-03	220	446

T-cell Average Spearman Rho	T-cell Average Spearman P-value	T-cell Average Q-value	T-cell Average Q-value Rank Anti-Correlated	T-cell Total Genes Significantly Anti-Correlated by Q-value		Number of samples
-0.40	2.70E-04	2.91E-03	445	1618		79
-0.29	1.41E-09	5.67E-09	1099	4305		414
0.29	1.54E-11	5.46E-11	NA	NA		1109
-0.12	1.21E-04	2.72E-04	2511	3768		288
NA	NA	N.S	NA	NA		306
NA	NA	N.S	NA	NA		36
-0.23	5.50E-07	1.88E-06	1036	2973		480
NA	NA	N.S	NA	NA		48
-0.28	2.77E-04	1.05E-03	2675	4355		162
NA	NA	N.S	NA	NA		169
NA	NA	N.S	NA	NA		502
-0.27	2.51E-10	2.36E-09	70	1564		65
-0.32	5.07E-08	4.66E-07	51	2360		538
NA	NA	N.S	NA	NA		374
-0.13	2.68E-03	7.51E-03	1627	2105		529
-0.14	1.31E-03	3.01E-03	2862	3736		502
NA	NA	N.S	NA	NA		535
NA	NA	N.S	NA	NA		470
-0.27	6.91E-08	6.09E-07	357	3397		86
-0.41	1.64E-08	1.05E-07	50	1420		379
NA	NA	N.S	NA	NA		178
-0.26	7.90E-09	2.89E-08	389	2123		180
-0.25	9.31E-04	4.64E-03	241	655		499
NA	NA	N.S	NA	NA		167
-0.31	7.38E-12	5.13E-11	54	2263		263
NA	NA	N.S	NA	NA		375
-0.32	7.66E-05	2.53E-04	2240	4160		150
NA	NA	N.S	NA	NA		119
-0.23	1.89E-07	5.95E-07	1664	4416		510
NA	NA	N.S	NA	NA		56
-0.15	5.22E-04	3.34E-03	497	1247		552
NA	NA	N.S	NA	NA		80

Supplemental table 4: GSEA from on-treatment non-responding biopsies compared to responding biopsies using Curated Gene Sets (C2), q < 0.2

NAME	GS follo	GS DETAILS	SIZE	ES	NES	NOM p-val	FDR q-val	FWER p-val
WELCSH_BRCA1_TARGETS_DN	WELCSH_BR	Details ...	139	0.6422657	3.163371	0	0	0
MANALO_HYPOXIA_DN	MANALO_HY	Details ...	270	0.5573447	3.0424507	0	0	0
SOTIRIOU_BREAST_CANCER_GRADE_1_VS_3_UP	SOTIRIOU_B	Details ...	141	0.58930874	2.9300787	0	0	0
YAO_TEMPORAL_RESPONSE_TO_PROGESTERONE_CLUSTER_14	YAO_TEMPO	Details ...	134	0.576613	2.8172123	0	0	0
MENSSEN_MYC_TARGETS	MENSSEN_M	Details ...	51	0.6932221	2.8031504	0	0	0
SCHUHMACHER_MYC_TARGETS_UP	SCHUHMACH	Details ...	77	0.6166993	2.7812567	0	0	0
LI_DCP2_BOUND_MRNA	LI_DCP2_BO	Details ...	84	0.5840576	2.7371175	0	0	0
WINTER_HYPOXIA_UP	WINTER_HY	Details ...	88	0.5884712	2.6980932	0	0	0
PENG_GLUTAMINE_DEPRIVATION_DN	PENG_GLUT	Details ...	325	0.48952675	2.660823	0	0	0
WINNEPENNINCKX_MELANOMA_METASTASIS_UP	WINNEPENN	Details ...	151	0.5144166	2.6306832	0	0	0
PENG_RAPAMYCIN_RESPONSE_DN	PENG_RAPA	Details ...	231	0.4946737	2.6215663	0	0	0
KOBAYASHI_EGFR_SIGNALING_24HR_DN	KOBAYASHI_	Details ...	241	0.4979802	2.620339	0	0	0
YAO_TEMPORAL_RESPONSE_TO_PROGESTERONE_CLUSTER_17	YAO_TEMPO	Details ...	171	0.5033298	2.6022208	0	0	0
RHODES_CANCER_META_SIGNATURE	RHODES_CA	Details ...	63	0.591095	2.5810163	0	0	0
PENG_LEUCINE_DEPRIVATION_DN	PENG_LEUCI	Details ...	182	0.49582386	2.5746064	0	0	0
KIM_ALL_DISORDERS_DURATION_CORR_DN	KIM_ALL_DIS	Details ...	142	0.50752264	2.55055	0	0	0
BILANGES_RAPAMYCIN_SENSITIVE_VIA_TSC1_AND_TSC2	BILANGES_R	Details ...	71	0.56648415	2.5071523	0	0	0
OXFORD_RALA_OR_RALB_TARGETS_UP	OXFORD_RA	Details ...	45	0.6142026	2.5067632	0	0	0
DANG_REGULATED_BY_MYC_UP	DANG_REGU	Details ...	70	0.55954903	2.4921827	0	0	0
FOURNIER_ACINAR_DEVELOPMENT_LATE_2	FOURNIER_A	Details ...	265	0.45493805	2.4844851	0	0	0
MOOTHA_VOXPHOS	MOOTHA_VOXPHOS		84	0.52912754	2.4148815	0	0	0
DANG_MYC_TARGETS_UP	DANG_MYC_TARGETS_UP		135	0.47602034	2.4082212	0	0	0
REACTOME_MITOCHONDRIAL_PROTEIN_IMPORT	REACTOME_MITOCHONDRIAL_I		47	0.57679176	2.403725	0	5.96E-05	0.001
FRASOR_RESPONSE_TO_SERM_OR_FULVESTRANT_DN	FRASOR_RESPONSE_TO_SERM		50	0.5865024	2.4022262	0	5.71E-05	0.001
REACTOME_MRNA_SPLICING_MINOR_PATHWAY	REACTOME_MRNA_SPLICING_M		40	0.5974374	2.3997123	0	5.48E-05	0.001
SANSOM_APC_TARGETS_REQUIRE_MYC	SANSOM_APC_TARGETS_REQU		192	0.4534387	2.3912604	0	5.27E-05	0.001
REACTOME_RESPIRATORY_ELECTRON_TRANSPORT	REACTOME_RESPIRATORY_ELE		64	0.55282086	2.39051	0	5.08E-05	0.001
REACTOME_TRNA_AMINOACYLATION	REACTOME_TRNA_AMINOACYL		42	0.59777385	2.3637283	0	4.89E-05	0.001
WONG_EMBRYONIC_STEM_CELL_CORE	WONG_EMBRYONIC_STEM_CE		330	0.43178394	2.3555942	0	4.73E-05	0.001
GRADE_COLON_AND_RECTAL_CANCER_UP	GRADE_COLON_AND_RECTAL_C		273	0.42499885	2.3476837	0	4.57E-05	0.001
STARK_HYPPOCAMPUS_22Q11_DELETION_DN	STARK_HYPPOCAMPUS_22Q11_		18	0.73649263	2.344347	0	4.42E-05	0.001
CHAUHAN_RESPONSE_TO_METHOXYESTRADIOL_UP	CHAUHAN_RESPONSE_TO_MET		50	0.5747056	2.341423	0	4.28E-05	0.001
REACTOME_RESPIRATORY_ELECTRON_TRANSPORT_ATP_SYNTHESIS	REACTOME_RESPIRATORY_ELE		80	0.50809836	2.3386672	0	4.15E-05	0.001
NIKOLSKY_BREAST_CANCER_16P13_AMPLICON	NIKOLSKY_BREAST_CANCER_16		108	0.48471385	2.3327332	0	7.92E-05	0.002
KEGG_AMINOACYL_TRNA_BIOSYNTHESIS	KEGG_AMINOACYL_TRNA_BIOS		41	0.59299195	2.330928	0	7.69E-05	0.002
WONG_MITOCHONDRIA_GENE_MODULE	WONG_MITOCHONDRIA_GENE		216	0.4337401	2.3259742	0	7.48E-05	0.002
KEGG_OXIDATIVE_PHOSPHORYLATION	KEGG_OXIDATIVE_PHOSPHORY		116	0.47559005	2.32503	0	7.28E-05	0.002
SCHLOSSER_MYC_TARGETS_AND_SERUM_RESPONSE_UP	SCHLOSSER_MYC_TARGETS_AN		46	0.5733477	2.3072815	0	7.08E-05	0.002
REACTOME_EXTENSION_OF_TELOMERES	REACTOME_EXTENSION_OF_TE		27	0.6444721	2.3045483	0	6.90E-05	0.002
REACTOME_BIOSYNTHESIS_OF_THE_N_GLYCAN_PRECURSOR_DOLI	REACTOME_BIOSYNTHESIS_OF_		28	0.64010525	2.3024354	0	1.01E-04	0.003
REACTOME_POST_TRANSLATIONAL_MODIFICATION_SYNTHESIS_OF	REACTOME_POST_TRANSLATIC		26	0.6318254	2.2874875	0	1.66E-04	0.005
PELLICCIOTTA_HDAC_IN_ANTIGEN_PRESENTATION_UP	PELLICCIOTTA_HDAC_IN_ANTIG		62	0.5263341	2.2845087	0	1.95E-04	0.006
WHITEFORD_PEDIATRIC_CANCER_MARKERS	WHITEFORD_PEDIATRIC_CANCE		111	0.46219832	2.2752745	0	2.24E-04	0.007
YAO_TEMPORAL_RESPONSE_TO_PROGESTERONE_CLUSTER_13	YAO_TEMPORAL_RESPONSE_TO		164	0.4360182	2.2726867	0	2.50E-04	0.008
REACTOME_GLUCONEOGENESIS	REACTOME_GLUCONEOGENESI		31	0.6132355	2.248203	0	4.27E-04	0.014
KEGG_RNA_POLYMERASE	KEGG_RNA_POLYMERASE		29	0.61928356	2.244533	0	4.47E-04	0.015

Supplemental table 5: Panel of immune markers for CyTOF

Tag	Target	Clone	Source
191/3 Ir	Single cells	-	Fluidigm
Cisplatin	Dead cells	-	Fluidigm
89Y	CD45	30-F11	DVS
142Nd	CD11c	N418	DVS
143 Nd	CD69	H1.2F3	DVS
146Nd	F4/80	BM8	DVS
148Nd	CD11b (Mac-1)	M1/70	DVS
149Nd	CD62L (L-selectin)*	MEL-14	
150Nd	Ly6C	Hk1.4	DVS
151Eu	Ly6G	1A8	DVS
152Sm	CD3e	145-2C11	DVS
153Eu	CD274_PDL-1		
155Gd	CD25 (IL-2R)*	3C7	Biolegend
159Tb	CD279_PD1	29F.1A12	DVS
160Gd	CD62L (L-selectin)	MEL-14	DVS
162Dy	CD366 (TIM3)	RMT3-23	DVS
166Er	CD19	6D5	DVS
167Er	CD335(Nkp46)	29A1.4	DVS
168Er	CD8a	53-6.7	DVS
170Er	CD161 (NK1.1)	PK136	DVS
171Yb	CD44	IM7	DVS
172Yb	CD4	RM4-5	DVS
174Yb	I-A/I-E (MHC class II)	M5/114.15.2	DVS
175 Lu	CD103		Biolegend
176Yb	CD45R_B220	RA3-6B2	DVS
	Intracellular		
115 IN	Ki67	SolA15	ThermoScientific
141Pr	TNF alfa	MP6-XT22	DVS
147Sm	Eomes	Dan11mag	ThermoScientific
158Gd	FoxP3	FJK-16s	DVS
161Dy	T-bet	B56	DVS

Chapter 3

PAK4 inhibition remodels the tumor microenvironment to increase PD-1 blockade efficacy

PAK4 inhibition remodels the tumor microenvironment to increase PD-1 blockade efficacy

Gabriel Abril-Rodríguez[1,2], Davis Y. Torrejon[1], Katie M. Campbell[1], Egmidio Medina[1], Justin D. Saco[1], Mildred Galvez[1], Ameya S. Champhekar[1], Ivan Perez-Garcilazo[1], Ignacio Baselga-Carretero[1], Jas Singh[3], Begoña Comin-Anduix[4,5], Cristina Puig-Saus[1,5,6], Antoni Ribas[1,2,4,5,6]

Affiliations:

1. Department of Medicine, Division of Hematology-Oncology, University of California, Los Angeles (UCLA).

2. Department of Molecular and Medical Pharmacology, UCLA

3. Arcus Biosciences, Inc., Hayward, CA

4. Department of Surgery, Division of Surgical Oncology, UCLA.

5. Jonsson Comprehensive Cancer Center, Los Angeles, CA 90095, USA

6. Parker Institute for Cancer Immunotherapy, San Francisco, CA 94129, USA

Correspondence: Antoni Ribas, M.D, Ph.D., Department of Medicine, Division of Hematology-Oncology, 11-934 Factor Building, Jonsson Comprehensive Cancer Center at UCLA, 10833 Le Conte Avenue, Los Angeles, CA 90095-1782, USA. Telephone: 310-206-3928. Fax: 310-825-2493. E-mail: aribas@mednet.ucla.edu.

Conflict of Interest

G.A-R. has received honoraria from consulting with Arcus Biosciences. A.R. has received honoraria from consulting with Amgen, Bristol-Myers Squibb, Chugai, Genentech, Merck, Novartis, Roche and Sanofi, is or has been a member of the scientific advisory board and

holds stock in Advaxis, Arcus Biosciences, Bioncotech Therapeutics, Compugen, CytomX, Five Prime, FLX-Bio, ImaginAb, Isoplexis, Kite-Gilead, Lutris Pharma, Merus, PACT Pharma, Rgenix and Tango Therapeutics. G.A-R., D.Y.T. and A.R. are inventors in a patent application covering the use of PAK4 inhibitors for cancer immunotherapy.

Abstract

PAK4 inhibition can sensitize tumors to immune checkpoint blockade (ICB) therapy, however, the underlying mechanisms remain unclear. We report that PAK4 inhibition reverses immune cell exclusion by increasing the infiltration of CD8 T cells and $CD103^+$ dendritic cells (DCs), a specific type of DCs that excel at cross-presenting tumor antigens and constitute a source of CXCL10. Interestingly, in melanoma clinical datasets, *PAK4* expression levels negatively correlate with the presence of *CCL21*, the ligand for CCR7 expressed in $CD103^+$ DCs. Furthermore, we extensively characterized the transcriptome of PAK4 knock out (KO) tumors, *in vitro* and *in vivo*, and established the importance of PAK4 expression in the regulation of the extracellular matrix, which can facilitate immune cell infiltration. Comparison between PAK4 wild type (WT) and KO anti-PD-1 treated tumors revealed how PAK4 deletion sensitizes tumors to ICB from a transcriptomic perspective. In addition, we validated genetically and pharmacologically that inhibition of PAK4 kinase activity is sufficient to improve anti-tumor efficacy of anti-PD-1 blockade. Therefore, this study provides novel insights into the mechanism of action of PAK4 inhibition and provides the foundation for a new treatment strategy that aims to overcome resistance to PD-1 blockade by combining anti-PD-1 with a small molecule PAK4 kinase inhibitor.

Introduction

Cancer immunotherapy has changed the treatment landscape of multiple tumor types, including advanced melanoma[1]. PD-1/PD-L1 blockade therapy works by releasing the brakes on the immune system and allowing the pre-existing anti-tumor response to resume and eradicate cancer cells[2]. Despite the unprecedented clinical success, with the approval by the FDA of multiple monoclonal antibodies blocking the PD-1/PD-L1 axis, the majority of patients with cancer do not respond to treatment or relapse shortly after[3,4]. Lack of tumor infiltration by immune cells, which results in low interferon-gamma signature, constitutes one of the main mechanisms of resistance to ICB therapies[2,5–7], and tumor-intrinsic oncogenic signaling pathways could drive immune cell exclusion from the tumor microenvironment[8–10]. Among the different pathways, WNT/β-catenin signaling has been associated with poor immune cell infiltration and resistance to anti-PD-1 blockade therapy in melanoma and other tumor types[11–13]. However, there is a paucity of targets that could potentially be inhibited in order to reverse immune cell exclusion and overcome resistance to PD-1 blockade therapies.

PAK4 is a member of the group II p21-activated kinases (PAKs) family and functions as a central player in the reorganization of the cytoskeleton[14]. PAK4 is also involved in several other cellular functions including cell survival and proliferation[15–17], but it is best known for its role in controlling cellular morphology, cell adhesion and cell migration[18–20]. Of note, *PAK4* overexpression is associated with tumorigenesis in several tumor types including breast, pancreatic, bladder, ovarian cancer and melanoma[21–26], and constitutes a potential target for cancer treatment. We have recently shown that in melanoma, *PAK4* overexpression is associated with lack of immune cell infiltration and resistance to PD-1 blockade immunotherapy, with its inhibition resulting in increased immune cell infiltration leading to overcoming resistance to anti-PD-1 therapy[13]. In addition, it has been shown that deletion of the *PAK4* gene in endothelial cells remodels the vascular microenvironment leading to increased T cell infiltration and improved responses to CAR-T immunotherapy in

glioblastoma[27]. However, the specific mechanisms underlying the improvement of effectiveness of ICB remain largely unknown.

Here, we show how PAK4 inhibition increases not only T cell infiltration, but also CD103$^+$ dendritic cell infiltration, an important subset of dendritic cells that excel at cross-presenting tumor antigens and priming T cells. We also describe how lack of *PAK4* expression alters the tumor microenvironment and sensitizes murine melanoma to anti-PD-1 therapy from a transcriptomic perspective. Finally, we demonstrate that the kinase activity of PAK4 is responsible for the improved response and show that pharmacological inhibition of PAK4 activity with a specific PAK4 kinase inhibitor improves the efficacy of anti-PD-1 immunotherapy. Taken together, these findings provide the rationale for a novel treatment strategy to overcome PD-1 blockade resistance by administering a combination of anti-PD-1 in combination with a specific PAK4 kinase inhibitor.

Results

PAK4 inhibition increases CD103$^+$ dendritic cell infiltration and its expression is associated with *CCL21* levels in biopsies of patients with melanoma

To elucidate how the lack of tumor *PAK4* expression sensitizes cancer cells to anti-PD-1 immunotherapy we aimed to characterize the tumor immune cell compartment. Previously, we described an increase in T cell infiltration in murine melanoma B16 PAK4 KO tumors[13]. In the current work, we sought to identify differences in the infiltration of other immune cell types that are key to orchestrating an anti-tumor response, such as dendritic cells. To do so, we implanted B16 PAK4 KO or B16 WT CRISPR control (CC) cells in the flanks of syngeneic C57BL/6 mice and treated them with murine anti-PD-1. To study the priming of T cells in the initial steps in the generation of anti-tumor immunity, we harvested tumors on day 6, after administering only one dose of anti-PD-1 therapy. A total of 44 murine melanoma B16 tumors (22 PAK4 KO and 22 WT) were then analyzed by flow cytometry using specific markers to

characterize dendritic cells (Supplementary Table 1 and Supplementary Figure 1). We observed that PAK4 KO tumors, regardless of anti-PD-1 treatment, significantly increased the percentage of $CD103^+$ DC (Fig. 1a), a subset of dendritic cells that have been described to excel at cross-presenting tumor antigens[28]. Almost half of the WT tumors analyzed (10/22) presented less than 5% $CD103^+$ DC infiltration while only three PAK4 KO tumors (3/22) had less than 5% $CD103^+$ DC infiltration. In line with the increase in dendritic cell infiltration, we also observed a significant increase in the percentage of $CD45^+$ $CD8^+$ cells in the PAK4 KO group compared to WT tumors (Fig. 1b). Furthermore, the expression of the T cell attracting chemokine CXCL10, was significantly enriched in PAK4 KO tumors (Fig. 1c). This is consistent with previous work in which it is shown that the expression of CXCL10 was dependent on the presence of $CD103^+$ DCs[29].

We then investigated differences in chemokine expression that could explain the increase in $CD103^+$ DC levels in the tumor microenvironment. To do so, we used transcriptomic data from multiple clinical datasets[7,13] and compared melanoma tumors with high *PAK4 expression* versus low *PAK4* expression. Interestingly, we found that among the different chemokines, high *PAK4* expression was strongly associated with decreased *CCL21* levels, which is the ligand for CCR7, the receptor expressed by $CD103^+$ DC (Fig. 1d). We also found significant changes in *CCL4* expression, a chemokine that has also been reported to facilitate the infiltration of this subset of dendritic cells[11], but to a lesser extent than *CCL21* levels (log2FC CCL21= 6.09, log2FC CCL4 = 2.34, Abril-Rodriguez cohort). Of note, we did not find any differences in CCL21 secretion between B16 WT CC and PAK4 KO cell lines *in vitro* (Ext Data Fig. 1). Altogether, our results show that genetic PAK4 deletion increases the infiltration of $CD103^+$ DCs, augments CXCL10 expression and results in higher CD8 T cell infiltration. Furthermore, this data is in line with our observation that in biopsies of patients with melanoma, *PAK4* expression is negatively associated with levels of *CCL21*, a chemokine that orchestrates $CD103^+$ DC migration.

Transcriptomic characterization of PAK4 KO cells reveals major changes in the tumor microenvironment followed by increased sensitivity to anti-PD-1

In order to tease out the transcriptomic differences between B16 PAK4 KO and WT cells, we performed RNA-seq on a total of 18 *in vitro* samples (12 KO and 6 WT), which included cultures that were treated with either IFNγ, TNF or Wnt3a. Principal component analysis showed that the main source of variance is due to lost *PAK4* expression (PC1 = 47% of variance, Fig. 2a). This was also validated by analyzing cell lines treated with IFNγ, TNF or Wnt-3a separately, which showed that there were no significant differences on how PAK4 WT or KO cells sense through these different stimuli (Ext. Data Fig. 2). Hence, these data also suggest that neither IFNγ nor TNF signaling in cancer cells plays a role in improving PD-1 blockade response in the context of PAK4 inhibition. Next, in order to gain statistical power, we compared all KO cells versus WT regardless of any additional cytokine (Fig. 2b, Supplementary Table 2). We performed differential gene expression (DGE) analysis and used the output to perform gene set enrichment analysis (GSEA) with GO signatures (C5), which showed that PAK4 KO cells were enriched in signatures associated with cell motility, cell adhesion and cytoskeleton (Fig. 2c). Due to its role in cytoskeleton organization, PAK4 loss might affect how cells interact with each other, which could impact the extracellular matrix, and hence, the tumor microenvironment. Interestingly, PAK4 KO cells had a higher expression of genes associated with blood vessel formation (*CERCAM1*, *ENPEP*, *ITGA3* and *LGALS3),* and antigen presentation (*H2-K1* and *H2-DMB1)* (Fig. 2d). However, MHC class I surface expression analysis by flow cytometry did not show any difference between PAK4 KO and WT cells (Ext. Data Fig. 3).

We next performed RNA-seq on murine melanoma B16 tumors implanted in the flanks of C57BL/6 mice that received treatment with either isotype or anti-PD-1. Here, tumors were harvested at two different time points: day 6 (early, 1 dose) and day 10 (late, 3 doses) so we could investigate the progression of transcriptomic changes over time. DGE analysis of day 6

tumors showed that anti-PD-1 treatment had no impact on either WT nor PAK4 KO tumors yet, as the mice had only have received one dose at this timepoint (Fig. 3a). Therefore, we focused solely on identifying the differences between WT and PAK4 KO tumors regardless of anti-PD-1 treatment status (Fig. 3b, Supplementary Table 3). We observed that 30% of the genes that were differentially expressed in PAK4 KO tumors at day 6 were also found differentially expressed in our *in vitro* analysis (Fig. 3c). B16 PAK4 KO tumors were also enriched in the same cell signatures as the PAK4 KO cells *in vitro*, such as cell motility, cell adhesion and blood vessel morphogenesis among others (Fig. 3d). In addition, the increased expression of CXCL10 in PAK4 KO tumors that we have previously described (Fig. 1c), was further validated in this RNA-seq analysis (Ext. Data Fig. 4).

When comparing B16 PAK4 KO and WT tumors harvested at day 10, we observed that PAK4 KO tumors underwent far more transcriptomic changes in response to anti-PD-1 (Fig. 4a). We found that only two genes changed in response to anti-PD-1 in WT tumors, which is consistent with the lack of anti-tumor response seen in this model, whereas up to 2995 genes were differentially expressed in PAK4 KO tumors (log2FC > 2 or < -2 and FDR < 0.05, Supplementary Table 4). Therefore, lack of *PAK4* expression facilitates changes in the tumor microenvironment, which become more evident when given anti-PD-1 therapy, to sensitize melanoma B16 tumors to anti-PD-1 treatment[13]. Among the differentially expressed genes, we found that the majority of changes occur in genes that are associated with or play a role in modulating the structure of the extracellular matrix (Fig. 4b). Furthermore, a cell adhesion signature with genes that play a role in the ECM and hence, could directly impact the tumor organization showed that the increase was specific for the PAK4 KO treated tumors (Fig. 4c). In addition, the comparison of PAK4 KO anti-PD-1 treated tumors with WT anti-PD-1 treated tumors yielded 2586 genes that were differentially expressed (log2FC > 1 or < -1 and FDR < 0.05, Supplementary Table 5). This included several gene families that could also impact the tumor architecture, including the collagen gene family (n = 20), the cadherin/protocadherin gene family (n=11), the integrin gene family (n=8) and the adam gene family (n=9) among

others (Supplementary Table 6). Additionally, we found that in B16 PAK4 KO tumors treated with anti-PD-1, there was an increase in the expression of a specific endothelial cell marker, *Cdh5* (Fig. 4d), indicating an increase in angiogenesis, which was already suggested in the *in vitro* and *in vivo* day 6 analyses (Fig. 2d and 3d). Of note, we performed IHC on a representative sample for each of the four groups (WT isotype, WT anti-PD-1, PAK4 KO isotype and PAK4 KO anti-PD-1) on day 10, to evaluate the protein expression of CD8 and CD31, which is required for leukocyte transendothelial migration. We observed that PAK4 KO tumors treated with anti-PD-1 presented higher levels of both, CD31 (WT: 4% and KO: 10%) and CD8 expression (WT: 1% and KO: 9%) (Fig. 4e). PAK4 KO anti-PD-1 treated tumors also showed a high level of spatial colocalization of these two markers, suggesting a proper functionality of these blood vessels and an active migration of $CD8^+$ cells into the tumor (Ext. Data. Fig. 5). In agreement with our results, recent work by Fan *et. al*.[27] demonstrated that knocking out *PAK4* in endothelial cells re-organize the whole tumor vascularity, increases immune cell infiltration and improves CAR-T cell therapy response in glioblastoma. Altogether, we characterized the tumor transcriptome of B16 PAK4 KO cells both, *in vitro* and *in vivo*, and determined that the main differences between PAK4 KO and WT transcriptomes are found in genes and cell signatures associated with the extracellular matrix. This suggests that the re-organization of the tumor architecture is necessary to increase immune cell infiltration and sensitize tumors to anti-PD-1 immunotherapy.

PAK4 kinase activity is responsible for the improved response to anti-PD-1 immunotherapy *in vivo*

We next aimed to investigate whether inhibition of PAK4 kinase activity was sufficient to recapitulate the improved responses to ICB. Our prior work had used genetic knockdown and a PAK4 inhibitor, KPT-9274, which works by degrading the whole protein[13,30,31], but did not directly demonstrate that the beneficial effects of PAK4 inhibition were due to inhibition of its kinase function. To this end, we first generated three different B16 PAK4 kinase dead (KD) cell lines by transducing PAK4 KO cells with a lentivirus containing the *PAK4* open reading

frame (ORF) with the lysine (K) at position 352 changed to a methionine (M) (Ext. Data Fig. 6), which was expected to inhibit PAK4 kinase activity[32,33]. In order to validate loss of functionality at the PAK4 kinase domain, we evaluated whether B16 PAK4 KD cells had decreased phosphorylation of β-catenin S675 and reduced response to Wnt-3a stimulation, as we have previously observed in B16 PAK4 KO cells as well as in human melanoma PAK4 KO cells (Ext. Data. Fig. 7). Indeed, B16 PAK4 KD cells had decreased β-catenin S675 phosphorylation (Fig. 5a) and reduced sensitivity to Wnt-3a at levels similar to the ones observed in B16 PAK4 KO cells (Fig. 5b). We next sought to determine if B16 PAK4 KD cell lines were as sensitive to anti-PD-1 immunotherapy as B16 PAK4 KO cells. We observed that blockade of PAK4 kinase activity was sufficient to overcome resistance to anti-PD-1 therapy in B16 melanoma cells as there was a significant reduction in tumor volume in B16 PAK4 KD cells treated with anti-PD-1 compared to those treated with isotype (Fig. 5c). In summary, B16 PAK4 KD cells behave as B16 PAK4 KO cells, an observation that has important implications in the development of novel PAK4 kinase inhibitors that could potentially be more potent and specific compared to total pharmacological PAK4 protein reduction.

A specific PAK4 kinase inhibitor synergizes with anti-PD-1 immunotherapy and improves responses *in vivo*

We next aimed to determine if pharmacological inhibition of PAK4 kinase activity recapitulated the effects previously observed in genetically modified cell lines. To this end, we used a novel and specific PAK4 kinase inhibitor, A0317859. First, in order to validate the efficacy of this compound *in vitro*, we studied its effect on the β-catenin/WNT signaling pathway. As observed in our PAK4 KO and KD cells, compound A0317859 succeeded in decreasing nuclear β-catenin phosphorylation at S675 (Fig. 6a) as well as in reducing sensitivity to Wnt-3a (Fig. 6b) in our B16 WT CC cells. We next investigated its activity *in vivo*. To do so, we treated murine melanoma B16 WT CC tumors with either vehicle, anti-PD-1, A0317859 or a combination of anti-PD-1 plus A0317859. The combination resulted in a significantly slower tumor growth compared to compound A0317859 or anti-PD-1 alone, which parallels the results of PAK4 KO

and KD tumors and provides a new rationale for the combination of PD-1 blockade with a specific PAK4 kinase inhibitor.

Discussion

Several signaling pathways have been associated with resistance to ICBs, such as WNT/β-catenin signaling pathway, mitogen-activated protein kinase (MAPK) signaling, MYC signaling activation, pathways activated by the loss of the tumor suppressor phosphoinositide phosphatase PTEN or loss of function of liver kinase B1 (LKB1) mediated immunosuppression[34]. Ideally, these pathways could be targeted pharmacologically and used in combination with ICBs to overcome resistance to ICB therapies. Although the association of these pathways with clinical responses to immunotherapy has become more evident, there is a lack of targets that could be pharmacologically inhibited to successfully re-wire these cancer-intrinsic oncogenic signaling pathways and sensitize tumors to ICB. We have previously shown that inhibition of the expression of *PAK4*, which encodes a serine-threonine kinase involved in the WNT/β-catenin pathway, increases T cell infiltration and overcomes resistance to PD-1 blockade in several mouse models[13]. However, the molecular mechanisms underlying the increased sensitivity to PD-1 blockade upon PAK4 inhibition are still unclear.

In the current study, we show that PAK4 inhibition not only increases T cell infiltration but also increases the infiltration of a specific subset of dendritic cells, $CD103^+$ DCs. We focused on this particular subset of dendritic cells since they have been previously associated with anti-tumor immunity in melanoma[11]. One study showed that T cell recruitment to the tumor was dependent on the presence of $CD103^+$ DCs producing CXCL10[29]. Similarly, our results showed an increase in $CD103^+$ DCs and demonstrated that *CXCL10* was the only chemokine up-regulated in PAK4 KO tumors at day 6. Moreover, these changes were observed when comparing PAK4 KO versus WT tumors, regardless of anti-PD-1 treatment status, which suggests that PAK4 inhibition alters the tumor microenvironment and facilitates the infiltration

of key immune cells that are required to mount an anti-tumor response. Nonetheless, these changes alone cannot generate a successful immune response as demonstrated by the similar growth rate of B16 PAK4 KO relative to B16 WT CC tumors. The observation that PAK4 KO tumors require the addition of anti-PD-1 in order to decrease tumor growth, highlights the importance of overcoming adaptive immune resistance mechanisms and blocking the PD-1/PD-L1 interaction. In line with these results, we found that *PAK4* expression negatively correlates with the expression of *CCL21*, the ligand for the CCR7 receptor expressed on $CD103^+$ DC. Importantly, a recent study showed that the expression of CCR7 in human melanoma correlates with the levels of T cell infiltration and patient survival[28]. The fact that PAK4 KO cells do not secrete any CCL21 suggests that, although another cell type is responsible for the secretion of this chemokine, the absence of PAK4 is necessary to increase its concentration in the tumor microenvironment. Furthermore, we have previously described that dendritic cells are the immune cell subtype that present the strongest negative correlation with *PAK4* expression in human melanoma tumors[13]. Altogether, our results suggest that PAK4 plays a key role in an initial step in the generation of an anti-tumor immune response.

The first described functional activities of PAK4 were related to cell morphology and cytoskeleton reorganization[35]. Currently, PAK4 kinase activity has also been shown to regulate β-catenin phosphorylation, which impacts WNT signaling pathway activity[36]. In addition, PAK4 scaffold functions include interaction with and regulation of the TNF signaling pathway. For instance, a recent study showed that PAK4 activated the TNF-survival pathway by directly facilitating the binding of TRADD to the TNF receptor[17]. In order to tease out which functions and signaling pathways are mediating the sensitivity to anti-PD-1, in this study we performed an extensive analysis of the transcriptomic changes that occur in PAK4 KO samples in both *in vitro* and *in vivo*. From our results, we conclude that PAK4 inhibition does not alter TNF nor IFNγ signaling pathways and we also were able to exclude the possibility of increased MHC class I presentation as a mechanism of action. Our analyses validate the role of PAK4 in β-catenin phosphorylation and WNT signaling activation. However, we have yet to

identify which key WNT-regulated genes are differentially stimulated in PAK4 KO cells. Therefore, the connection between PAK4, β-catenin and ICB efficacy requires further investigation. On the other hand, our transcriptomic data supports the importance of PAK4 in cell morphology, cell adhesion and extracellular matrix organization. *In vitro*, lack of *PAK4* expression impacts the expression of genes that encode for membrane proteins involved in cell-cell interaction. Importantly, these changes are maintained in early *in vivo* samples (day 6) and could potentially affect the tumor architecture and impact its immunogenicity. Interestingly, we also observed changes in genes that were related to blood vessel formation. This became more relevant after Yi Fan's group demonstrated that blocking *PAK4* expression in endothelial cells could reprogram the tumor vascular microenvironment, thus, facilitating the infiltration of CAR-T cells and improving the efficacy of immunotherapy in glioblastoma[27]. Although *PAK4* expression is specifically knocked out in endothelial cells, there are some similarities with our melanoma PAK4 KO cells, stressing the importance of PAK4 in modulating the tumor microenvironment and impacting immunotherapy effectiveness. For instance, our immunohistochemistry analyses show an increase of CD31 in PAK4 KO anti-PD-1 treated tumors, as well as an increase of CD8, which is spatially co-localized with CD31. While this analysis does not provide any information on the quality of the blood vessels, it shows that immune cells are able to infiltrate the tumor through them, suggesting that the blood vessels are functional. Of note, these results are limited by the sample size. Furthermore, the importance of PAK4 deletion is also supported by our late *in vivo* RNA-seq data, where anti-PD-1 treatment only changed the transcriptome of melanoma PAK4 KO tumors. The main differences were observed in genes related to the extracellular matrix and angiogenesis, and are accompanied by an improved response to ICB in our B16 melanoma mouse model. Nevertheless, whilst the association between PAK4 and the tumor microenvironment is evident, further studies are needed to elucidate the key changes that facilitate the infiltration of immune cells and overcomes the resistance to ICB.

The identification of oncogenic-driven resistance mechanisms to ICB can provide novel candidates for clinical intervention. However, discovering targets that could be exploited pharmacologically remains a challenge. Specifically, the β-catenin/WNT signaling pathway has been extensively associated with poor immune infiltration and lack of response to PD-1 blockade, but to date, there are no clinical trials that have successfully combined WNT-inhibitors with ICB inhibitors. This is in part due to the complexity and importance of this signaling pathway in regulating several essential cellular functions, which could narrow the therapeutic window. The link between PAK4 and β-catenin is consistent in our model, however we need to further investigate how PAK4 inhibition re-wires the WNT signaling pathway and examine whether these changes impact anti-PD1 efficacy. Our results demonstrate that lack of *PAK4* expression modifies the sensitivity to the main WNT ligand, Wnt-3a, while other WNT-dependent cellular functions, such as cell proliferation, remain intact. Importantly, we demonstrate that PAK4 kinase function is responsible for both: WNT signaling alteration and increased sensitivity to PD-1 blockade immunotherapy. Yet, we cannot completely exclude the possibility that other kinase-independent PAK4 functions may contribute to the phenotype we observe *in vivo*. Previous attempts to block PAK4 activity pharmacologically have failed due to a dearth of selective inhibitors or due to issues with the compound pharmacokinetics, as observed in the terminated clinical trial evaluating the pan-PAK inhibitor, PF-03758309[37]. Here, we provide the initial results of a specific and novel PAK4 kinase inhibitor, A0317859. Importantly, this compound is able to recapitulate the *in vivo* efficacy observed in our B16 PAK4 KO and PAK4 KD *in vivo* models.

In summary, in this study we showed how PAK4 inhibition remodels the tumor microenvironment, enabling the infiltration of key immune cell subtypes and changing the expression of genes involved in the tumor architecture. In addition, we established that blocking PAK4 kinase function is sufficient to overcome PD-1 blockade resistance *in vivo* and demonstrated how a novel PAK4 kinase inhibitor could potentially overcome resistance to PD-1 blockade. To date, there is only a single clinical trial (NCT02702492), combining an anti-PD-

1 antibody with a dual PAK4 and NAMPT inhibitor, KPT-9274, which decreases whole PAK4 protein expression. Our work lays the foundation for the translation of a novel, unique and specific PAK4 kinase inhibitor that could be used in combination with PD-1 blockade immunotherapy.

Acknowledgments

This study was funded in part by the Parker Institute for Cancer Immunotherapy, NIH grants R35 CA197633 and P01 CA168585, the Ressler Family Fund and the support from Ken and Donna Schultz (to A.R.). G.A-R. was supported by the Isabel & Harvey Kibel Fellowship award and the Alan Ghitis Fellowship Award for Melanoma Research. D.Y.T was supported by a Young Investigator Award from ASCO, a grant from the Spanish Society of Medical Oncology for Translational Research in Reference Centers and the V Foundation-Gil Nickel Family Endowed Fellowship in Melanoma Research. J.D.S. is a pre-doctoral fellow supported by the UCLA Tumor Immunology Training Grant (USHHS Ruth L. Kirschstein Institutional National Research Service Award # T32 CA009120). M.G. is a pre-doctoral fellow supported by the UCLA Tumor Cell Biology Training Program (USHHS Ruth L. Kirschstein Institutional National Research Service Award # T32 CA009056) and the UCLA Medical Scientist Training Program (MSTP) NIH NIGMS Training Grant T32-GM008042. C.P.S was funded by the Senior Parker Fellow from the Parker Institute for Cancer Immunotherapy (PICI). We acknowledge Jia Min Chen and Jacqueline Trent from PICI Center at UCLA for administrative support. Flow and mass cytometry were performed in the UCLA Jonsson Comprehensive Cancer Center (JCCC) and Center for AIDS Research Flow Cytometry Core Facility that is supported by NIH awards P30 CA016042 and 5P30 AI028697, and by the JCCC, the UCLA AIDS Institute, and the David Geffen School of Medicine at UCLA. The authors thank Arcus Biosciences for providing the compound, A0317859.

Author Contributions

Conception and design: G.A.-R., A.R.

Development of methodology: G.A.-R., D.Y.T., K.M.C., E.M., J.S., C.P.-S., B.C-A., A.R.

Acquisition of data (provided animals, acquired and managed patients, provided facilities, etc.): I.B.C., I.P.G., A.R.

Analysis and interpretation of data (e.g., statistical analysis, biostatistics, computational analysis): G.A.-R., D.Y.T., K.M.C., E.M., J.D.S., M.G., A.S.C., B.C-A., C.P.-S., A.R.

Writing of manuscript: G.A.-R., A.R.

Review of manuscript: All authors

References

1. Ribas, A. & Wolchok, J. D. Cancer immunotherapy using checkpoint blockade. *Science* **359**, (2018).
2. Tumeh, P. C. *et al.* PD-1 blockade induces responses by inhibiting adaptive immune resistance. *Nature* **515**, 568–571 (2014).
3. Abril-Rodriguez, G. & Ribas, A. SnapShot: Immune Checkpoint Inhibitors. *Cancer Cell* **31**, (2017).
4. Sharma, P., Hu-Lieskovan, S., Wargo, J. A. & Ribas, A. Primary, Adaptive, and Acquired Resistance to Cancer Immunotherapy. *Cell* **168**, 707–723 (2017).
5. Chen, P. L. *et al.* Analysis of immune signatures in longitudinal tumor samples yields insight into biomarkers of response and mechanisms of resistance to immune checkpoint blockade. *Cancer Discov.* **6**, 827–837 (2016).
6. Ayers, M. *et al.* IFN-γ-related mRNA profile predicts clinical response to PD-1 blockade. *J. Clin. Invest.* **127**, (2017).
7. Riaz, N. *et al.* Tumor and Microenvironment Evolution during Immunotherapy with Nivolumab. *Cell* **171**, 934-949.e15 (2017).
8. Spranger, S. & Gajewski, T. F. Impact of oncogenic pathways on evasion of antitumour immune responses. *Nat. Rev. Cancer* **18**, 139–147 (2018).
9. Peng, W. *et al.* Loss of PTEN promotes resistance to T cell–mediated immunotherapy. *Cancer Discov.* **6**, (2016).

10. Liu, C. *et al.* BRAF inhibition increases tumor infiltration by T cells and enhances the antitumor activity of adoptive immunotherapy in mice. *Clin. Cancer Res.* **19**, (2013).
11. Spranger, S., Bao, R. & Gajewski, T. F. Melanoma-intrinsic β-catenin signalling prevents anti-tumour immunity. *Nature* **523**, 231–235 (2015).
12. Luke, J. J., Bao, R., Sweis, R. F., Spranger, S. & Gajewski, T. F. WNT/b-catenin pathway activation correlates with immune exclusion across human cancers. *Clin. Cancer Res.* **25**, (2019).
13. Abril-Rodriguez, G. *et al.* PAK4 inhibition improves PD-1 blockade immunotherapy. *Nat. Cancer* **1**, (2020).
14. Qu, J., Cammarano, M. S., Shi, Q. & Ha, K. C. Activated PAK4 Regulates Cell Adhesion and Anchorage-Independent Growth Activated PAK4 Regulates Cell Adhesion and Anchorage-Independent Growth. *Mol Biol Cell* **21**, 3523–3533 (2001).
15. Lu, Y., Pan, Z. Z., Devaux, Y. & Ray, P. p21-activated protein kinase 4 (PAK4) interacts with the keratinocyte growth factor receptor and participates in keratinocyte growth factor-mediated inhibition of oxidant-induced cell death. *J. Biol. Chem.* **278**, (2003).
16. Li, Q. *et al.* p21-activated kinase 4 as a switch between caspase-8 apoptosis and NF-κB survival signals in response to TNF-α in hepatocarcinoma cells. *Biochem. Biophys. Res. Commun.* **503**, (2018).
17. Li, X. & Minden, A. PAK4 functions in tumor necrosis factor (TNF) α-induced survival pathways by facilitating TRADD binding to the TNF receptor. *J. Biol. Chem.* **280**, (2005).
18. King, H. *et al.* PAK4 interacts with p85 alpha: Implications for pancreatic cancer cell migration. *Sci. Rep.* **7**, (2017).
19. Vershinin, Z., Feldman, M. & Levy, D. PAK4 methylation by the methyltransferase SETD6 attenuates cell adhesion. *Sci. Rep.* **10**, (2020).
20. Baskaran, Y. *et al.* Proximity proteomics identifies PAK4 as a component of Afadin-Nectin junctions. *Nat. Commun.* **12**, 5315 (2021).

21. Rane, C. K. & Minden, A. P21 activated kinase signaling in cancer. *Seminars in Cancer Biology* **54**, (2019).

22. Chandrashekar, D. S. *et al.* Therapeutically actionable PAK4 is amplified, overexpressed and involved in bladder cancer progression. *bioRxiv* (2019). doi:10.1101/740316

23. Siu, M. K. Y. *et al.* P21-Activated Kinase 4 Regulates Ovarian Cancer Cell Proliferation, Migration, and Invasion and Contributes To Poor Prognosis in Patients. *Proc. Natl. Acad. Sci.* **107**, 18622–18627 (2010).

24. Zhao, M. *et al.* Role of PAK4 in pancreas development and pancreatic cancer progression. *Pancreatology* **15**, (2015).

25. He, L. F. *et al.* Activated-PAK4 predicts worse prognosis in breast cancer and promotes tumorigenesis through activation of PI3K/AKT signaling. *Oncotarget* **8**, (2017).

26. Costa, T. D. F. *et al.* PAK4 suppresses RELB to prevent senescence-like growth arrest in breast cancer. *Nat. Commun.* **10**, (2019).

27. Ma, W. *et al.* Targeting PAK4 to reprogram the vascular microenvironment and improve CAR-T immunotherapy for glioblastoma. *Nat. Cancer* **2**, (2021).

28. Roberts, E. W. *et al.* Critical Role for CD103+/CD141+ Dendritic Cells Bearing CCR7 for Tumor Antigen Trafficking and Priming of T Cell Immunity in Melanoma. *Cancer Cell* **30**, (2016).

29. Spranger, S., Dai, D., Horton, B. & Gajewski, T. F. Tumor-Residing Batf3 Dendritic Cells Are Required for Effector T Cell Trafficking and Adoptive T Cell Therapy. *Cancer Cell* **31**, (2017).

30. Rane, C. *et al.* A novel orally bioavailable compound KPT-9274 inhibits PAK4, and blocks triple negative breast cancer tumor growth. *Sci. Rep.* **7**, 1–12 (2017).

31. Li, N. *et al.* Dual PAK4-NAMPT inhibition impacts growth and survival, and increases sensitivity to DNA-damaging agents in Waldenstrom € macroglobulinemia. *Clin. Cancer Res.* **25**, (2019).

32. Foxall, E. *et al.* PAK4 Kinase Activity Plays a Crucial Role in the Podosome Ring of Myeloid Cells. *Cell Rep.* **29**, (2019).

33. Gnesutta, N. & Minden, A. Death Receptor-Induced Activation of Initiator Caspase 8 Is Antagonized by Serine/Threonine Kinase PAK4. *Mol. Cell. Biol.* **23**, (2003).

34. Kalbasi, A. & Ribas, A. Tumour-intrinsic resistance to immune checkpoint blockade. *Nature Reviews Immunology* **20**, (2020).

35. Eby, J. J. *et al.* Actin cytoskeleton organization regulated by the PAK family of protein kinases. *Curr. Biol.* **8**, (1998).

36. Li, Y. *et al.* Nucleo-cytoplasmic shuttling of PAK4 modulates β-catenin intracellular translocation and signaling. *Biochim. Biophys. Acta - Mol. Cell Res.* **1823**, 465–475 (2012).

37. Murray, B. W. *et al.* Small-molecule p21-activated kinase inhibitor PF-3758309 is a potent inhibitor of oncogenic signaling and tumor growth. *Proc. Natl. Acad. Sci. U. S. A.* **107**, (2010).

38. Kim, D., Langmead, B. & Salzberg, S. L. HISAT: A fast spliced aligner with low memory requirements. *Nat. Methods* **12**, (2015).

39. Anders, S., Pyl, P. T. & Huber, W. HTSeq-A Python framework to work with high-throughput sequencing data. *Bioinformatics* **31**, (2015).

40. Love, M. I., Huber, W. & Anders, S. Moderated estimation of fold change and dispersion for RNA-seq data with DESeq2. *Genome Biol.* **15**, (2014).

41. Subramanian, A. *et al.* Gene set enrichment analysis: A knowledge-based approach for interpreting genome-wide expression profiles. *Proc. Natl. Acad. Sci. U. S. A.* **102**, (2005).

Figure 1

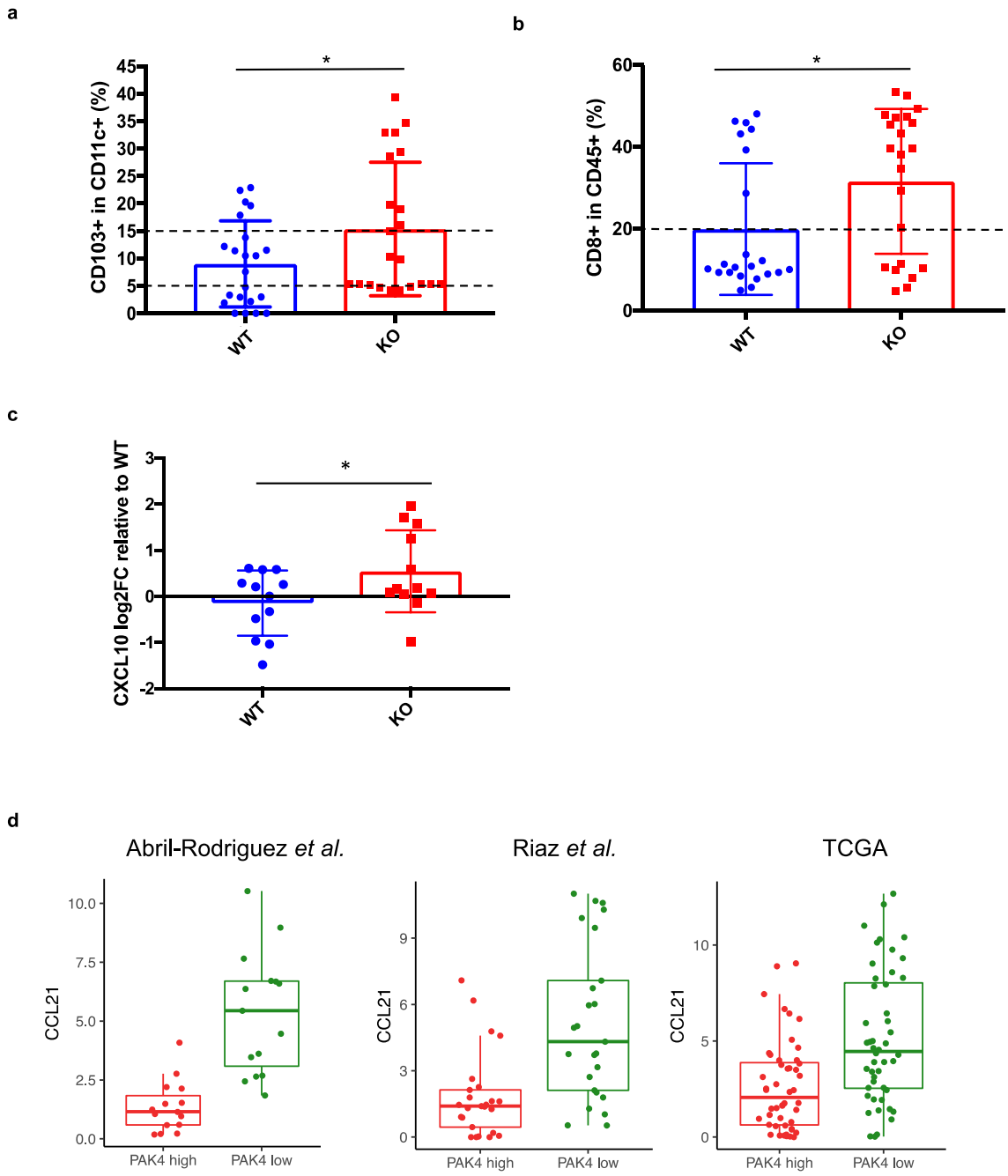
a
CD103+ in CD11c+ (%)
45
40
35
30
25
20
15
10
5
0
*
WT
KO
b
CD8+ in CD45+ (%)
60
40
20
0
*
WT
KO
c
CXCL10 log2FC relative to WT
3
2
1
0
-1
-2
*
WT
KO
d
Abril-Rodriguez et al.
Riaz et al.
TCGA
CCL21
10.0
7.5
5.0
2.5
0.0
9
6
3
0
10
5
0
PAK4 high
PAK4 low

Figure 1: PAK4 expression levels are negatively associated with the presence of CD103$^+$ dendritic cells *in vivo* and the levels of their ligand, CCL21 in biopsies of patients with melanoma. a, Differences in the infiltration of CD103$^+$ dendritic cells in B16 WT CC and PAK4 KO tumors (n = 44, 22 per group). Tumors were collected on day 6, after one dose of anti-PD-1. After processing and staining, CD103$^+$ DCs were gated for singlets, live cells, CD45$^+$, MHC-II$^+$, CD11c$^+$ and CD103$^+$ cells. B16 PAK4 KO tumors had significantly higher levels of CD103$^+$ DCs compared to B16 WT CC tumors (P = 0.04). **b,** Differences in the infiltration of CD8$^+$ cells. Samples were gated for singlets, live cells, CD45$^+$ and CD8$^+$ population to have an estimate of the number of CD8 T cells. B16 PAK4 KO samples showed a significant increase of CD45$^+$/CD8$^+$ cells compared to WT CC tumors (P = 0.02). **c,** RNA from a total of 24 samples (n = 12 per each group) were collected to perform RT-PCR. The cycle threshold (Ct) of each sample was normalized by the mean of the WT isotype group. CXCL10 expression is significantly increased in the PAK4 KO group. **d,** Differences in CCL21 log2FPKM expression levels between high and low PAK4 in biopsies of patients with melanoma (based on the upper and lower quartile) across three different clinical datasets: Abril-Rodriguez *et. al.*, Riaz *et. al.*, and TCGA. In all 3 cohorts, CCL21 levels were significantly enriched ($P < 0.05$) in patients with low PAK4 expression.

Figure 2

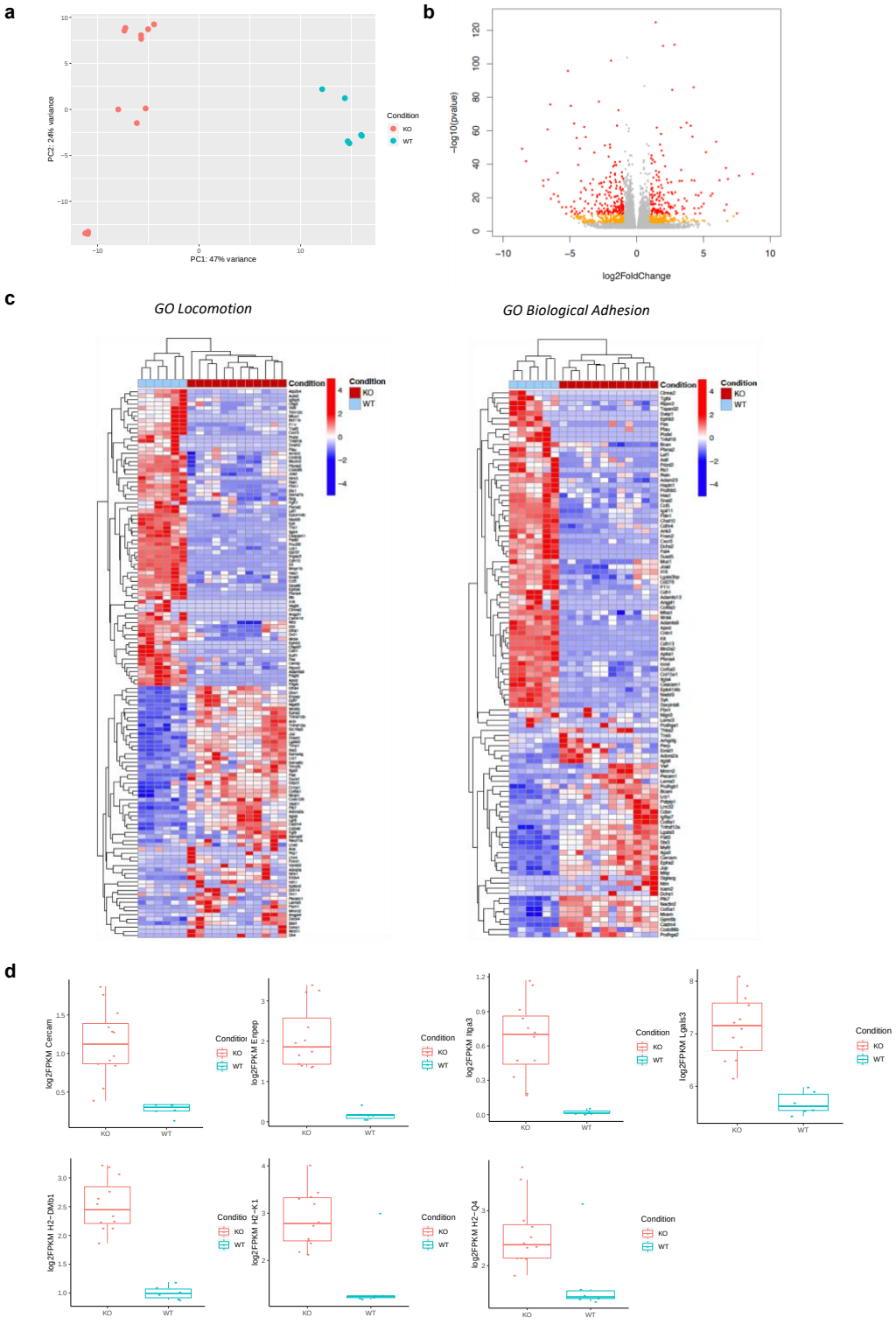
a
PC2: 24% variance
PC1: 47% variance
Condition
KO
WT
b
−log10(pvalue)
log2FoldChange
c
GO Locomotion
GO Biological Adhesion
Condition
KO
WT
d
log2FPKM Cercam
log2FPKM Entpp
log2FPKM Itga3
log2FPKM Lgals3
log2FPKM H2−DMb1
log2FPKM H2−K1
log2FPKM H2−Q4

Figure 2: *In vitro* transcriptomic comparison of PAK4 KO and WT cells shows differences in extracellular matrix genes. a, Principal component analysis (PCA) of 18 *in vitro* samples (12 KO and 6 WT CC). Principal component 1 (PC1) is related to PAK4 expression and explains almost half of the variance of this cohort (47%). **b,** Volcano plot derived from the differential gene expression analysis between PAK4 KO and WT CC samples. In red, genes with log2FC > 1 or < -1 and p-value < 5e-05. In orange, genes with log2FC > 1 or < -1 and p-value < 0.05. In grey, genes that do not fall in any of the two previous categories. **c,** Heatmap of two selected signatures: locomotion and biological adhesion from Gene Ontology (GO), after performing Gene Set Enrichment Analysis with the list of differentially expressed genes (q < 0.05 and log2FC >1 or <-1) resulted from KO vs WT CC comparison. Samples are separated based on PAK4 expression (condition: WT and KO). Plotting the raw z-score. **d,** Differences between PAK4 KO (n = 12) and WT CC (n = 6) cells in the expression of genes associated to blood vessel formation: *Cercam*, *Enpep*, *Itga3*, *Lgals3*, and antigen presentation machinery: *H2-Dmb1*, *H2-K1* and *H2-Q4* (*P* < 0.05 for all genes).

Figure 3

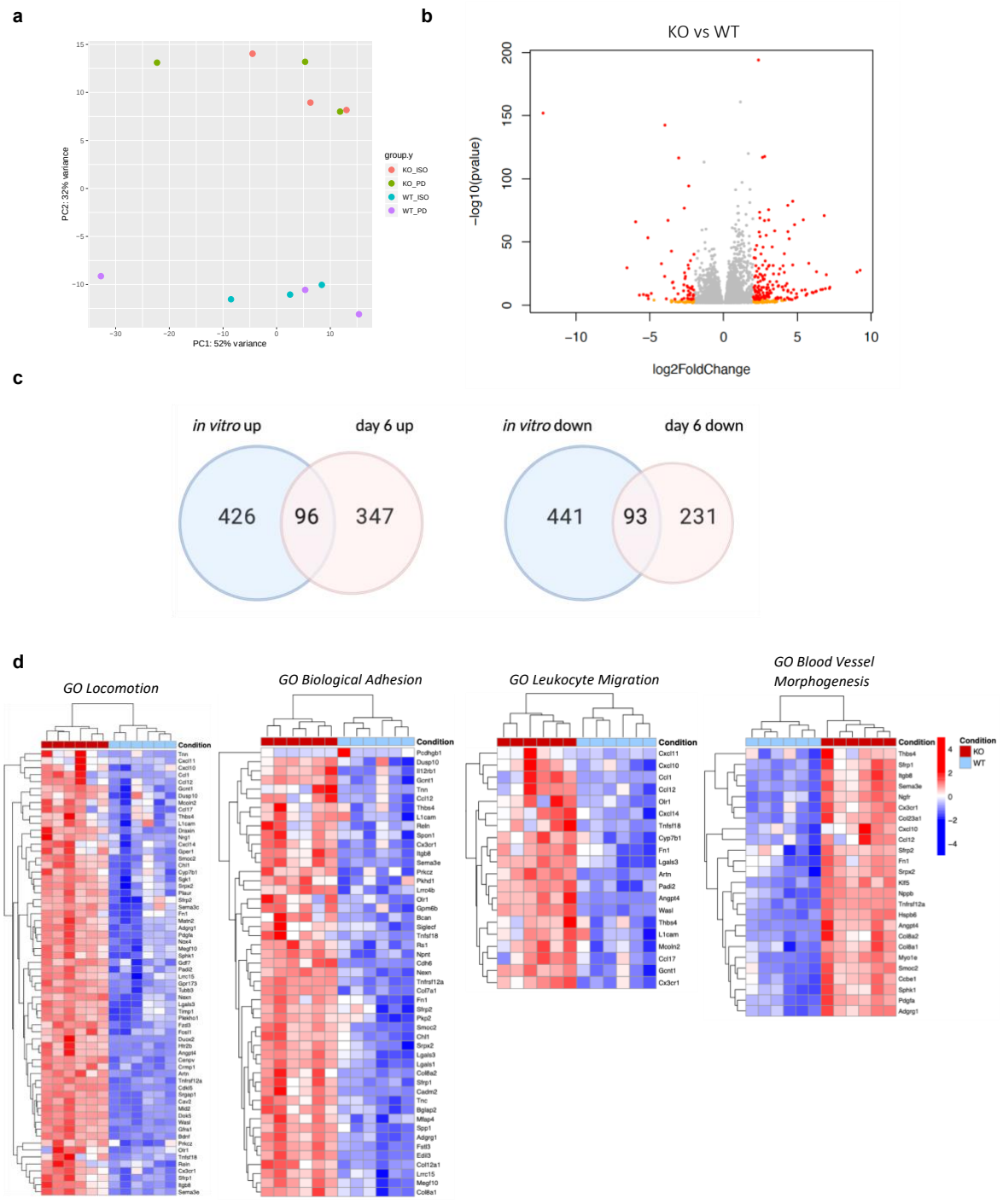
a
PC2: 32% variance
PC1: 52% variance
group.y
KO_ISO
KO_PD
WT_ISO
WT_PD
b
KO vs WT
−log10(pvalue)
log2FoldChange
c
in vitro up
day 6 up
426
96
347
in vitro down
day 6 down
441
93
231
d
GO Locomotion
GO Biological Adhesion
GO Leukocyte Migration
GO Blood Vessel Morphogenesis
Condition
KO
WT

Figure 3: Transcriptomic characterization of early *in vivo* PAK4 KO tumors reveals major changes in the tumor microenvironment. a, Principal component analysis (PCA) of 12 *in vivo* samples (6 KO and 6 WT CC). In this case, principal component 2 (PC2) is related to PAK4 expression and explains almost 32% of the variance of this cohort. **b,** Volcano plot derived from the differential gene expression analysis between PAK4 KO and WT CC tumors, regardless of anti-PD-1 treatment. In red, genes with log2FC > 1 or < -1 and p-value < 5e-05. In orange, genes with log2FC > 1 or < -1 and p-value < 0.05. In grey, genes that do not fall in any of the two previous categories. **c,** Venn diagram showing the overlap between DEG (q < 0.05 and log2FC >1 or <-1) *in vitro* and early *in vivo* samples. **d,** Heatmap (raw z-score) of four enriched GO signatures: locomotion, biological adhesion, leukocyte migration and blood vessel morphogenesis, after GSEA with the DEG from comparing KO vs WT CC tumors. Again, samples are separated based on PAK4 expression (condition: WT and KO).

Figure 4

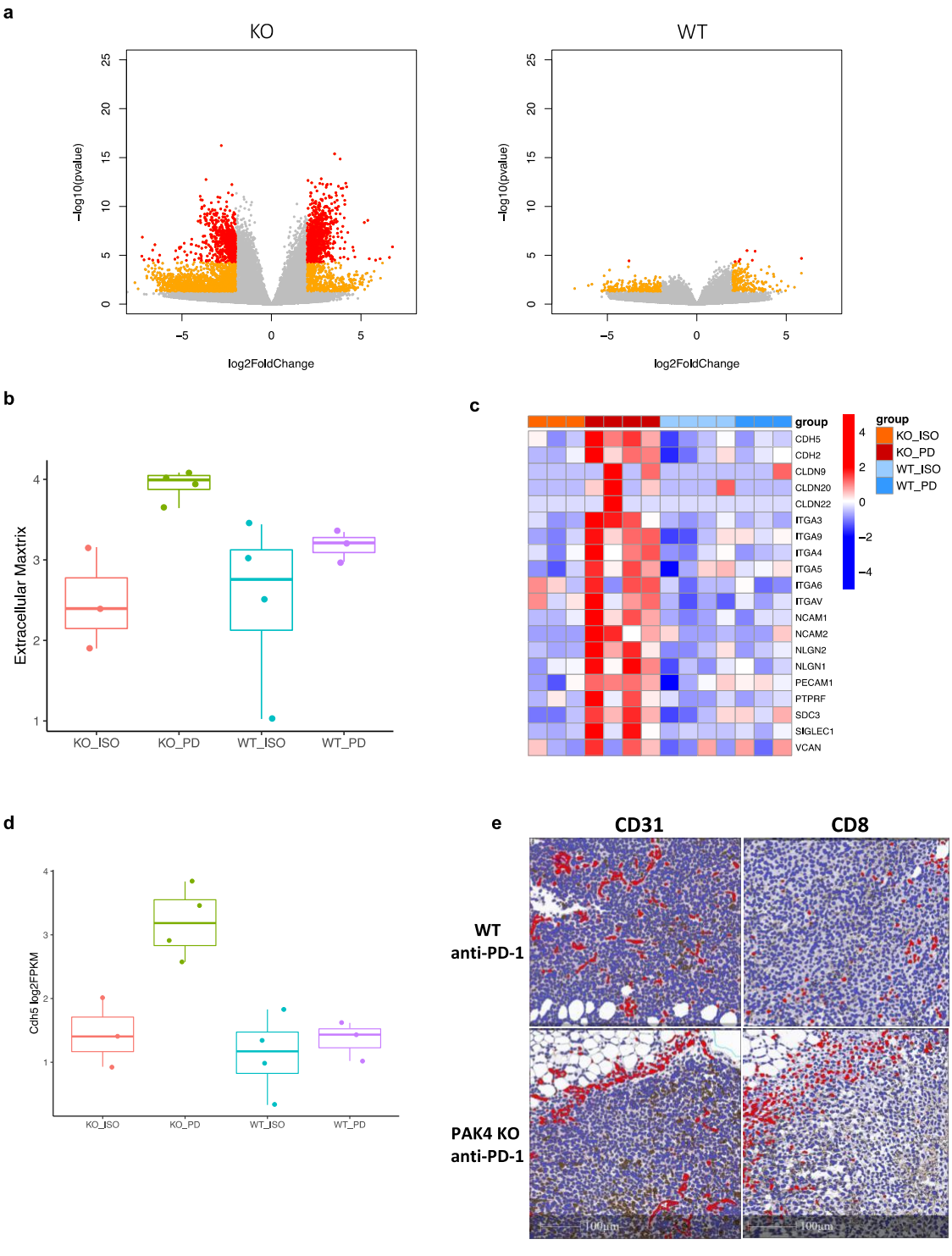
a
KO
WT
−log10(pvalue)
log2FoldChange
b
Extracellular Maxtrix
KO_ISO
KO_PD
WT_ISO
WT_PD
c
group
CDH5
CDH2
CLDN9
CLDN20
CLDN22
ITGA3
ITGA9
ITGA4
ITGA5
ITGA6
ITGAV
NCAM1
NCAM2
NLGN2
NLGN1
PECAM1
PTPRF
SDC3
SIGLEC1
VCAN
d
Cdh5 log2FPKM
e
CD31
CD8
WT
anti-PD-1
PAK4 KO
anti-PD-1
100μm

Figure 4: Transcriptome analysis of PAK4 KO deletion resulting in tumor sensitization to anti-PD-1 treatment. a, Volcano plots derived from the differential gene expression analysis between untreated and anti-PD-1 treated PAK4 KO tumors (left, n = 7) or WT CC tumors (right, n= 7). In red, genes with log2FC > 1 or < -1 and p-value < 5e-05. In orange, genes with log2FC > 1 or < -1 and p-value < 0.05. In grey, genes that do not fall in any of the two previous categories. **b,** Comparison of the geometric mean of a signature related to the extracellular matrix (Reactome ECM) for each of the different four groups: KO Isotype (KO ISO), KO anti-PD-1 (KO PD), WT Isotype (WT ISO) and WT anti-PD-1 (WT PD). Only PAK4 KO tumors significantly change upon anti-PD-1 treatment. **c,** Heatmap of selected genes related to the ECM such as cadherins, claudins and integrins among others. Again, anti-PD-1 treatment affects the expression of these genes only in PAK4 KO tumors. Plotting the raw z-score. **d,** Differences between PAK4 WT and KO anti-PD-1 treated tumors in the expression of genes specific for endothelial cells. **e,** Images from two representative B16 WT anti-PD-1 (top) and PAK4 KO anti-PD-1 (bottom) tumors. Slides were stained with CD8 and CD31. Scale bar, 100µm.

Figure 5

a

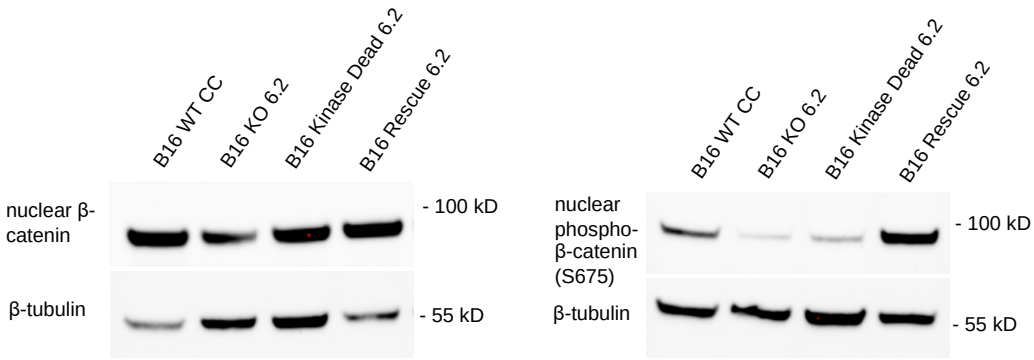
B16 WT CC
B16 KO 6.2
B16 Kinase Dead 6.2
B16 Rescue 6.2
nuclear β-catenin
- 100 kD
β-tubulin
- 55 kD
B16 WT CC
B16 KO 6.2
B16 Kinase Dead 6.2
B16 Rescue 6.2
nuclear phospho-β-catenin (S675)
- 100 kD
β-tubulin
- 55 kD

b

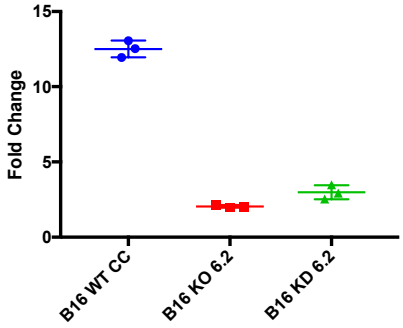
Fold Change
15
10
5
0
B16 WT CC
B16 KO 6.2
B16 KD 6.2

c

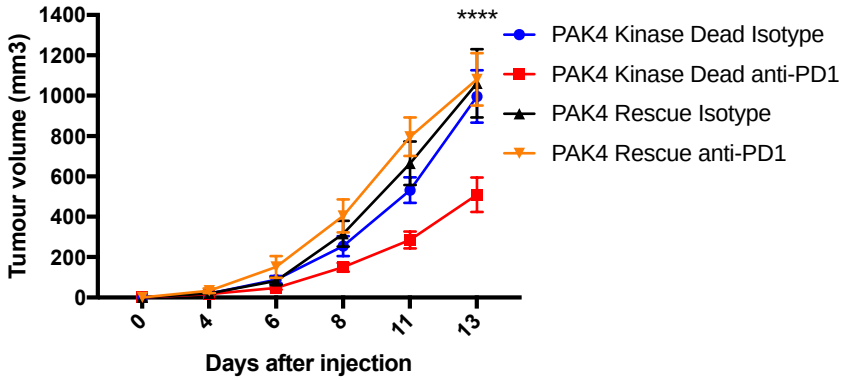
Tumour volume (mm3)
1400
1200
1000
800
600
400
200
0
****
0
4
6
8
11
13
Days after injection
PAK4 Kinase Dead Isotype
PAK4 Kinase Dead anti-PD1
PAK4 Rescue Isotype
PAK4 Rescue anti-PD1

Figure 5: Genetic inhibition of PAK4 kinase activity sensitizes tumors to anti-PD-1 *in vivo*. a, Immunoblot for nuclear β-catenin expression (left) and nuclear phospho-β-catenin S675 (right) in B16 WT CC, PAK4 KO, PAK4 Kinase Dead and B16 PAK4 Rescue cells. PAK4 KD cells recapitulates the effects on β-catenin observed in B16 PAK4 KO cells. **b,** Topflash experiment to quantify β-catenin/WNT signaling activation. Cells were treated with ligand Wnt-3a at 200ng/mL for 8 hours. Showing the fold change in luciferase activity between untreated and WNTA-3a treated samples for B16 WT CC, KO and KD cells. Inhibition of PAK4 kinase activity decreases sensitivity to WNT-3a *in vitro*. Results are representative from three independent experiments. **c,** Tumor growth curves for B16 PAK4 Kinase Dead tumors treated with isotype (n = 12, blue), anti-PD-1 (n = 14, red) and B16 PAK4 rescue tumors treated with isotype (n = 9, black) and anti-PD-1 (n = 9, orange). PAK4 Kinase Dead tumors are able to overcome resistance to anti-PD-1 in melanoma B16 cells (P = 2.1e-09) day 13, comparison between PAK4 KD anti-PD-1 and Rescue anti-PD-1). Statistical significance and correction for multiple comparisons was calculated using Holm-Sidak method. ****$P < 0.0001$.

Figure 6

a

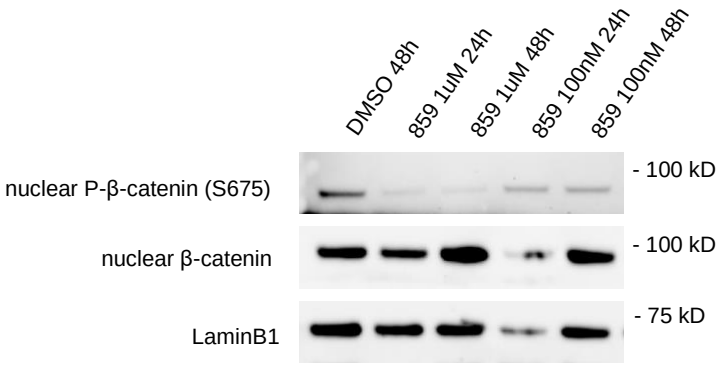
DMSO 48h
859 1uM 24h
859 1uM 48h
859 100nM 24h
859 100nM 48h
nuclear P-β-catenin (S675)
- 100 kD
nuclear β-catenin
- 100 kD
LaminB1
- 75 kD

b

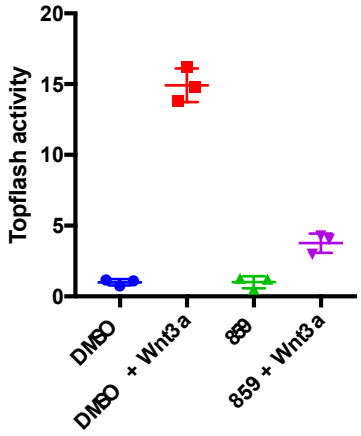
Topflash activity
20
15
10
5
0
DMSO
DMSO + Wnt3a
859
859 + Wnt3a

c

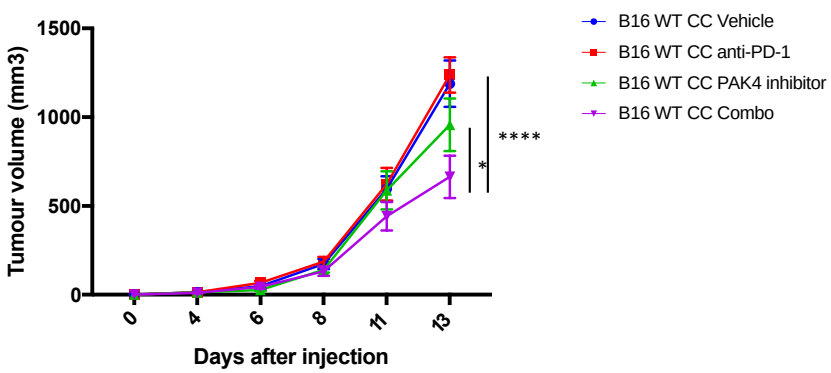
Tumour volume (mm3)
1500
1000
500
0
0
4
6
8
11
13
Days after injection
****
*
B16 WT CC Vehicle
B16 WT CC anti-PD-1
B16 WT CC PAK4 inhibitor
B16 WT CC Combo

Figure 6: Pharmacological inhibition of PAK4 kinase activity with A0317859 synergizes with anti-PD-1 immunotherapy *in vivo*. a, Immunoblot for nuclear β-catenin expression (middle lane) and nuclear phospho-β-catenin S675 (top lane) in B16 WT CC cells treated with the PAK4 inhibitor, A0317859, at two different concentrations: 1uM and 100mM, and two different timepoints 24h and 48h. A0317859 is able to reduce S675 β-catenin phosphorylation in all four conditions without having an impact on total nuclear β-catenin expression. **b,** Topflash experiment to test efficacy of PAK4 inhibitor on β-catenin/WNT signaling activation. The four groups include: cells treated with DMSO only, DMSO and Wnt-3a at 200ng/mL for 8 hours, A0317859 at 1uM for 24h and A0317859 at 1uM for 24h together with Wnt-3a at 200ng/mL for 8 hours. A0317859 is able to reduce sensitivity to Wnt-3a stimulation as observed in B16 PAK4 KD cells. Results are representative from three independent experiments. **c,** Tumor growth curves for B16 PAK4 WT tumors treated with isotype (n = 8, blue), anti-PD-1 (n = 8, red), A0317859 (n = 6, green) and combination of A0317859 and anti-PD-1 (n = 8, purple). Pharmacological inhibition of PAK4 kinase activity has a significantly higher anti-tumor activity compared to anti-PD-1 treatment alone (P = 3.7e-09 day 13). Statistical significance and correction for multiple comparisons was calculated using Holm-Sidak method. ****$P < 0.0001$.

Methods

Cell lines and PAK4 Kinase Dead generation

Murine B16 cells were maintained in DMEM medium, supplemented with 10% FBS, 100 units/mL penicillin, and 100 µg/mL streptomycin at 37°C in a humidified atmosphere of 5% CO_2. In order to generate a B16 PAK4 Kinase Dead cell line we took advantage of the previously generated lentiviral vector with the PAK4 open reading frame and performed site directed mutagenesis with the following primers containing the mutation to change AAG codon to ATG (K352M): 5-GGCAAACTGGTGGCCGTCATGAAGATGGACTTGCGCAAGC-3 and 5-GCTTGCGCAAGTCCATCTTCATGACGGCCACCAGTTTGCC-3. After cloning and vector amplification on Stbl3, 293T cells were used for lentiviral particle generation and B16 PAK4 KO cells were transduced at 20% confluency. 24 hours after transduction, media was changed and cells were expanded and sorted based on Thy1.1 expression. PAK4 expression and loss of kinase activity was validated by Western Blot and Topflash assay.

Mouse model studies

All mouse studies were performed under the UCLA Animal Research Committee protocol #2004-159-23. C57BL/6 mice were bred and kept under defined-flora pathogen-free conditions at the Association for Assessment and Accreditation of Laboratory Animal Care approved animal facility of the Division of Experimental Radiation Oncology, UCLA. To study the *in vivo* effects of genetically blocking the kinase activity of PAK4 effect on PD-1 blockade efficacy, we subcutaneously injected $0.3x10^6$ B16 PAK4 Kinase Dead and B16 PAK4 Rescue into the flanks of C57BL/6 syngeneic mice. 96 hours after tumor injection mice were randomly assigned into the different groups. Anti PD-1 (Cat. No. BE0146, clone RMP1-14, BioXCell, West Lebanon, NH) treatment was injected intraperitoneally three times per week at 300 µg per dose. We followed the same protocol to test the impact of pharmacological inhibition of PAK4 kinase activity. In this case, we established four treatment groups of B16 WT CC melanoma cells: 1) vehicle, 2) anti-PD-1, 3) PAK4 inhibitor (A0317859) and 4) combination.

The PAK4 inhibitor was administered by oral gavage at 300mg/kg daily and anti-PD-1 was injected intraperitoneally three times per week at 200 µg per dose. In all *in vivo* studies, tumor progression was monitored three times per week by measuring two perpendicular dimensions with a caliper.

Flow cytometry

In order to characterize and quantify the dendritic cell population, we collected mouse tumor samples from B16 WT CC or PAK4 KO melanoma cells treated with anti-PD-1 or vehicle at two different time points, day 6 and day 10. As described previously[13], tumor samples were processed using the mouse tumor dissociation kit (Miltenyi, Bergisch Gladbach, Germany) following manufacture's protocol. Samples were stained using the antibodies listed in Supplementary Table 1. Following staining, samples were analyzed using the Attune Flow Cytometer (Thermo Fisher Scientific, Waltham, MA) platform at the UCLA Flow Cytometry core. Samples were analyzed using FlowJo software (v10.4.2, Ashland, OR) and the gating strategy is provided on Supplementary Figure 1.

RNA-seq analysis

To study the transcriptomic differences between PAK4 KO and WT cells, we harvested and collected RNA from a total of 18 in vitro samples (12 KO and 6 WT), using the RNeasy mini kit (Qiagen, Hilden, Germany). These samples also included some that have been previously stimulated with either TNF at 100ng/mL for 6 hours (Peprotech, Rocky Hill, NJ), IFNg at 100UI/mL for 6 hours (Peprotech, Rocky Hill, NJ) or Wnt-3a at 200ng/mL for 8 hours (R&D Systems, Minneapolins, MN). We also isolated RNA from *in vivo* B16 WT CC and KO tumors as described previously[13]. Samples were sequenced using the Illumina NextSeq500 platform with a read length of 1x75 at the UCLA Technology Center for Genomics & Bioinformatics. Raw FASTQ files were aligned to the GRCh38 genome (human) and GRCm38 genome (mouse) using HISAT2 version 2.1.0[38] using the default parameters and counted with HTseq version 0.6.1p1[39]. Differential gene expression was performed based on the negative binomial

distribution with the DESeq2 package using default settings. To perform principal component analyses with the DESeq2 package[40], raw reads were previously normalized using the variance stabilizing transformation (vst) function. We also used Gene Set Enrichment Analysis (GSEA) analysis with the following gene sets: C2 Curated Gene Sets and C5 Gene Ontology Gene Sets[41] to identify which signaling pathways were enriched in each of the different groups.

IHC analysis

Tissues were fixed in 10% neutral buffered formalin, processed and embedded in paraffin, and sectioned at 4µm thickness using standard histological procedures. Slides were dewaxed using xylene and rehydrated with a graded series of ethanol using a DAKO Coverstainer (DAKO, Agilent Technologies, Santa Clara, CA). Antigen retrieval was performed in a high pH buffer using PT Link (DAKO, Agilent Technologies, Santa Clara CA) at 95 °C for 20 minutes. Immunohistochemistry was carried out using a DAKO Autostainer Link 48 platform (DAKO, Agilent Technologies, Santa Clara, CA). Briefly, slides were blocked for endogenous peroxidases and subsequently stained using the following primary antibodies: rabbit anti-mouse CD8 (D4W27 at 1:200), Rabbit anti-mouse CD45 (Cell Signaling Technologies D3F8Q at 1:200), and Rabbit anti-mouse CD31 antibodies (Abcam EPR17259 at 1:500) in Da Vinci diluent (Biocare Medical, Pacheco CA). MACH2 Rabbit AP polymer (Biocare Medical, Pacheco CA) was used to detect primary antibodies, followed by detection using Enzo Red chromogen (Enzo Life Sciences, Farmingdale, NY). Slides were then counterstained with Tacha's Hematoxylin (Biocare Medical, Pacheco CA), dehydrated, and coverslipped using the DAKO Coverstainer. Once dried, slides were scanned using a 3D Histech Pannoramic MIDI II Scanner (3DHISTECH, Budapest, Hungary), then image/spatial analyses were performed using HALO software (Indica Labs, Albuquerque, NM).

WNT activity assays

Protein levels and S675-phosphorylation of β-catenin were evaluated by Western Blot as described previously[13] using the following antibodies: β-catenin (Cat. No. 9587) and phospho-

β-catenin (S675) (Cat. No. 9567) from Cell Signaling Technology, Danvers, MA. Nuclear and cytoplasmic extractions were performed with NE-PERTM Nuclear and Cytoplasmic Extraction Reagents (Thermo Fisher Scientific, Waltham, MA) following the manufacture's protocol. Topflash WNT activity assay were performed as described previously[13] using pSV-β-galactosidase control vector (PR-E1081, Promega, Madison, WI), pTopflash (Addgene, Cat. No. 12456) and mouse recombinant Wnt-3a (R&D Systems, Minneapolins, MN). For luciferase activity detection, we used the Bright-Glo Luciferase Assay System (Promega, Cat. No. PR-E2610) and the Beta-Glo Assay System (Promega, Cat. No. PR-E4720).

Protein level quantification

CXCL10 expression was measured by RT-PCR following the manufacturer's protocol for the Power SYBR® Green RNA-to-CT™ 1-Step Kit (Applied Biosystems, Foster City, CA) and using the following FW and RV primers: 5-AATCATCCCTGCGAGCCTAT-3 and 5-TTTTTGGCTAAACGCTTTCAT-3.

CCL21 protein expression was measured with the mouse 6-Ckine (CCL21A) ELISA kit (Thermo Fisher Scientific, Waltham, MA) following the manufacturer's protocol.

Mouse MHC Class I and II were analyzed by flow cytometry with the following antibodies: MHC Class I (H-2Kb) monoclonal antibody (AF6-88.5.5.3), APC, eBioscience and MCH Class II (I-A/I-E) monoclonal antibody (M5/114.15.2), APC, eBioscience.

Statistics & Reproducibility

GraphPad Prism7 (GraphPad Software, Inc, La Jolla, CA), R software (v3.5.1) and FlowJo™ Version 10.7.1 (Ashland, OR) was used for graphic representation and statistical analysis. Comparisons of $CD103^+$ DC were performed using an unpaired t-test with Welch's correction. As described previously[13], differential gene expression was performed using the R package DESeq2 in which p-values were calculated using the negative binomial generalized linear model fitting and the Wald significance test. The adjusted p values (q) were obtained by applying the Benjamini Hochberg method. For *in vivo* studies, statistical significance and

correction for multiple comparisons was calculated using the Holm-Sidak method. Differences were considered statistically significant if $P < 0.05$.

Supplementary Data

Extended Data Figures and Supplementary Figures to “PAK4 inhibition remodels the tumor microenvironment to increase PD-1 blockade efficacy” by Gabriel Abril-Rodríguez, Davis Y. Torrejon, Katie M. Campbell, Egmidio Medina, Justin D. Saco, Ameya S. Champhekar, Ivan Perez-Garcilazo, Ignacio Baselga-Carretero, Jas Singh,Begoña Comin-Anduix, Cristina Puig-Saus, Antoni Ribas.

Ext. Data Fig. 1

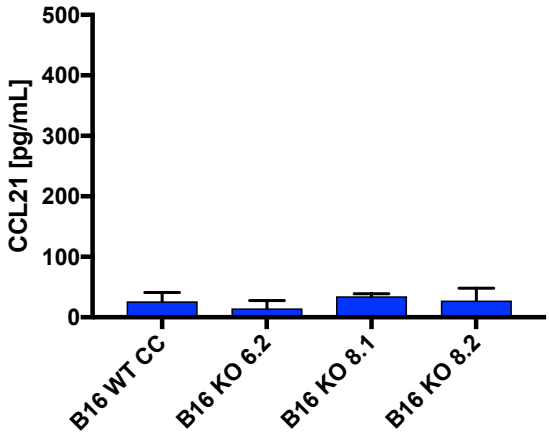

Extended Data Figure 1: PAK4 deletion does not affect CCL21 secretion. Cells were seeded in 96 well plates by triplicate and media from B16 WT CC and three independent PAK4 KO cell lines were collected to measure CCL21 protein levels by ELISA. No differences between WT and KO cells were observed.

Ext Data Fig. 2

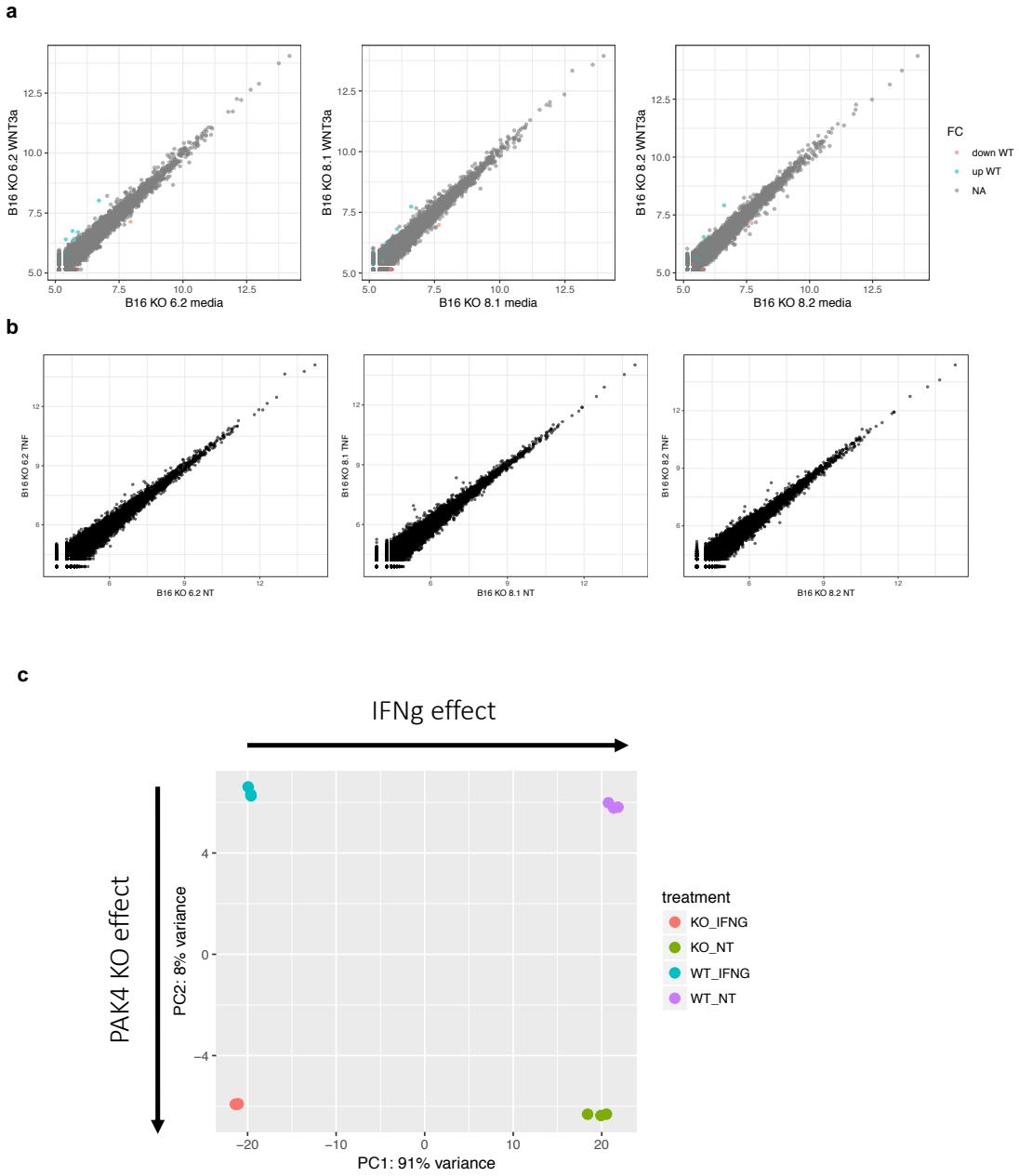

Extended Data Figure 2: No difference in signalling through different stimuli between PAK4 KO and WT cells. a, We collected RNA and sequenced cells treated with Wnt-3a at 200ng/mL for 8 hours. Scatter plot of the log2FPKM expression of all genes between untreated (X axis) and treated (Y axis) cells for each of the different PAK4 KO clones. To visualize that the same genes that change upon Wnt-3a stimuli in KO cells, also change in WT cells, we coloured them in red (up-regulated) and blue (down-regulated). **b,** Cells were treated with TNF at 100ng/mL for 6 hours before extracting RNA for sequencing. As in a, showing scatter plot of the log2FPKM expression of all genes between untreated and treated cells. TNF does not affect the transcriptome of B16 PAK4 KO cells. **c,** We collected RNA and sequenced cells treated with IFNg at 100ng/mL for 6 hours. Principal component analysis reveals that there are no differences in IFNg signalling between PAK4 KO and WT cells as both fall in the same position of the PC1 axis which explains the effect of adding IFNg.

Ext. Data Fig. 3

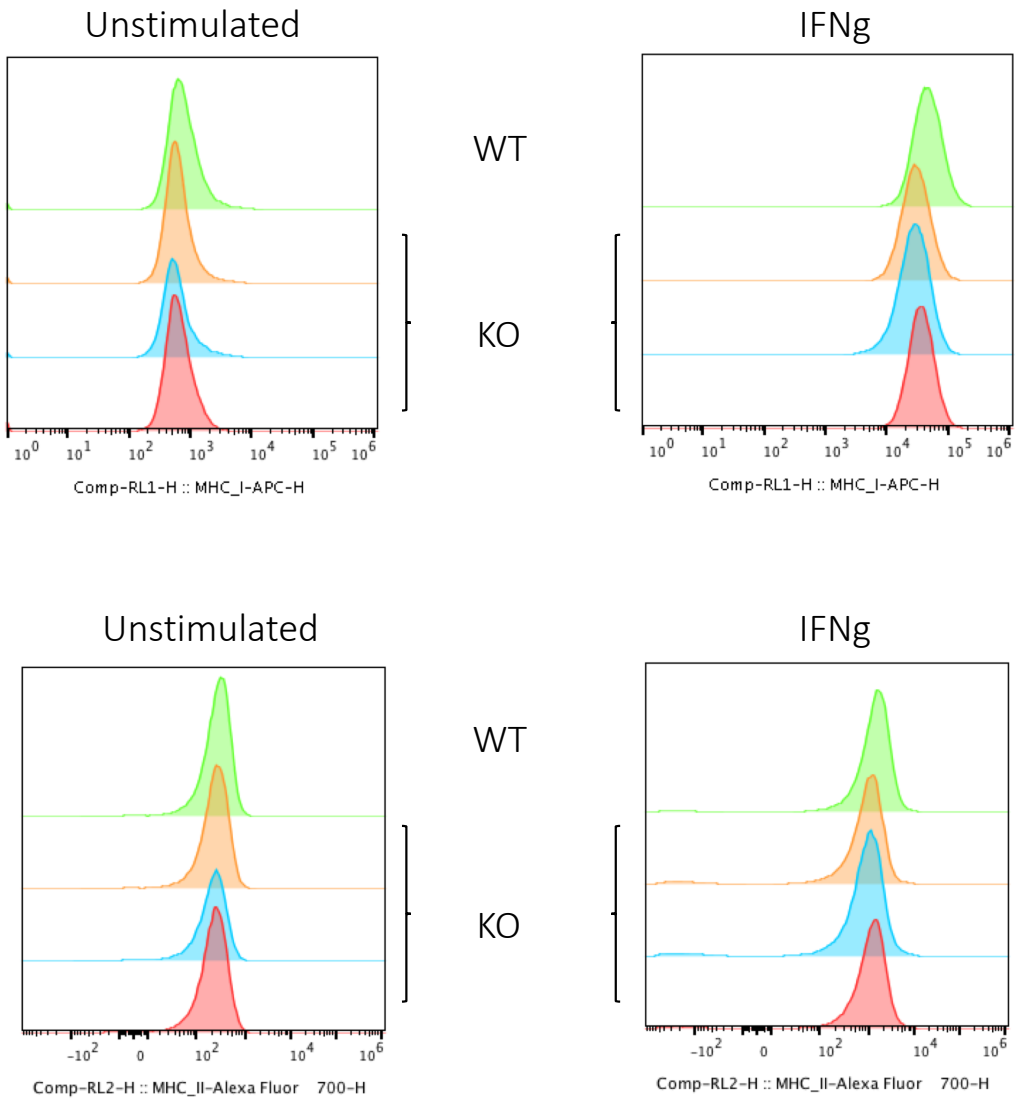

Extended Data Figure 3: PAK4 deletion does not affect MHC-I and II surface expression. B16 WT and KO cells were treated with IFNg at 100ng/mL for 6 hours and stained for MHC-I and II expression. No statistical differences between the MHC surface up-regulation in WT and KO cells was found.

Ext. Data Fig. 4

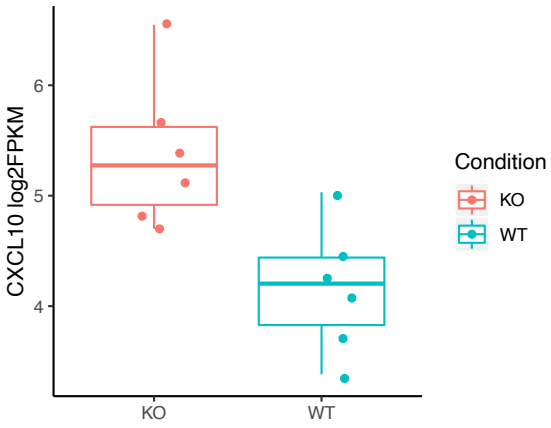

Extended Data Figure 4: PAK4 deletion increases CXCL10 expression *in vivo*. Boxplot showing the log2FPKM for CXCL10 at day 6 in PAK4 KO tumors (n= 6) and WT tumors (n = 6). CXCL10 expression in enriched in KO tumors.

Ext. Data Fig. 5

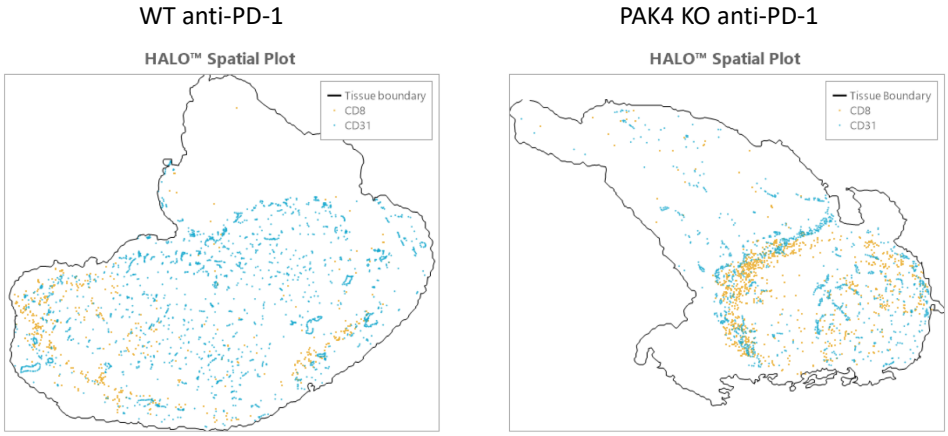

Extended Data Figure 5: Spatial colocalization of CD8 and CD31 positive cells. PAK4 KO tumors treated with anti-PD-1 show a high overlap between CD8 and CD31 while WT anti-PD-1 tumors show a more diffuse CD31 distribution without $CD8^+/CD31^+$ clusters.

Ext. Data Fig. 6

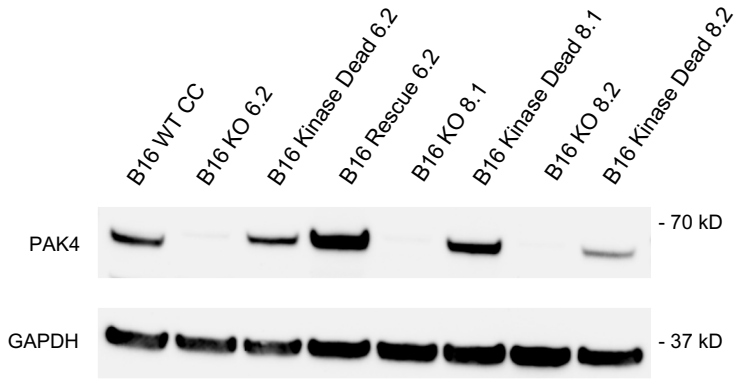

Extended Data Figure 6: PAK4 protein expression levels in the different cell lines. Cells were cultured and harvested for protein isolation upon reaching 80% confluency. Showing immunoblot for PAK4 expression protein levels in WT, PAK4 KO, Kinase Dead and Rescue cell lines.

Ext. Data Fig. 7

a

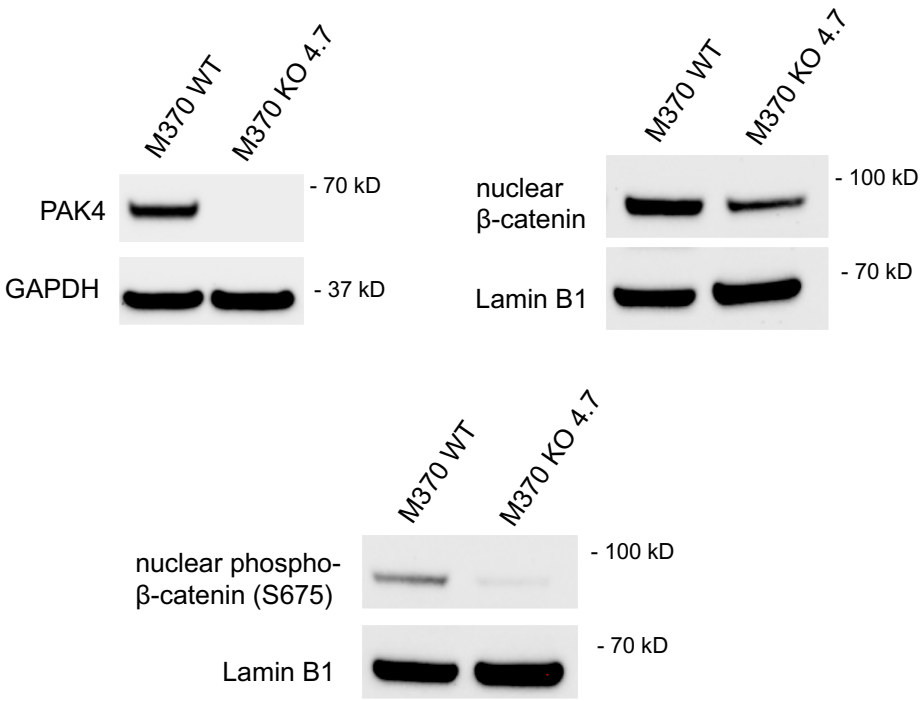

b

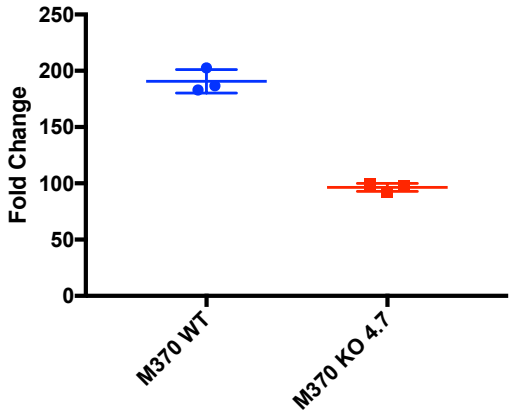

Extended Data Figure 7: PAK4 KO in human melanoma cells impairs B-catenin/WNT signalling. a, Immunoblot for PAK4, nuclear B-catenin and S675 phospho-B-catenin in human melanoma M370 cells. **b,** M370 WT and KO cells were treated with Wnt-3a at 200ng/mL for 8 hours to perform a Topflash assay. Showing the fold change between Wnt-3a treated and untreated cells for both groups. As observed in B16 PAK4 KO cells, PAK4 deletion decreases S675 phosphorylation and reduces sensitivity to Wnt-3a stimulation.

Supplementary Figure 1

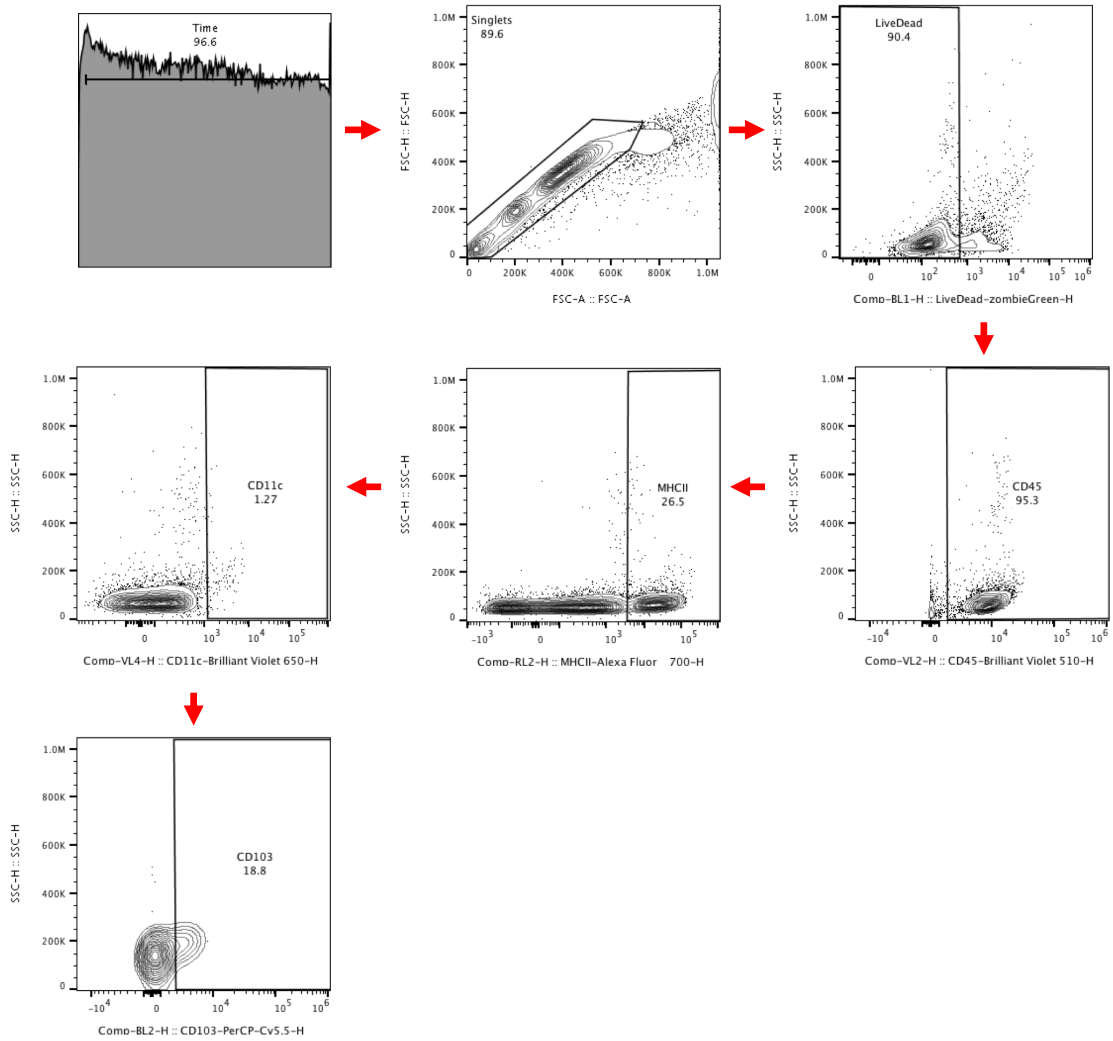

Supplementary Figure 1: Gating strategy for CD103⁺ dendritic cells. Tumor cells were gated to exclude doublets using FSC-H vs FSC-A. Then singlets were selected for viable cells (LiveDead vs SSC-H) and then gated for CD45 positive cells (CD45 BV510 vs SSC-H). Then, MHC-II (MHC-II AF700 vs SSC-H) and CD11c (CD11c BV650 vs SSC-H) positive cells were selected to quantify the percentage of CD103 positive cells (CD103 PerCP-Cy5 vs SSC-H).